

Viridian (Gen X) Final Design Report

Table of Contents

1. [Introduction](#)
 - 1.1. [Critical Dimensions](#)
 - 1.2. [Center of Gravity](#)
2. [Aerobody](#)
3. [Mechanical](#)
 - 3.1. [Front Suspension](#)
 - 3.2. [Rear Suspension](#)
 - 3.3. [Fatigue Analysis](#)
 - 3.4. [Shock and Spring](#)
 - 3.5. [Steering](#)
 - 3.6. [Wheel System](#)
 - 3.7. [Brakes](#)
 - 3.8. [Connection Methods](#)
4. [Chassis](#)
5. [Electrical](#)
6. [Appendix](#)

1. Introduction

Blue Sky Solar Racing's tenth generation solar electric vehicle is a cruiser class vehicle designed to meet the regulations of the 2019 World Solar Challenge. A major change from previous generations is the pod style design of the aerobody compared to catamaran styles used previously. This change is anticipated to significantly improve the aerodynamic performance of the vehicle and result in a more efficient car overall. The driver will also be located at the center of the vehicle instead of to the side.

The team's main goal for the design was to achieve the highest ratio of total energy intake by the array over the drag coefficient. The latest theoretical team goal value calculated was 98.84, which is a major improvement over Polaris value of 84.20. The derivation of the team goal can be seen below where Total Energy over CdA is the optimized parameter.

$$P_{aero} = 0.5 * \rho * v^3 * C_d A$$
$$P_{array} = \frac{\text{Total Power}}{\text{Total Time}}$$
$$\text{Total Time} = \frac{3022000}{v}$$
$$\frac{\text{Total Energy}}{3022000} = 0.5 * \rho * v^2 * C_d A$$
$$v = \sqrt{\left(\frac{2 * \text{Total Energy}}{3022000 * \rho * C_d A} \right)}$$

The following assumptions and conventions will be used throughout this report:

- The x, y, z components refer to the lateral, longitudinal and vertical components of the vehicle respectfully as shown in the figure.
- The origin of the global coordinate axis system is on the ground between the two front tires

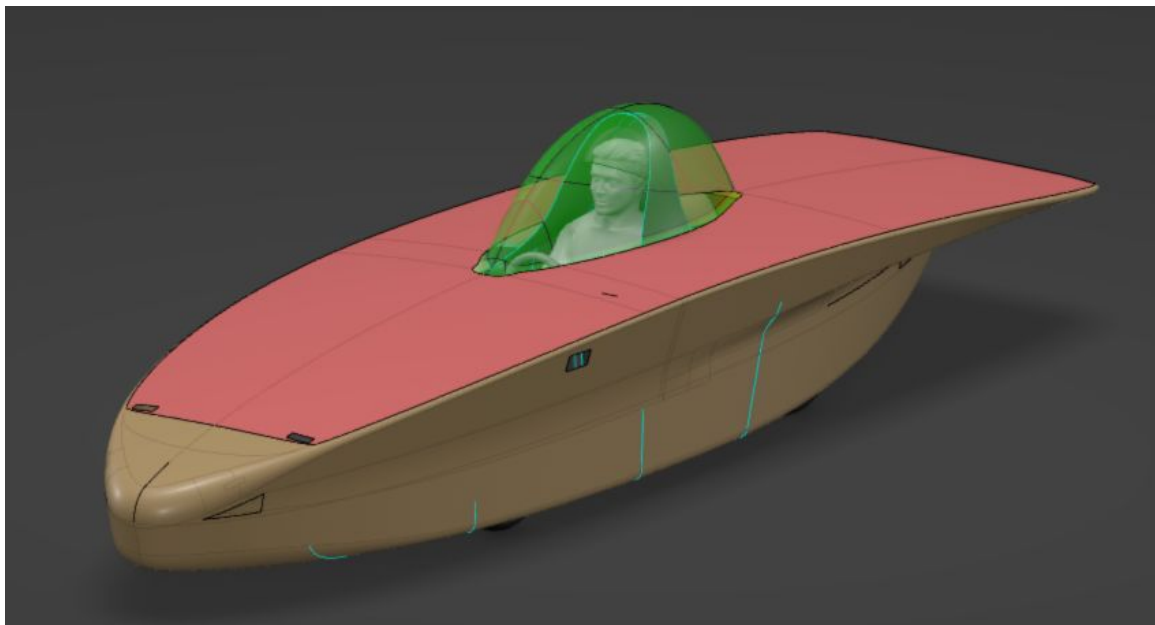


Figure 1.1 Car isometric view

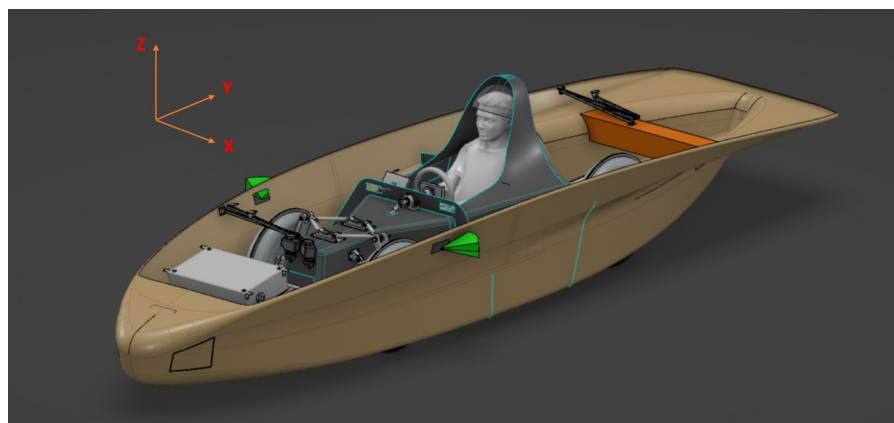


Figure 1.2 Coordinate System

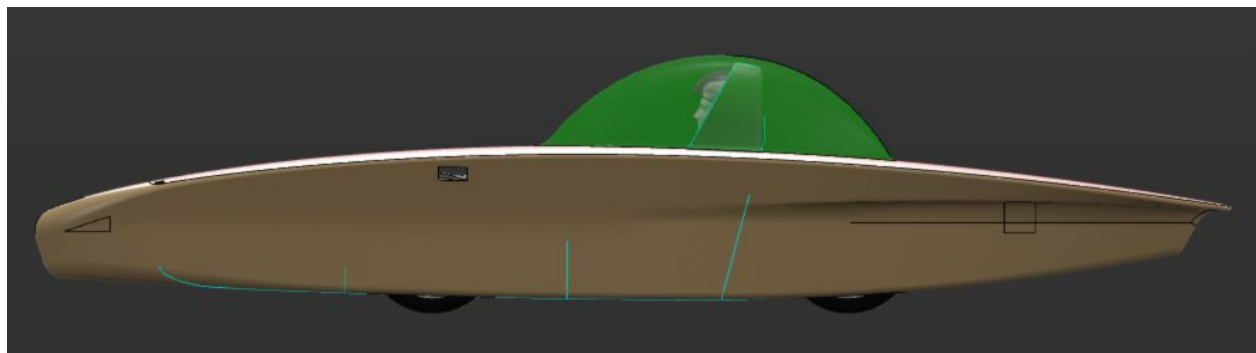


Figure 1.3 Side View of the car

1.1. Critical Dimensions

Table 1.1.1 Key parameters of Viridian

Parameter	Value
Length	4.969 m
Width	1.26 m
Height	1.066 m at max height
Front Track Width	0.7 m
Rear Track Width	0.68 m
Wheelbase	1.727 m
Ride Height	0.06 m at lowest point

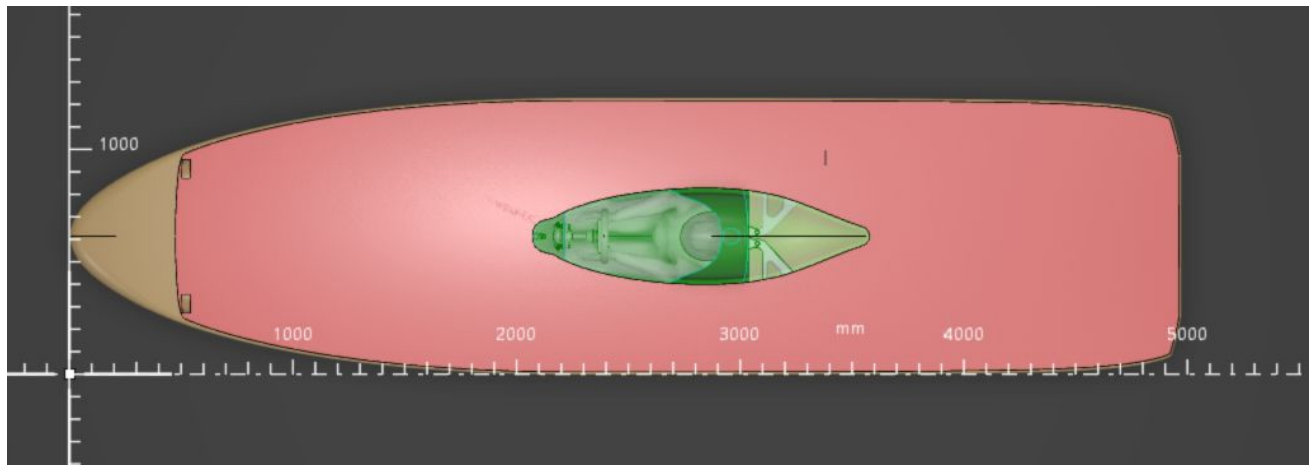


Figure 1.1.1 Top view dimensions of the car

A highly disputed issue with the design concept has been the ground clearance and the ability of the vehicle to handle typical road conditions. Currently the vehicle can handle the following conditions:

- Can pass over a 60mm object
- Can mount a 50mm curb
- Can fully bump the front suspension and droop the rear suspension and maintain 5mm of ground clearance

The most concerning issue regarding the ride height is ensuring the vehicle does not hit curbs while being pushed onto high platforms (sidewalks, ramps, etc.). While driving, it is not anticipated that the vehicle will have enough ground clearance issues.

The figures below demonstrate the analysis done on the ground clearance:

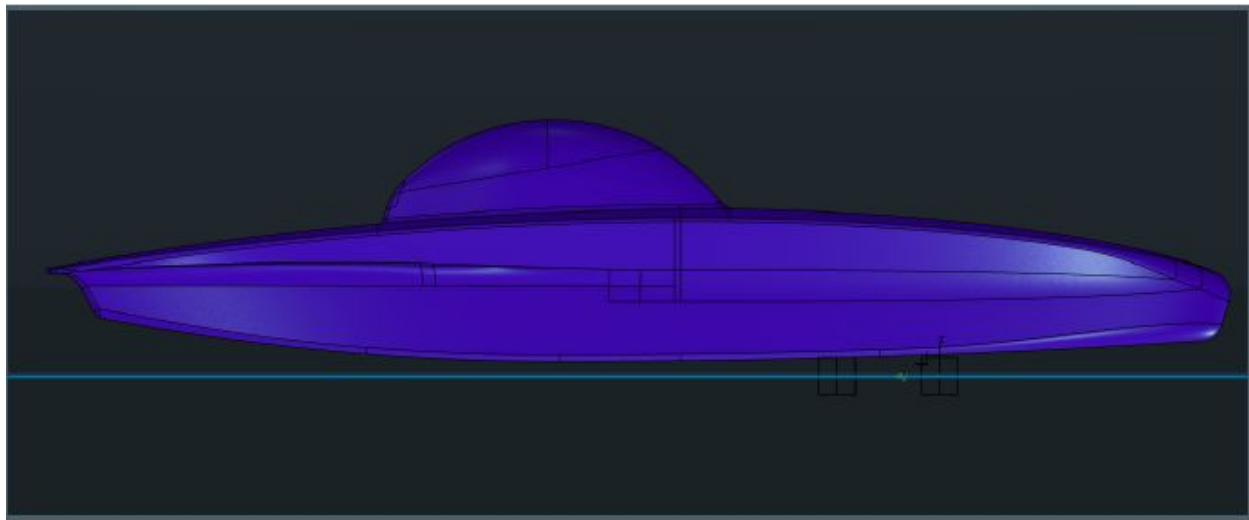


Figure 1.1.2 Ground Clearance

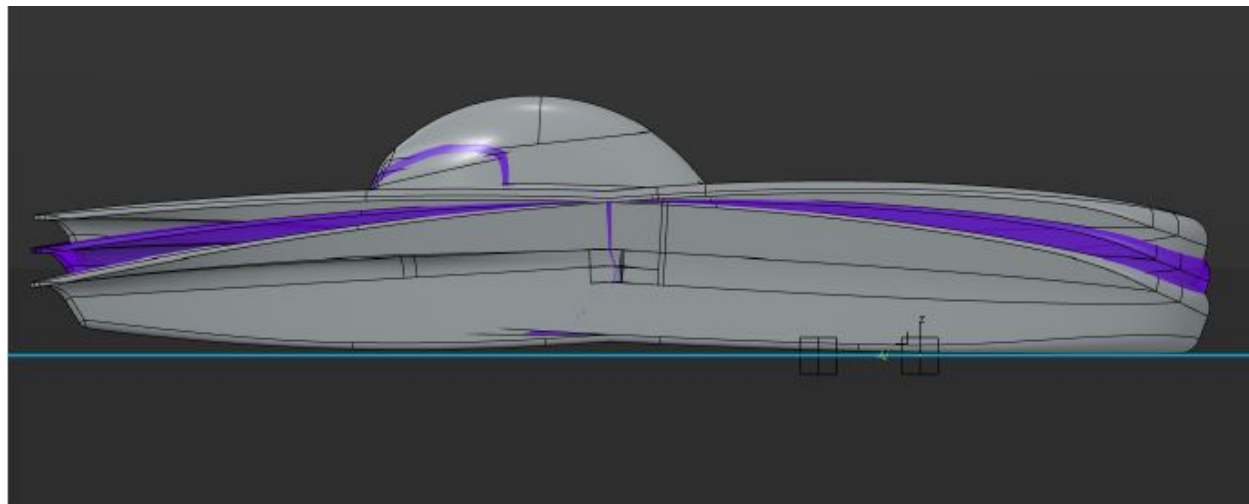


Figure 1.1.3 Bump and Droop

1.2. Center of Gravity Information

The driver location and the components of the car are positioned relative to the global coordinate axis system. The individual masses are used to calculate the center of gravity shown in Table 1. For the car to have an understeer configuration, it was necessary to have more than 50% of the weight on the front wheels.

The CG was calculated using the formulas:

$$CG_x = \frac{\sum(W_i \times CG_{x,i})}{\sum W_i}$$

$$CG_y = \frac{\sum(W_i \times CG_{y,i})}{\sum W_i}$$

$$CG_z = \frac{\sum(W_i \times CG_{z,i})}{\sum W_i}$$

where i represents the different components on the car. The table and figure below show the location of the major components in the car with their relative mass:

Table 1.2.1 Mass approximation of vehicle components

Component	Approximate Mass [kg]
Driver + Ballast	80
Battery Box	22.5
PPT Box	9.8
Top + Array	19.5
Motor	13.00
Chassis + Roll cage + Bottom	40
Steering	4.5
Accelerator + Brake	4
Front Wheels + Suspension	25
Rear Wheels + Suspension	23
CG position	

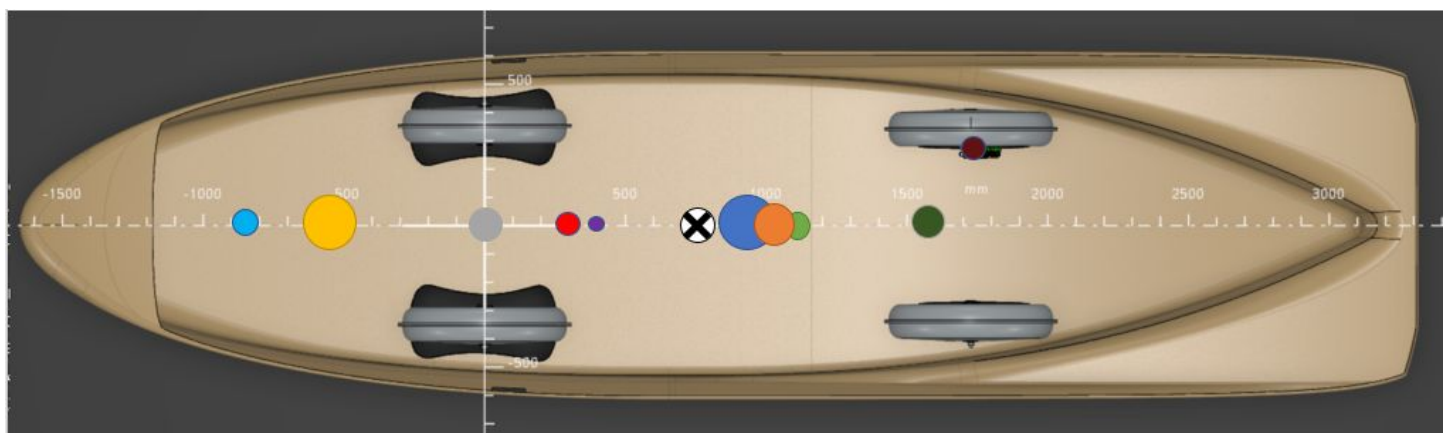


Figure 1.2.1 CG layout

Table 1.2.2 CG location of the car w.r.t the origin

CG	Location from origin [m]
CGX	0
CGY	0.732
CGZ	0.32

Static Weight Distribution:

When static, the weight distribution of the car is as follows:

Table 1.2.3

Side	Weight Ratio
Front	57.6 %
Rear	42.4 %
Left	50 %
Right	50 %

In dynamic conditions, the vehicle can experience certain bump, brake and load conditions. The weight distribution of the vehicle will change in these scenarios based on the amount of weight transfer. The following formulas were used to determine the longitudinal weight transfer when braking, and the lateral weight transfer when turning:

$$\text{Longitudinal Weight Transfer} = CGZ * \text{Longitudinal Acceleration} / \text{Wheelbase} = 0.186$$

$$\text{Lateral Weight Transfer} = CGZ * \text{Lateral Acceleration} / \text{Track Width} = 0.467$$

The lateral weight transfer was calculated using the rear track width as it is narrower and can lead to more weight transfer.

The table below displays the different percentages that each wheel experiences in certain conditions. The cases are Bump, turn and brake respectively.

Table 1.2.4

Case [Bump, Turn, Brake]	Static	2,1,1	2,1,-1	2,0,1	2,0,-1	2,1,0
Front Left	29%	74%	3%	56%	2%	39%
Front Right	28%	2%	73%	2%	55%	38%
Rear Left	21%	23%	1%	41%	2%	12%
Rear Right	22%	1%	23%	1%	41%	11%

As all percentages are above zero, the car will not lift from the ground in any scenario. BWSC requires drivers to navigate a Figure-8 course where the smallest turning radius is 6.5m. This scenario is anticipated to impose the largest turning force (1G) on the vehicle. With the above calculations, the car will be able to navigate the figure 8 course without any lifting of the tires.

2. Aerobody

The aerobody design was optimized by performing 5 Design of Experiments (DOEs) on different parameters and then selecting the best performing configuration. The parameters of the DOEs were:

1. Front & Rear Track Width and Fairing Length
2. Driver Position, Canopy rear fillet and Canopy top style
3. Airfoil Types and front & rear taper
4. Top and side curvatures
5. Fillets

The array from this cycle is unique from those of previous cycles in that it has curvature in two directions. Although this was more difficult to design for and will likely result in slightly more complicated manufacturing, the aerodynamic benefits from having the aerobody curved in two axis outweighed the potential costs.

The array layout was decided on with the cooperation of the aerodynamics design. Around 200 different, array, aerobody, and canopy combinations were ranked according to the team goal with the help of simulations. The current array layout uses the maximum allowable number of Me1 cells (260). The current array design will produce approximately 7kWh of energy during racing hours on an average sunny day, around 10% higher than the amount estimated from simulations run on polaris' array.

The resultant aerobody shape can be seen in the below figures:

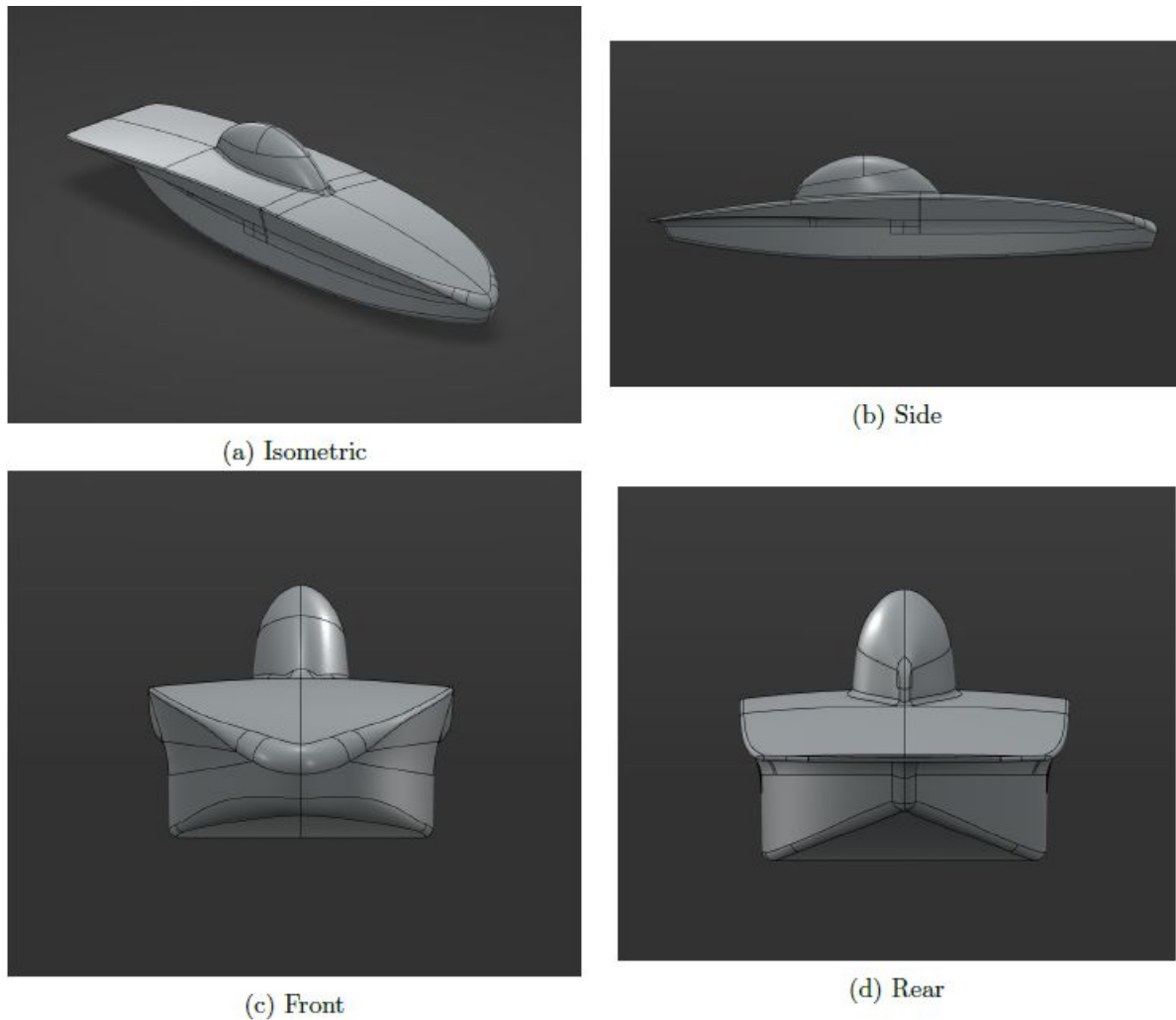
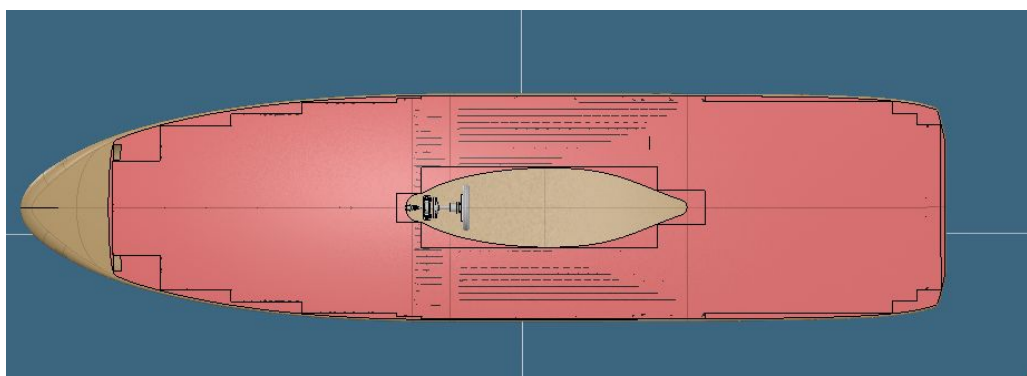


Figure 2.1



Array Layout

2.1. Center of Pressure:

The center of pressure is the point where the pressure fields act on a body. In this case, any pressure applied from oncoming flows/winds will be applied to the Cp. The table below shows the Cp and Cg locations relative to the origin of the car.

Table 2.1.1 CG and CP comparison

	X [m]	Y [m]	Z [m]
Center of Pressure	0	0.82	0.57
Center of Gravity	0	0.732	0.32

The fact that the CP point is behind the CG point ensure that the vehicle has a self correcting effect in cross wind situations. A restoring yaw moment will be produced when crosswinds are applied to the vehicle.

2.2. Crosswind: Yaw and Pitch

3 crosswind study cases were done for wind angles of attack of 8 degrees, 15 degrees and 35 degrees. Based on statistical data of wind directions and magnitude at major cities along the racing route, we found that the strongest wind, in the record of 5 years, is happening in Alice Spring, with the wind due East at magnitude of about 50 km/hr. Combining this wind stats with our ideal speed of 70 km/hr, we have used wind direction of 35 degree at magnitude of

$\sqrt{50^2 + 70^2} = 86 \text{ km/hr}$, which is roughly 24 m/s. Also, similar method is used for the case of 15 degrees. As expected, the drag was increased noticeably. However, in terms of stability, the lift force is still negative, and the side force is only 11.60 N and 37.87 N, which turns into small yaw moment considering that the Cpy and CGy are in close proximity.

Table 2.2.1 Crosswind Performance

Angle	X-force [N]	Y-force [N]	Z-force [N]
Head On (18 m/s)	0	13.352	-44.30
8 degrees (18 m/s)	3.50	13.83	-43.57
15 degrees (20 m/s)	11.60	21.45	-54.35
35 degrees (24 m/s)	37.87	37.55	-54.23

Note that the moment about x-axis using CG as the moment center is minute, only 86.79 N.m (referring to table 10), so the most pitching up the car can be, before it is limited by the suspension system, will not pose the safety concern to the driver or the car itself.



Figure 2.2.1 Alice Spring Wind Data

Table 2.2.3 “Pitch Up” wind Performance

Angle	X-force [N]	Y-force [N]	Z-force [N]
3.323 deg	0	16.70	13.45

Table 2.2.4 “Pitch Up” Moment

Moment Axis	X-Axis
Moment Value [N-m]	86.79 (Pitching Up)

From 2 figures below, we can see that the pressure difference between the top and bottom aerobody at location close to the trailing edge are similar to each other; hence, no significant moment is generated.

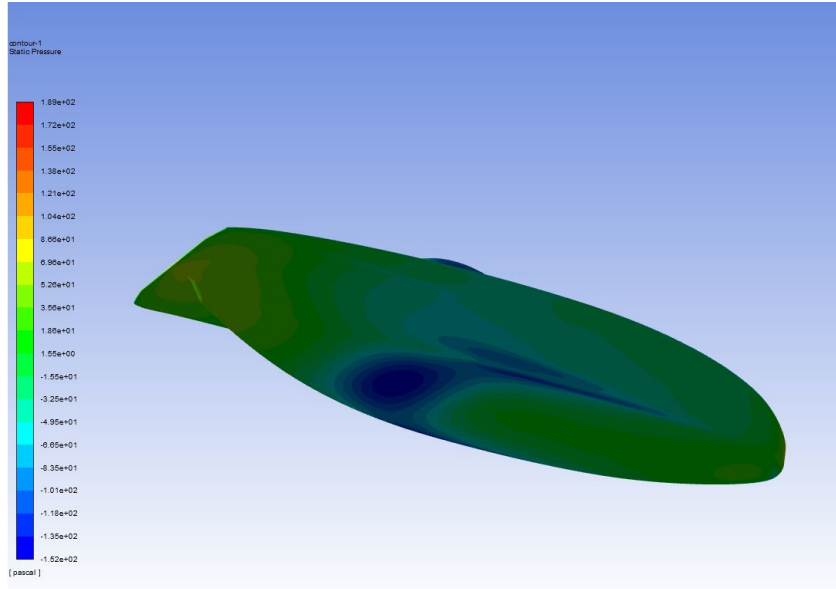


Figure 2.2.2: Pressure Plot on the bottom of aerobody

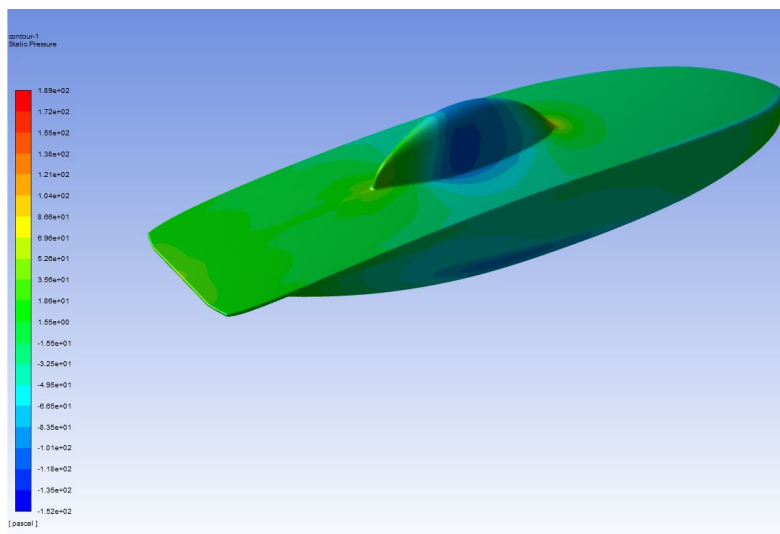


Figure 2.2.3: Pressure Plot on the top of aerobody

2.3. Effect of sharp edges: flow visualization

The flow field visualization on some edges of the aerobody is shown in the following figures. Note that this is the case of cross wind $\tan^{-1}(5/7)$, which are worse than the head on case.

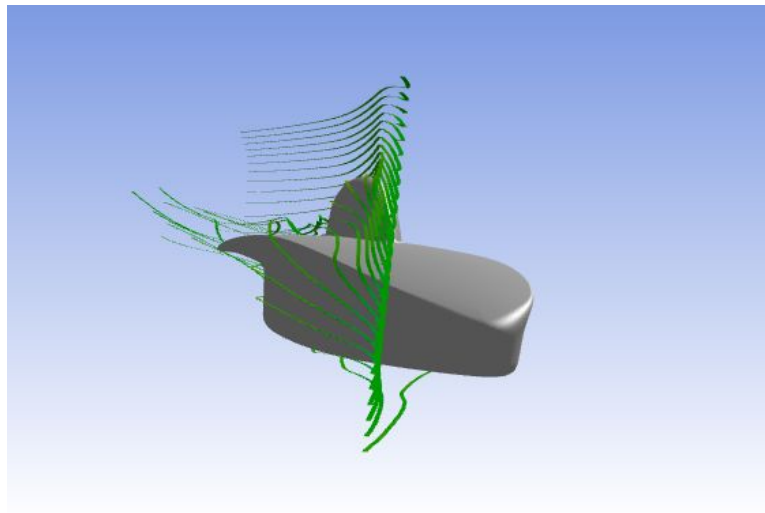


Figure 2.3.1 Sharp Edge 1

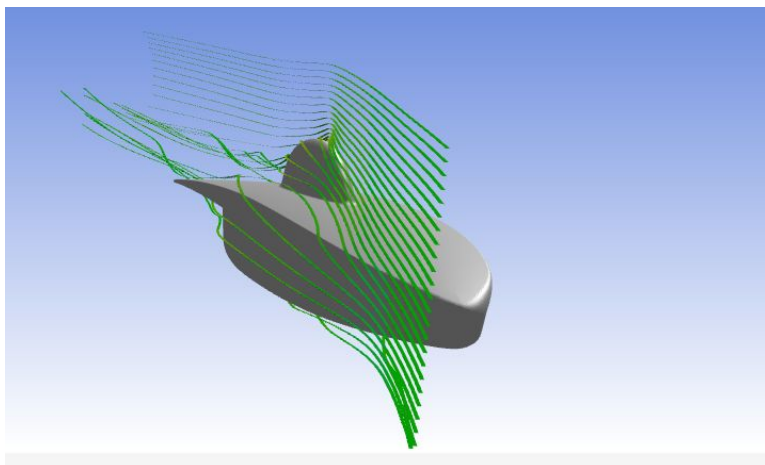


Figure 2.3.2 Sharp Edge 2

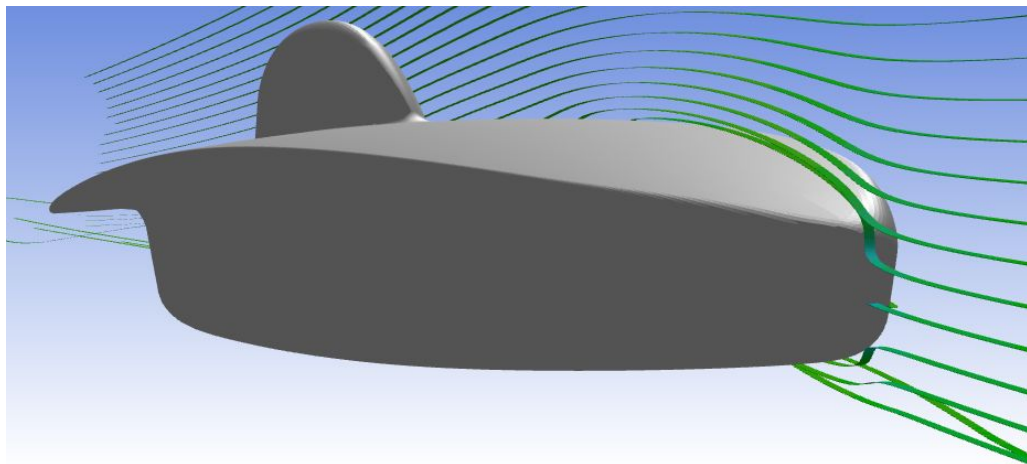


Figure 2.3.3 Sharp Edge 3

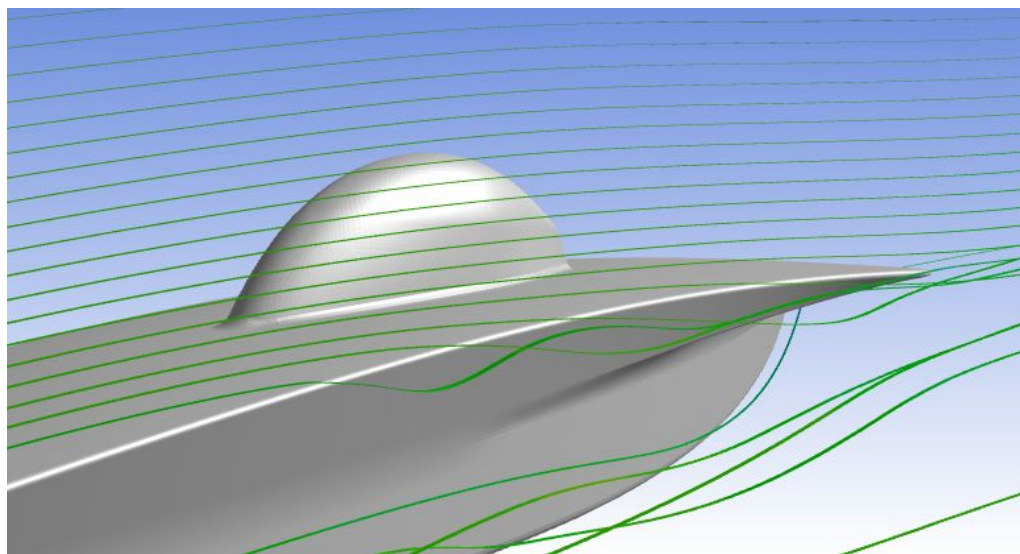


Figure 2.3.4 Sharp Edge 4

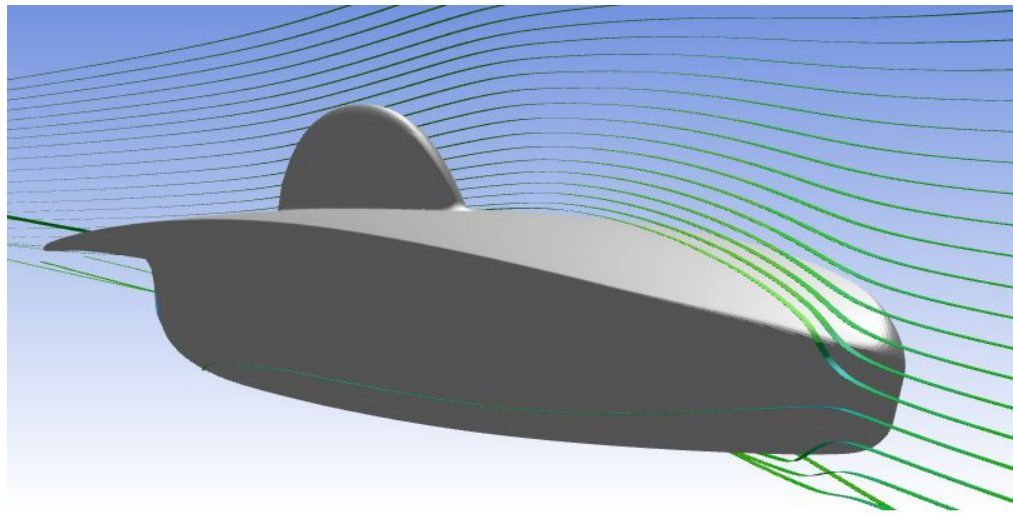


Figure 2.3.5 Sharp Edge 5

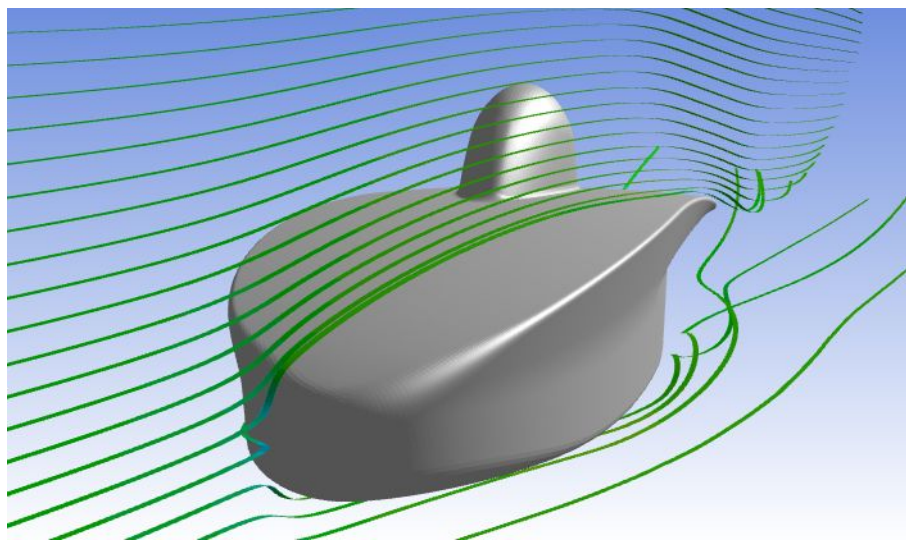


Figure 2.3.6 Sharp Edge 6

3. Mechanical

3.1. Front Suspension

The front suspension of Viridian is a double wishbone suspension with parallel but unequal length control arms. The mechanism is comprised of four main components:

- Upright
- Top AARM
- Bottom A-Arms

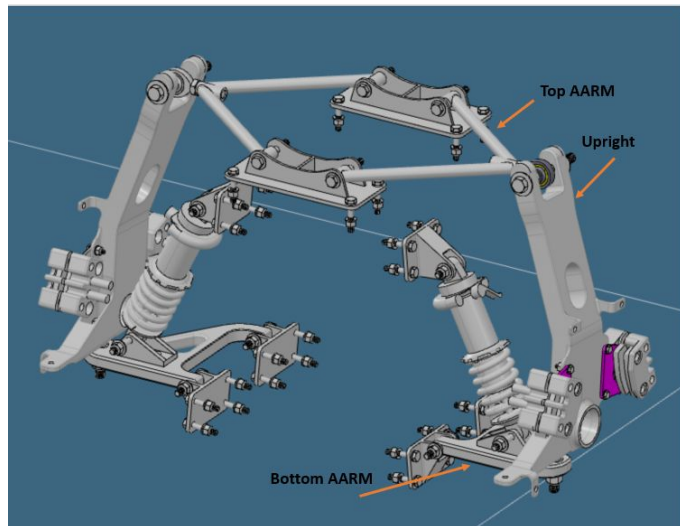


Figure 3.1.1

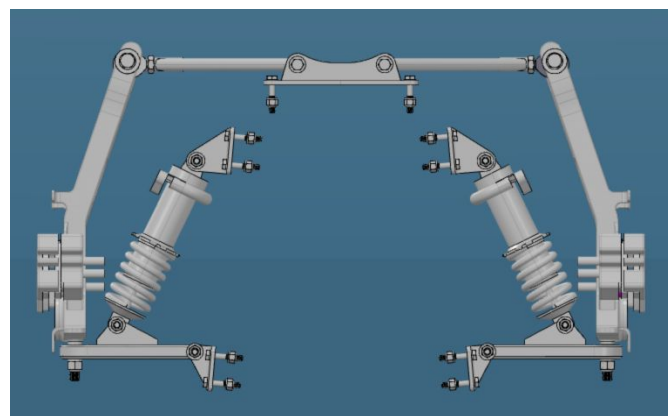


Figure 3.1.2

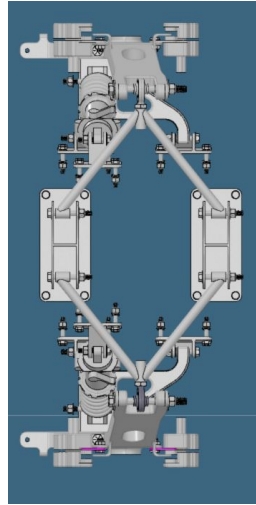


Figure 3.1.3

The report will first discuss the 2D suspension geometry and properties before detailing the 3D aspects of the design.

3.1.1. 2-D Suspension

The design of the suspension system of the car started with a 2D skeleton sketch of the mechanism. This was done in order to experiment with various suspension geometries so that the important parameters could be optimized. Several iterations of the 2D suspension were created throughout the conceptual design and detailed design phase. The following geometry was selected based on packaging constraints of the chassis/aerobody and the optimization of parameters discussed later.

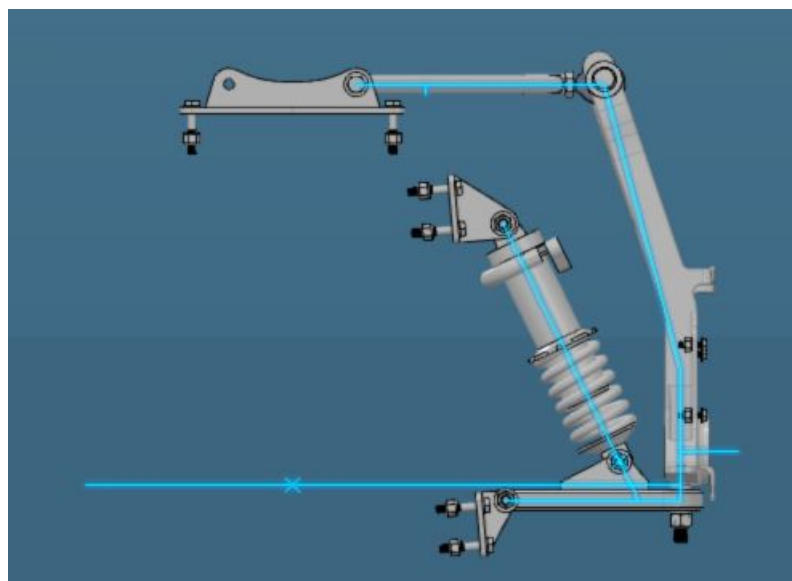


Figure 3.1.1.1 2D front suspension

Summary of suspension parameter

Parameter (at Neutral)	Value
Scrub Radius	0.89 mm
Bump Steer	0.16 degrees
Roll Center Height [Neutral]	0 mm (on the ground)
Camber Change	0.489 degrees
Track Change [each]	9.536 mm
Caster Angle	10 degrees
Mechanical Trail	90 mm

- **Suspension Travel**

The suspension is designed for 2" of travel in each of bump and droop.

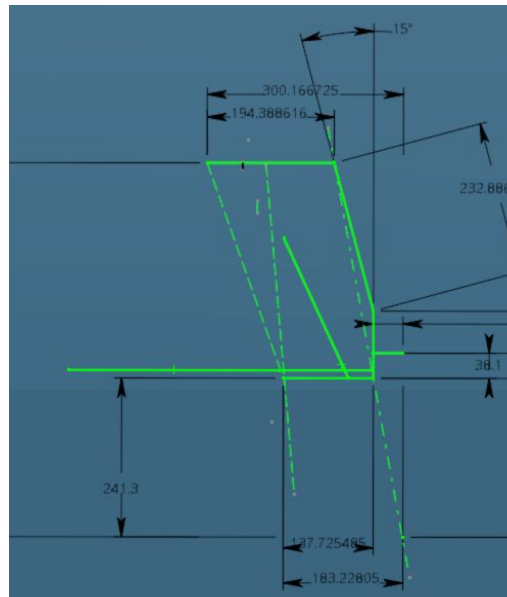


Figure 3.1.1.2 Neutral

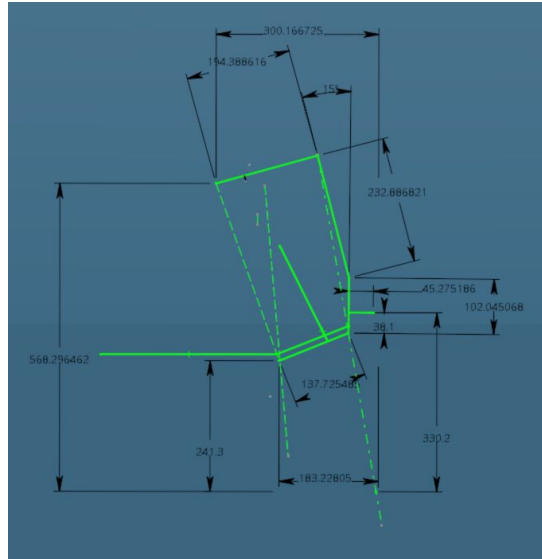


Figure 3.1.1.3 Bump

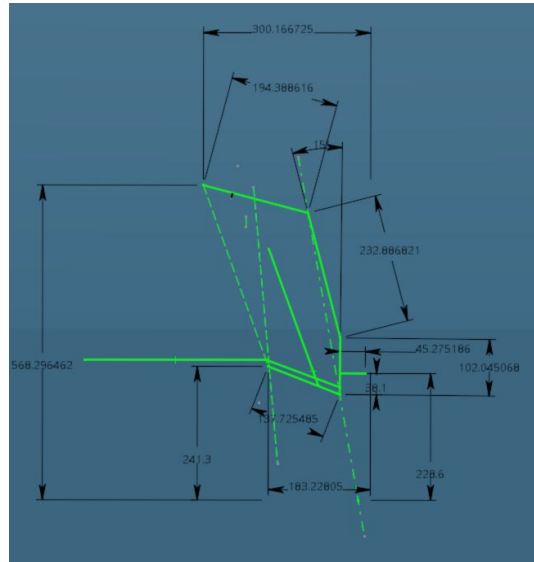


Figure 3.1.1.4 Droop

- **Scrub Radius:**

Scrub radius was minimized to a value of 0.89 mm by optimizing the location of the top and bottom ball joints. This value will allow for easier steering (less resistance) and will reduce energy loss due to friction between the tire patch and the road.

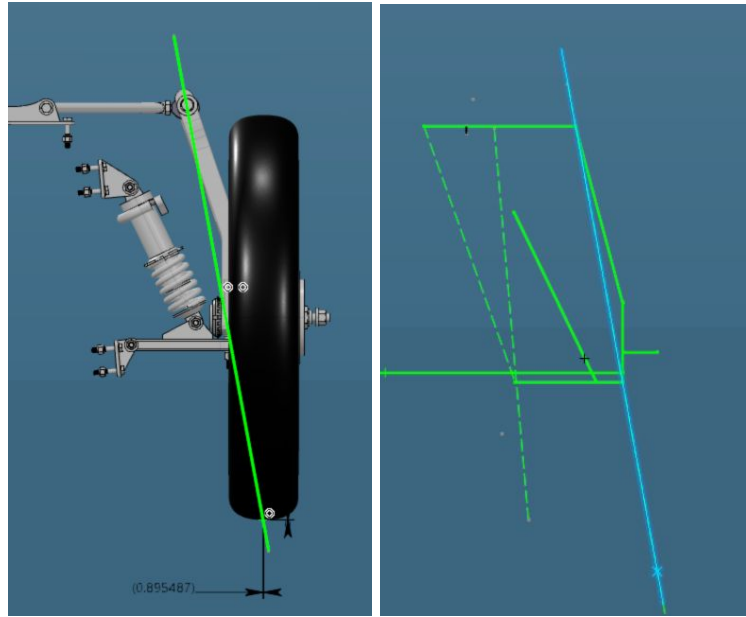


Figure 3.1.1.5 Scrub Radius

- **Bump Steer:**

The amount of bump steer experienced by the car has been minimized to 0.08 degrees on bump and droop for a total of 0.16deg. This was achieved by modifying the geometry of the suspension and steering systems and ensuring that the control arms and the steering tie rod shared the same instantaneous center of rotation.

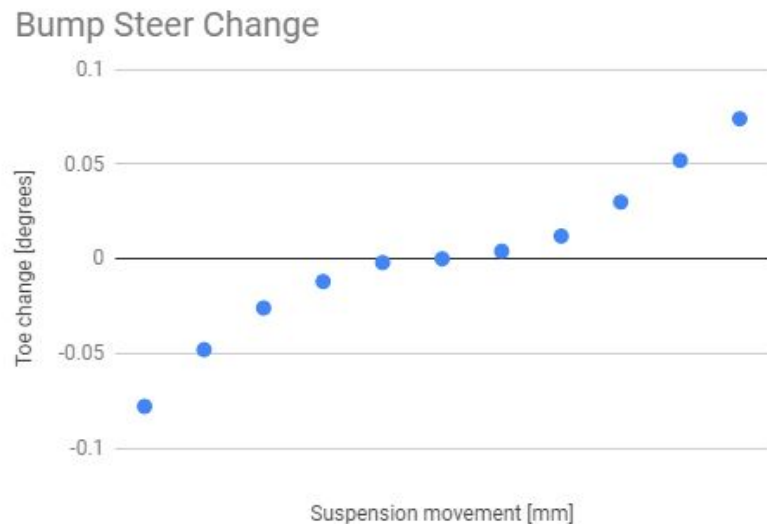


Figure 3.1.1.5 Bump Steer Change

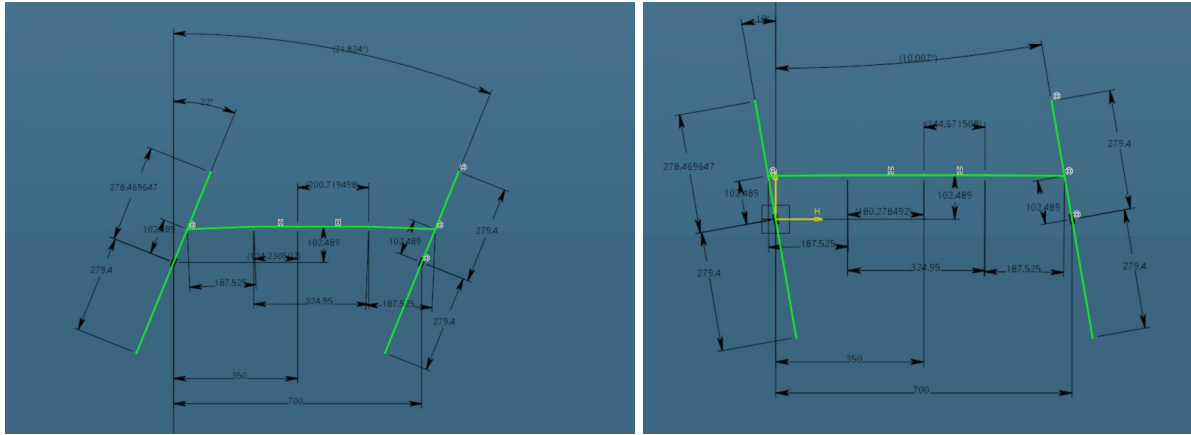


Figure 3.1.1.6 2D Steering geometry

- **Roll Center Height (RCH):**

The roll center is the theoretical point around which the chassis/car rolls. The roll center height of the suspension at neutral is on the ground due to the parallel control arms. As the suspension moves through its travel, the roll center height changes based on Figure 3.1.1.7. The amount of movement that the RCH experiences is minimal (150mm) and its distance from the CGZ is not considerable. Therefore the car will not experience significant roll.

The roll axis from the rear RCH to the front RCH is also going to be either pointing down or slightly up which is again not a major concern, as the weight of the car will shift to the front while turning which causes understeer.

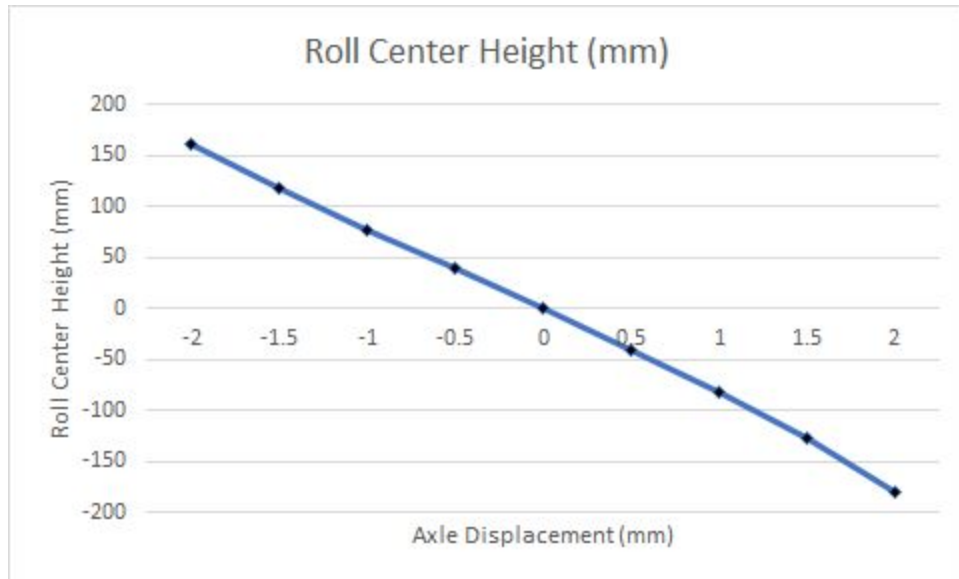


Figure 3.1.1.7 RCH change through suspension movement

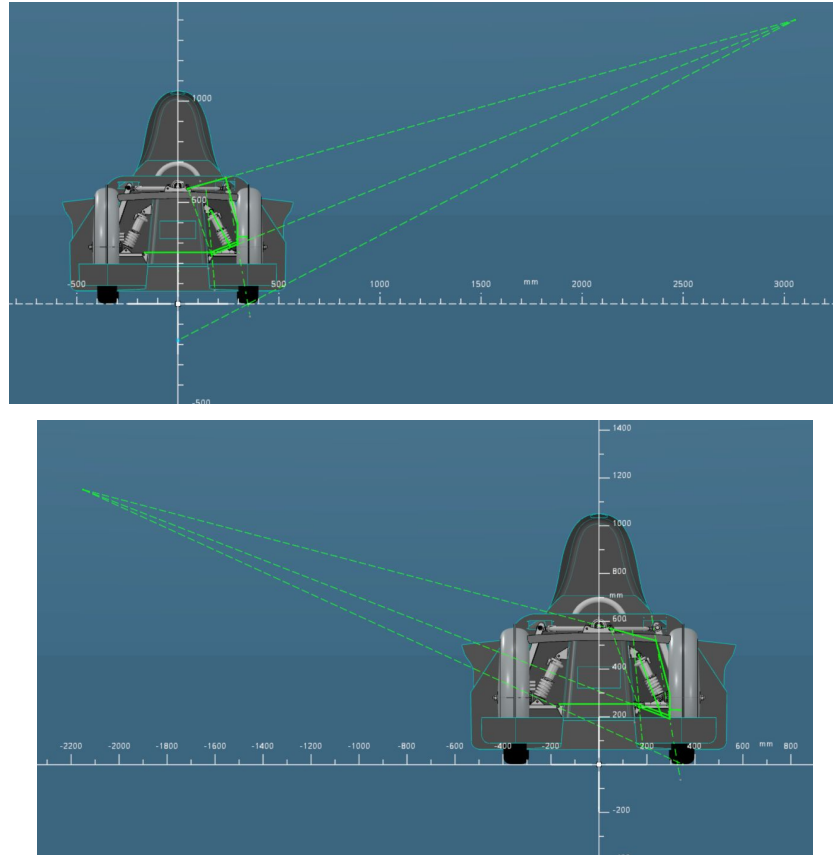


Figure 3.1.1.8 RCH location at bump and droop

- **Camber and Track Change (Scrub):**

The suspension experiences minimal camber change (0.489 degrees) as it travels through its motion. This ensures that the wheel contact patch remains in contact with the ground to ensure traction and stability.

There is some track change present in the current suspension configuration. The maximum anticipated track change is 9.536 mm, which is considerably less than the previous generation car (roughly 15mm for Polaris)

- **Caster Angle**

A 10-degree caster angle is present with a positive mechanical trail of 90 mm. This will ensure that the suspension has a self-centering effect and that the front wheels will straighten themselves as the vehicle travels forward.

3.1.2. Load Calculations

The forces experienced by the suspension and transmitted to the chassis were determined using the 2D model as well. The diagram below shows the forces at the tire patch where N is the bump force, F_t is the turning force, and F_b is the braking force.

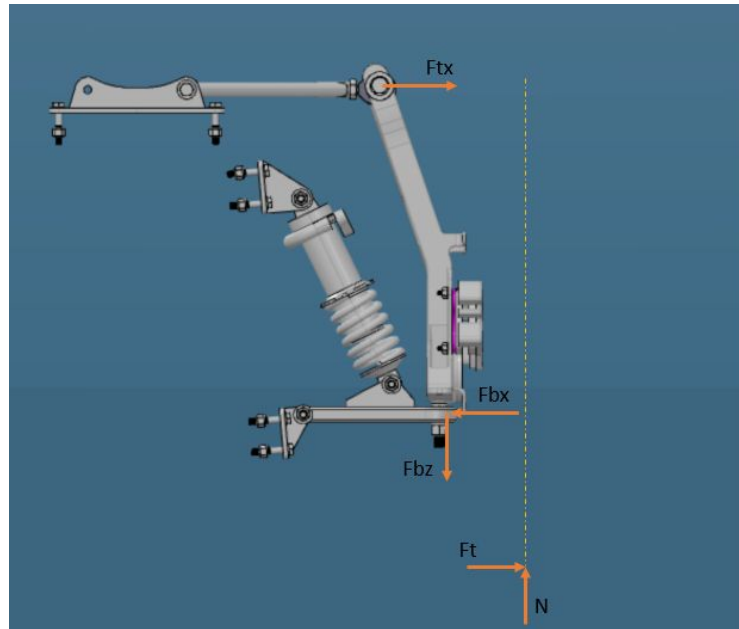


Figure 3.1.2.1 Forces at joints - Side view

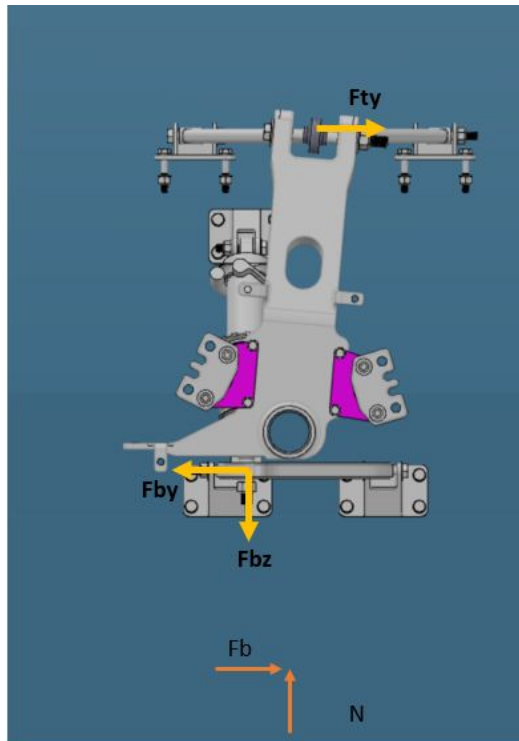


Figure 3.1.2.2 - Front View

To determine the value of wheel contact patch forces (N, Ft, Fb), the following formula was used:

$$N/Ft/Fb = M * g * G's * P$$

Where M = mass of the car, which is taken as 300 kg for all calculations, g is acceleration due to gravity, G's is the number of G's of force experienced, and P is the weight ratio of the wheel at a certain scenario (Refer to CG calculations above).

The different cases and G forces used for calculations were:

Table 3.1.2.1 Load Cases

Case	Bump [G]	Brake [G]	Corner [G]
Bump only (cattle grid, curb strike)	6	0	0
Bump, brake and left turn	2	1	1
Bump, brake and right turn	2	1	-1
Bump and left turn	2	0	1
Bump and right turn	2	0	-1
Bump and Brake	2	1	0

The forces acting at the joints were then calculated using static equilibrium equations ($\sum M = 0$, $\sum F = 0$).

The diagrams below show the reaction forces at the clevises:

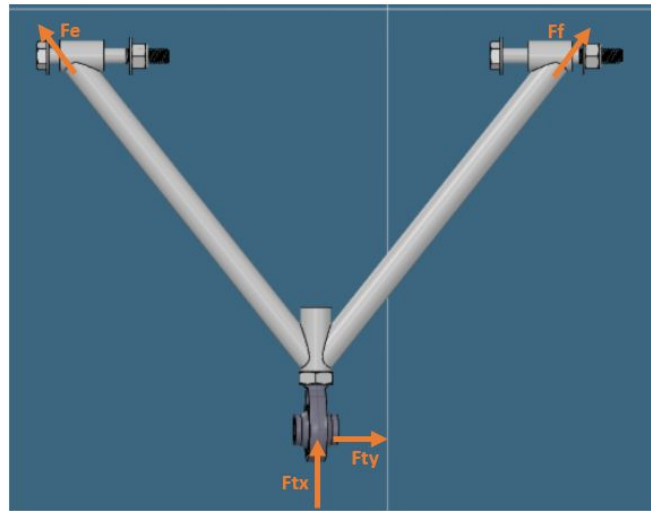


Figure 3.1.2.3 Top AARM forces

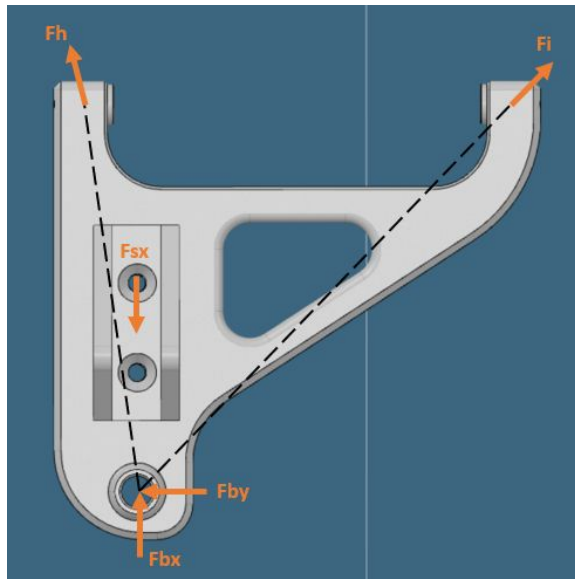


Figure 3.1.2.4 Bottom AARM forces Top view

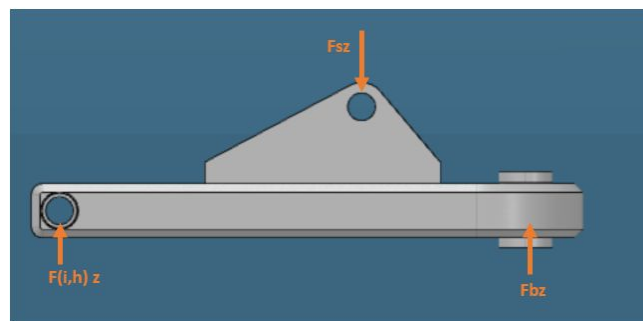


Figure 3.1.2.4 Bottom AARM forces Side View

Static equilibrium equations were again used to solve for these reaction forces.

3.1.3. 3-D Suspension

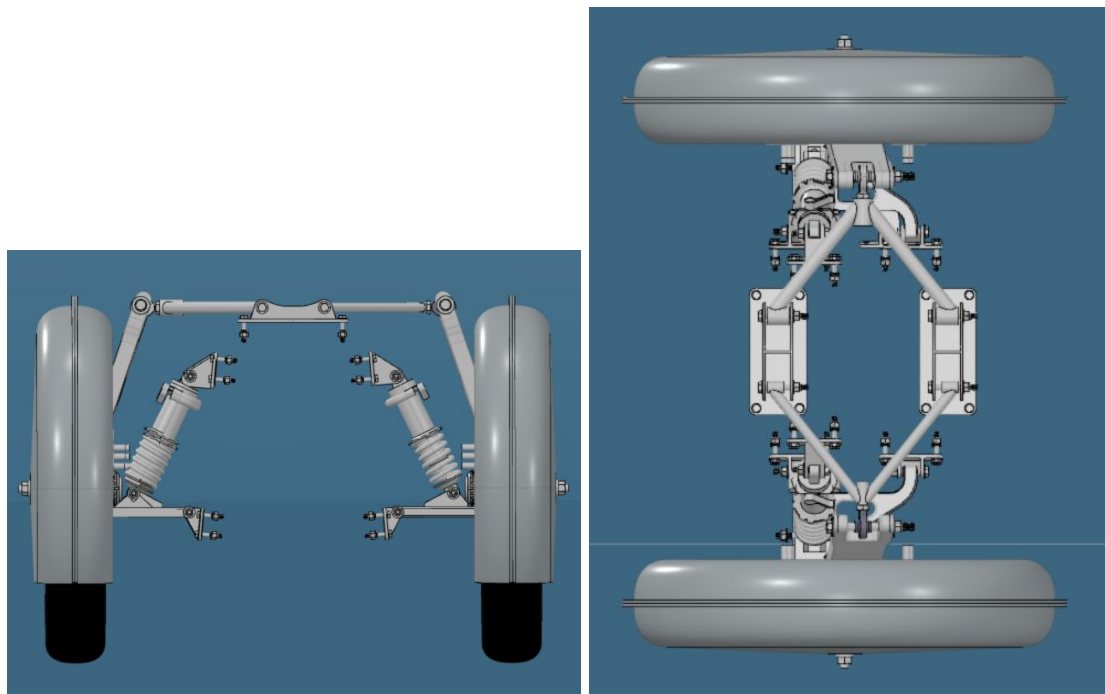


Figure 3.1.3.1

- **Top AARM**

Description

The Tom Control Arm (AARM) connects the top portion of the upright to the chassis. It is connected to the upright using an HXAM-7T rod end. This rod end allows for adjustability of the suspension in alignment. It allows the caster and camber to be adjusted as desired.

Material and Manufacturing

All components of the Top AARM are manufactured using 4130 steel due to its ease of machining and welding. As the top AARM may need to be modified in the future to make modifications to the suspension, using 4130 steel was determined to be the best choice. The components of the top AARM are:

- Main Body
 - 9/16" OD with 0.035 wall thickness

- Clevis Attachment
 - $\frac{5}{8}$ " OD with 0.151 wall thickness
- Rod End Attachment
 - $\frac{5}{8}$ " OD with 0.093 wall thickness

The components will be manufactured separately and welded together using a jig to ensure accurate assembly.

Diagrams

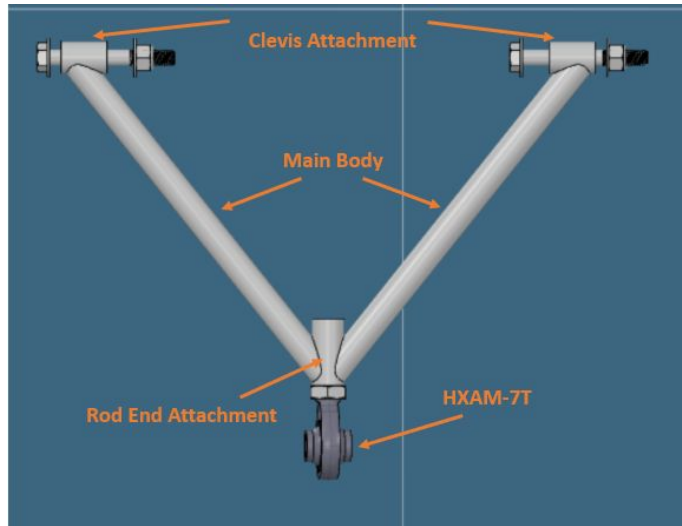


Figure 3.1.3.2

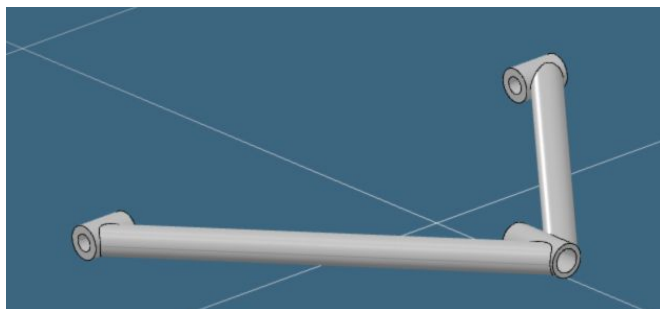


Figure 3.1.3.3

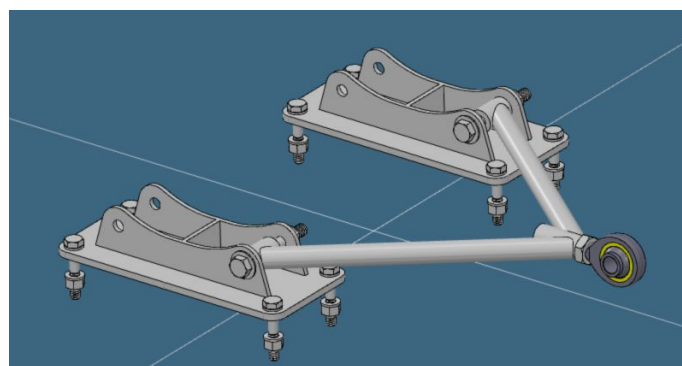


Figure 3.1.3.4

Simulation summary

The top AARM is simulated with a force applied to the hole of the rod end. The clevis mounting holes are set as cylindrical supports, allowing rotation.

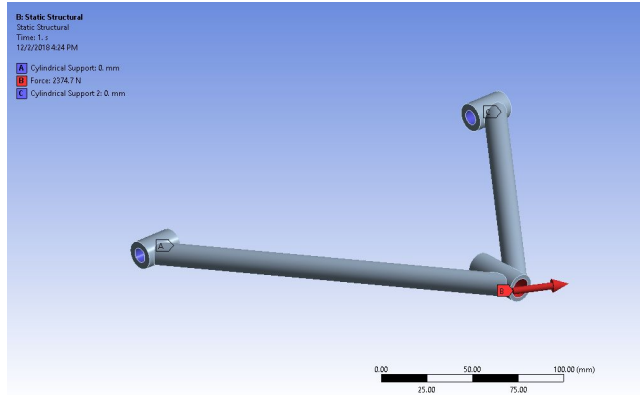


Figure 3.1.3.5

Table 3.1.3.1 Simulation results

Case	Safety Factor	Max Stress (MPa)	Max Deformation (mm)
2,1,1	1.73	251.5	0.14
2,1,-1	1.66	262.2	0.14
2,0,1	6.1	71.3	0.036

- **Bottom AARM**

Description

The bottom control arm (AARM) connects to the bottom portion of the upright to the chassis. It is connected to the upright using a HAB 7T high misalignment spherical bearing which facilitates the adjustability of the suspension. The bearing has a misalignment angle of 22 degrees which covers the max misalignment that the bottom aarm will experience (21 degrees). The bearing in combination with a bolt acts as a ball joint. The front suspension shock is attached on the bottom AARM using a bolt-on clevis.

Material + Manufacturing

The bottom AARM will be CNC cut using Aluminum 7075. Aluminum was chosen as the material due to its lower density compared to steel. CNC was picked as the manufacturing method due to the simple 2D shape of the arm. Some major parts of the bottom aarm:

- 7075 Aluminum CNC cut
- HAB-7T Spherical Bearing with 22 degrees misalignment
- Steel bushing for connection to clevises
- Bolt on clevis for the shock/spring

Diagrams

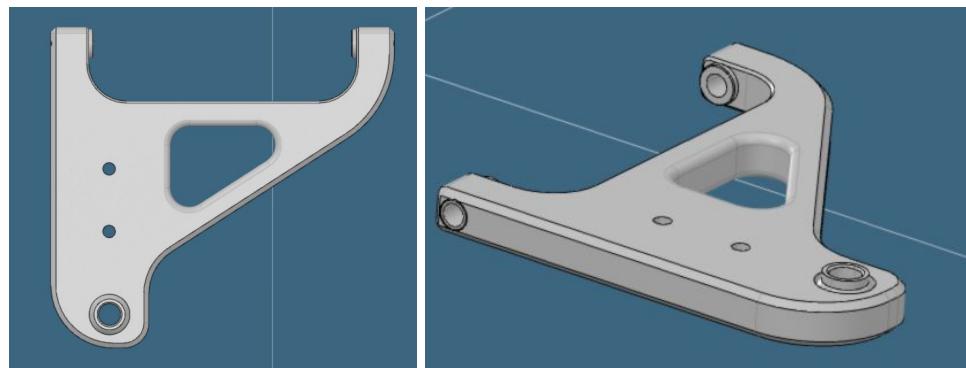


Figure 3.1.3.6 Top and Iso views

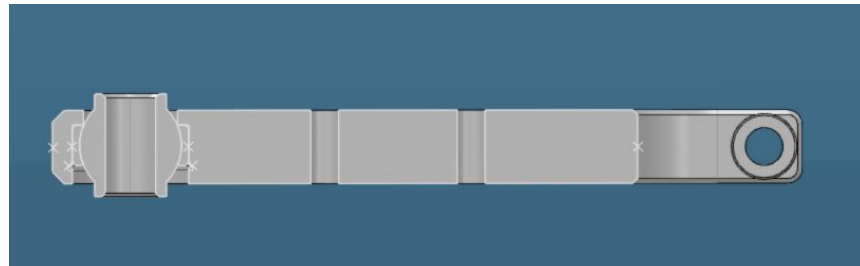


Figure 3.1.3.7 Section view

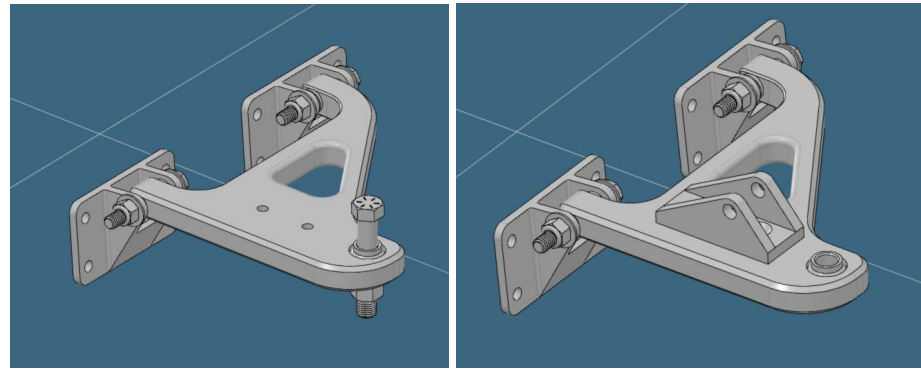


Figure 3.1.3.8

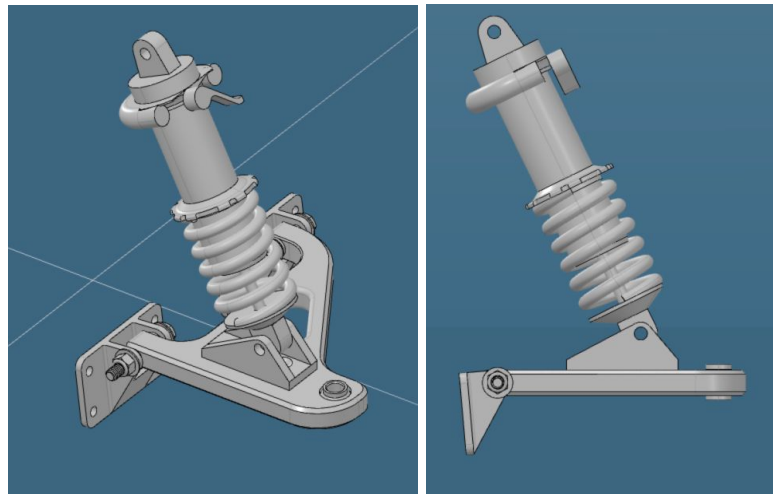


Figure 3.1.3.9

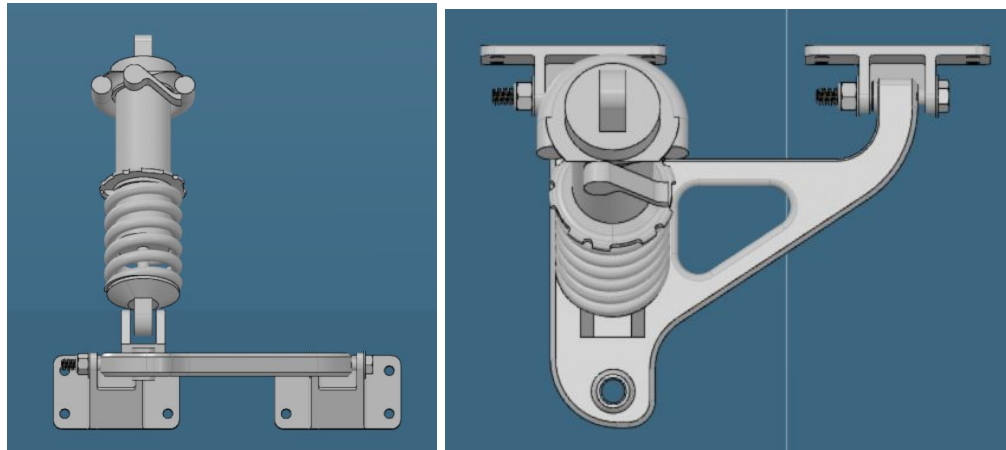


Figure 3.1.3.10

Simulation summary (Jane)

The bottom A ARM is simulated with clevis forces applied to the two holes that will be attached to clevises and upright and a remote displacement applied to the shock clevis projection area and the bolt clearance holes, while all degrees of freedom are a lock

around the center of shock clevis hole. (See the following diagram). Refer to the table for key simulation results.

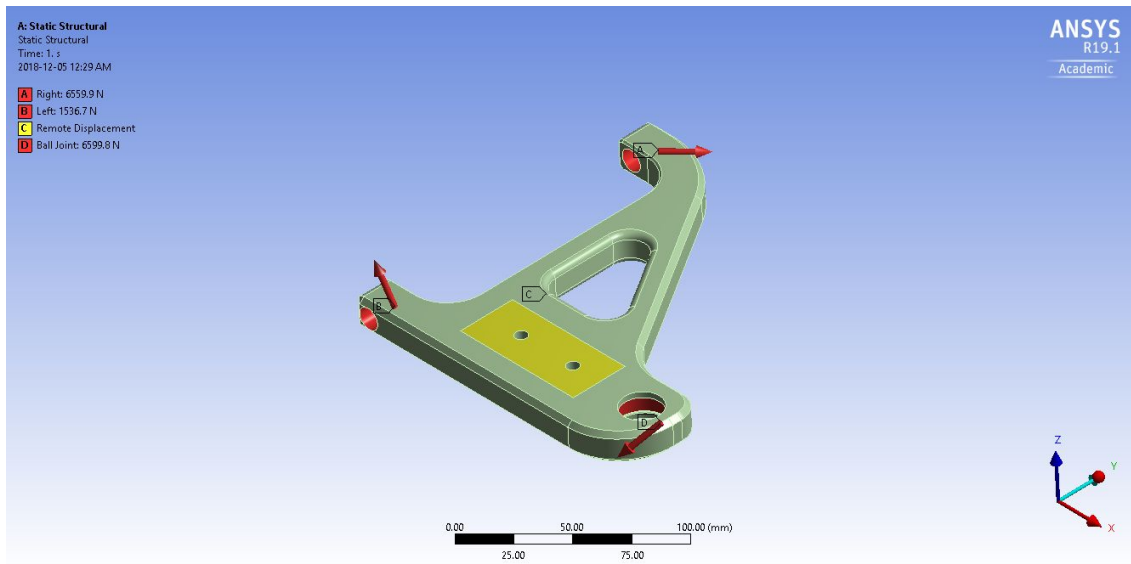


Table 3.1.3.2 Simulation results

Case	Safety Factor	Stress (MPa)	Deformation (mm)
2,1,1	1.9463	258.44	1.1603
2,1,-1	1.722	292.1	1.302
6,0,0	3.543	141.97	0.3551

Please refer to the Appendix for more information.

- **Upright**

Description

The upright connects to the axle, the top, and bottom control arm, steering rod, brake as well as inner fairing. It provides a positive kingpin angle at which the control arms will be mounted.

Material + Manufacturing

The upright will be casted out of Aluminum C355 , AMS 4215, T6 Tempered. Aluminum is going to provide a lighter product compared to steel alternatives. A main advantage of a casted aluminum piece is that several features on the upright can be integrated into the cast part, instead of having the need to weld/bolt additional pieces to the upright.

These features include brake ears, inner fairing attachments and other pieces. Additionally, the upright along with the trailing arms will be sponsored by a company free of charge.

Diagrams

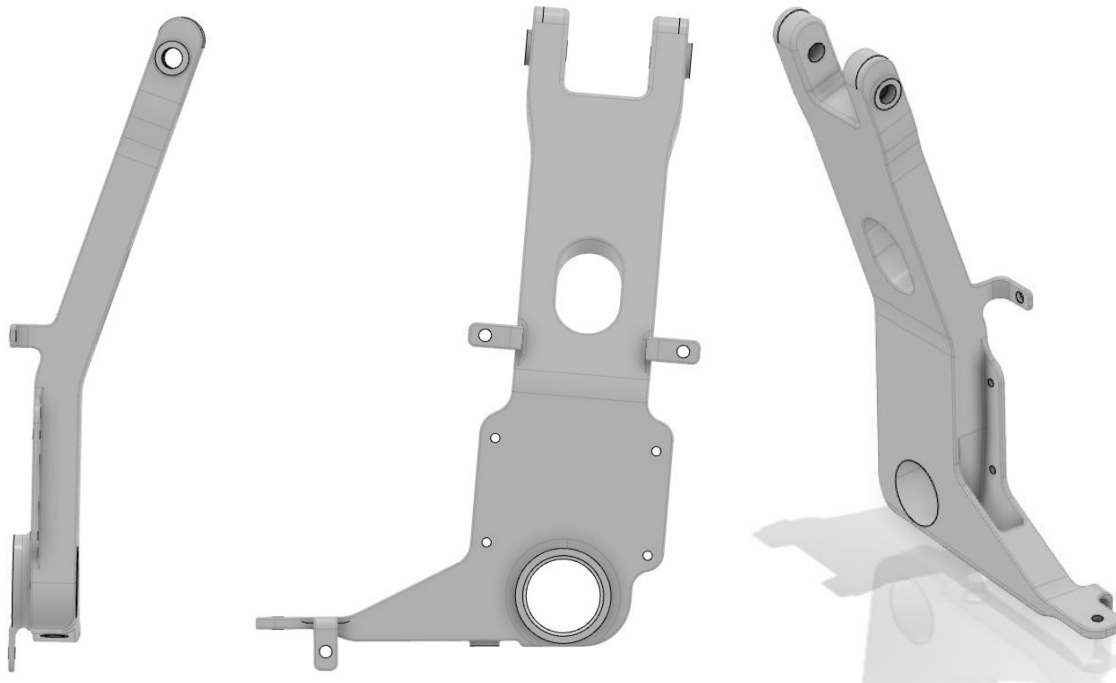


Figure 3.1.3.11

FRONT

SIDE

ISOMETRIC



Figure 3.1.3.12

Simulation summary

The upright simulation is simulated with a remote force applied to the axle attachment hole, from the front (left) wheel contact point with the ground, a force applied to bottom control arm attachment hole and cylindrical support applied to the top control arm attachment hole with all degrees of freedom locked (See the following diagram). The table below lists the key simulation results.

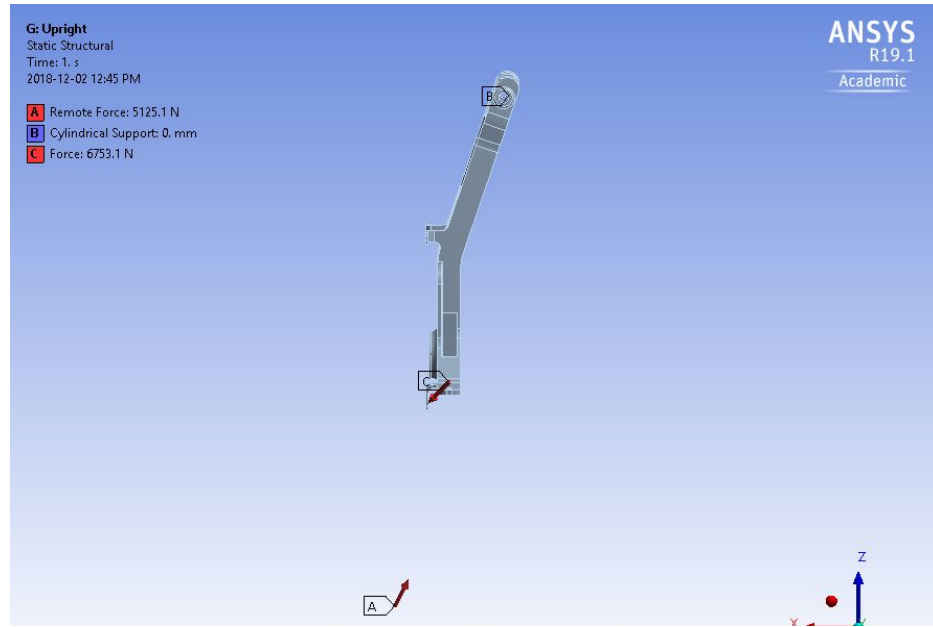


Figure 3.1.3.13

Table 3.1.3.3 Simulation results: Upright (Left) Simulation Summary

Case	Safety Factor	Stress (MPa)	Deformation (mm)
2,1,1	1.7601	0.846	109.68
2,0,1	2.2724	84.956	0.7353
6,0,0	1.7995	107.28	1.692

Please refer to the Appendix for more information.

3.1.4. Rigid Dynamics

Bump/droop and steering cases are examined in using ANSYS Rigid Dynamics to optimize front suspension geometry and prevent clashing in dynamic conditions. Issues mainly occur around axle, upright, bottom control arm and bottom shock clevis. These issues have been addressed based on the simulation results. Refer to the Appendix for more information.

3.2. Rear Suspension

3.2.1. 2D Rear Suspension

The suspension is designed for 2" of travel in each of bump and droop.

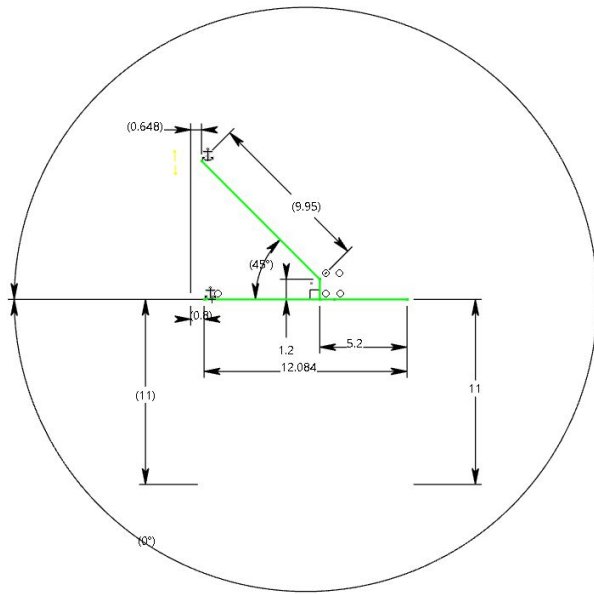


Figure 3.2.1.1 Neutral

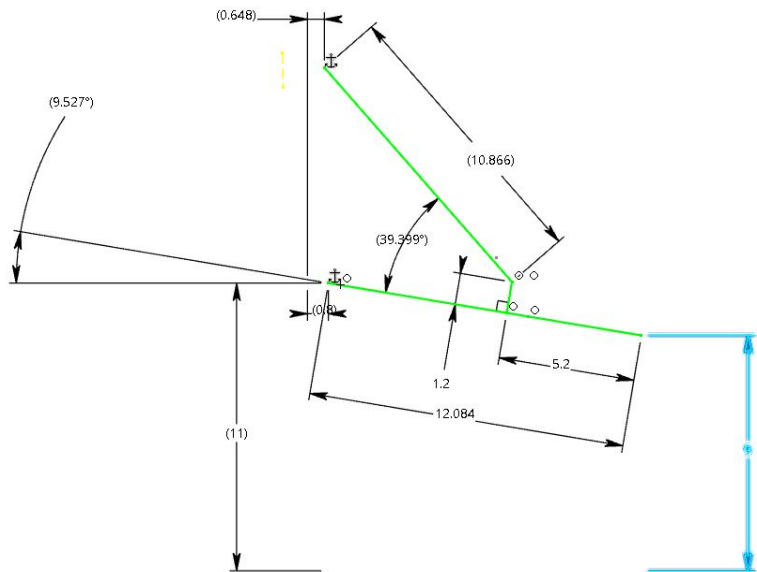


Figure 3.2.1.2 Bump

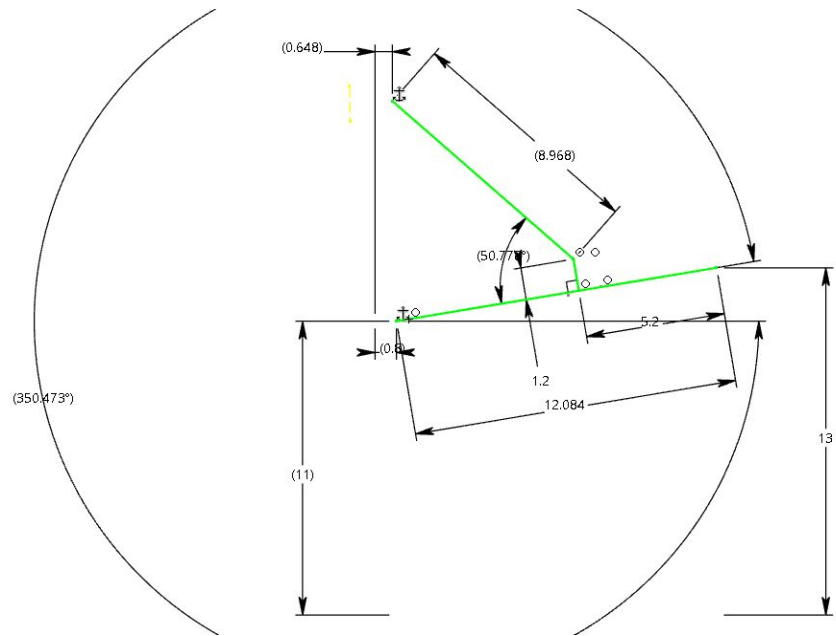


Figure 3.2.1.3 Droop

3.2.2. Force Calculations

The forces experienced by the suspension and transmitted to the chassis were determined using the 2D model as well. The diagram below shows the forces at the tire patch where N is the bump force, F_t is the turning force, and F_b is the braking force.

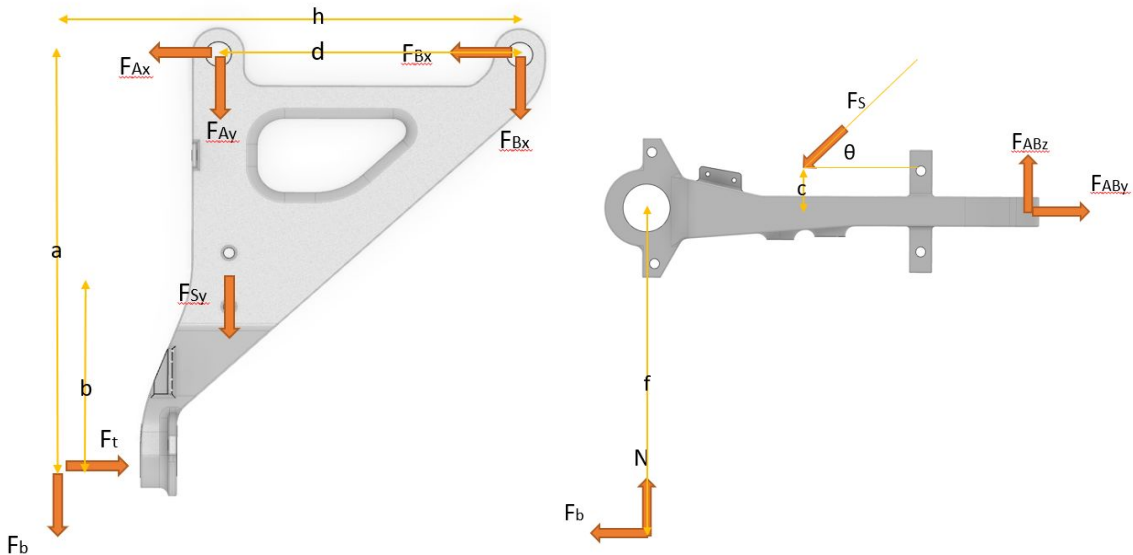


Figure 3.2.2.1 FBD of Trailing Arm (Left)

Based on the FBD, we built the system of equations based on the balance of force and moment.

$$\begin{aligned}\Sigma F &= \begin{pmatrix} F_{Ax} + F_{Bx} + F_t \\ F_{Ay} + F_{By} + F_b \\ F_{Az} + F_{Bz} + N \end{pmatrix} = \begin{pmatrix} 0 \\ 0 \\ 0 \end{pmatrix} \\ \Sigma M_B &= r_A \vec{F}_A + r_S \vec{F}_S + r_0 \vec{F}_0 = \begin{pmatrix} d \\ 0 \\ 0 \end{pmatrix} \begin{pmatrix} F_{Ax} \\ F_{Ay} \\ F_{Az} \end{pmatrix} + \begin{pmatrix} d \\ a-b \\ c \end{pmatrix} \begin{pmatrix} 0 \\ F_S \cos \theta \\ F_S \sin \theta \end{pmatrix} + \begin{pmatrix} h \\ a \\ -f \end{pmatrix} \begin{pmatrix} F_t \\ F_b \\ N \end{pmatrix} \\ &= \begin{pmatrix} 0 \\ -dF_{Az} \\ dF_{Ay} \end{pmatrix} + \begin{pmatrix} -(a-b)F_S \sin \theta - cF_S \cos \theta \\ dF_S \sin \theta \\ dF_S \cos \theta \end{pmatrix} + \begin{pmatrix} aN + fF_b \\ -fF_t - hN \\ hF_b - aF_t \end{pmatrix}\end{aligned}$$

We will notice that F_{Ax} and F_{Bx} end up indeterminate. Here, we assume they are equal. Therefore, we will have the following expressions for each force:

$$F_{Ax} = \frac{1}{2} F_t$$

$$F_{Ay} = \frac{-hF_b + aF_t - d\cos \theta F_s}{d}$$

$$F_{Az} = \frac{-d\sin \theta F_s + fF_t + hN}{d}$$

$$F_{Bx} = \frac{1}{2} F_t$$

$$F_{By} = -F_b - F_s \cos \theta - F_{Ay}$$

$$F_{Bz} = -N + F_S \sin \theta - F_{Az}$$

$$F_S = \frac{aN + fF_b}{(a-b)\sin \theta + c\cos \theta}$$

Similarly, we can get the expressions for the right side:

$$\begin{aligned}
F_{Ax} &= -\frac{1}{2}F_t \\
F_{Ay} &= -F_b - F_s \cos\theta - F_{By} \\
F_{Az} &= -N + F_s \sin\theta - F_{Az} \\
F_{Bx} &= -\frac{1}{2}F_t \\
F_{By} &= \frac{-hF_b + aF_t + d\cos\theta F_s}{d} \\
F_{Bz} &= \frac{d\sin\theta F_s + fF_t - hN}{d} \\
F_s &= \frac{aN + fF_b}{(a - b)\sin\theta + c\cos\theta}
\end{aligned}$$

3.2.3. 3D Rear Suspension:

- **Trailing Arm**

Description

The Trailing Arm connects to the rear of the chassis through HAB 6T through high misalignment spherical bearing. It also provides support to rear brakes and inner fairing. The rear left and right trailing arm are asymmetric due to the motor on the rear right. Therefore, the left side connects to the wheel through the axle attachment hole while the rear right will be attached directly to the motor using the screws. A shock and spring is attached to the arm through a bolt-on clevis, in a similar way as the front suspension bottom control arms.

Materials + Manufacturing

- Main Body: Aluminum 355, casting
- Shock and spring clevis: Steel 4310, welding
- HAB-6T Spherical Bearing with 23 degrees misalignment

Diagrams

- **Rear Left Trailing Arm**

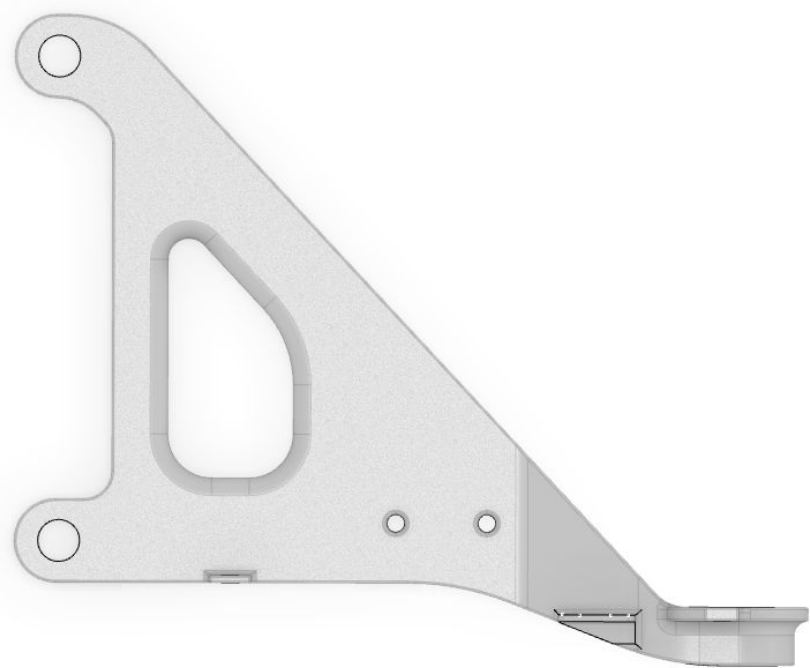


Figure 3.2.2.1 Top View

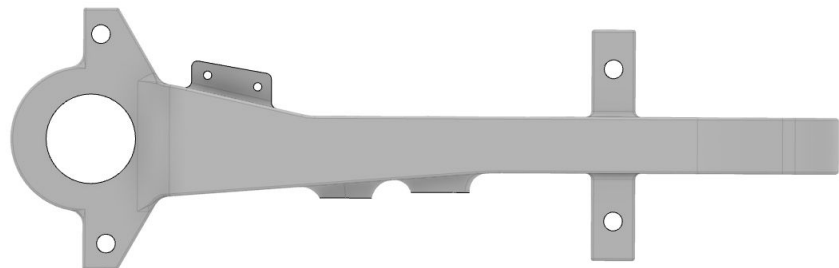


Figure 3.2.2.2 Side View

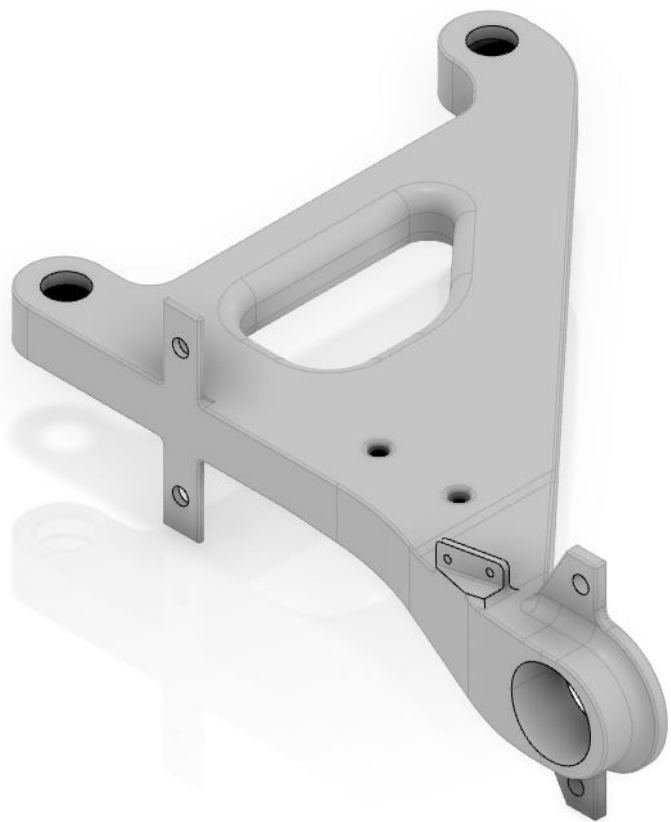


Figure 3.2.2.3 Spherical Bearing Interference

- **Rear Right Trailing Arm**



Figure 3.2.2.4 Top View

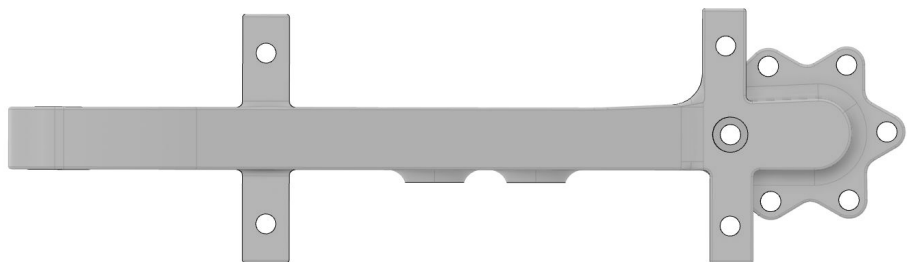


Figure 3.2.2.5 Side View

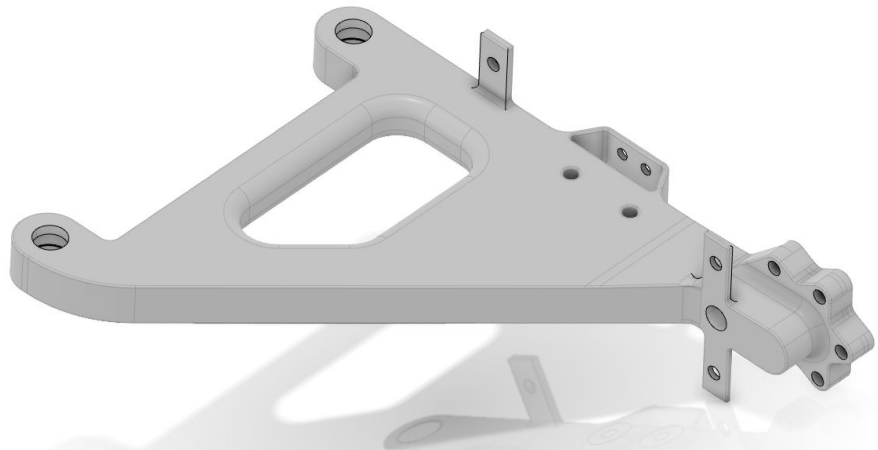


Figure 3.2.2.6 ISO View

Simulation summary

The rear left trailing arm simulation set consists of two forces at ball bearing holes, a remote force from where the wheel contacts the ground and a remote displacement applied at the center of bottom shock clevis holes, with all six degree of freedom locked (See the following diagrams). The remote displacement is applied to the projection of the clevis, half of the screw holes in the direction of shock applied force and the bottom surface where the nut will be bolted to. The reaction force at the remote displacement is checked against the hand-calculated force exerted by the shock, and the two forces match up with a minor discrepancy. Table 3.1.3.3 lists the key simulation results.

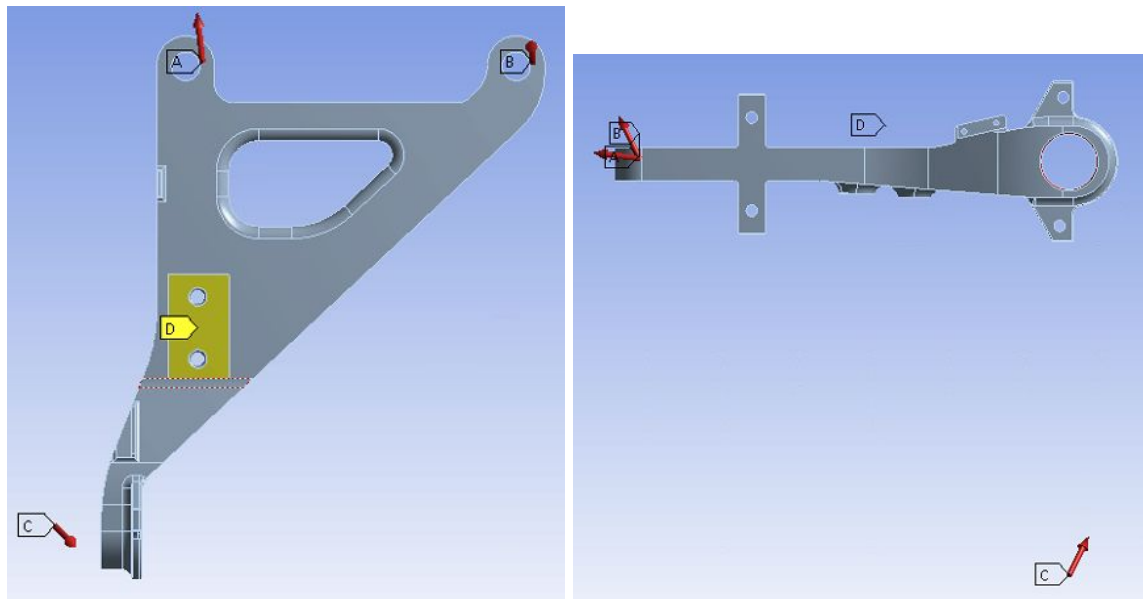


Figure 3.2.2.7 Rear Left Trailing Arm simulation Setup

Table 3.2.3.1 Rear Left

Case	Safety Factor	Stress (MPa)	Deformation (mm)
(2,1,1)	1.90	101.4	2.34
(2,0,1)	1.58	122.1	1.46
(6,0,0)	1.46	132.5	1.72

Please refer to the Appendix for more information.

The rear right is setup in a similar manner except that due to the motor, the axle attachment hole is replaced by a flower-shaped adapter bolted onto the motor as the motor specification required. Therefore, the remote force is applied at a same location but to the six screw holes and the adapter surface pressing against the motor (See the following diagrams). Refer to Table 3.1.3.3 for key simulation results.

Figure 3.2.2.8 Rear Right Trailing Arm Simulation Setup

Case	Safety Factor	Stress (MPa)	Deformation (mm)
(2,1,-1)	1.77	109.0	0.59
(2,0,-1)	1.45	122.05	1.46
(6,0,0)	2.56	132.5	1.72

3.3. Fatigue Analysis

As many of the suspension components are made of Aluminum, specifically Aluminum C355, fatigue analysis was performed to ensure the components do not fail under cyclic loading. A stress-life analysis was chosen to analyse the high cycle fatigue regime. Aluminum like other metals dulls the initiated crack (cause of fatigue failure) which makes it more difficult to fail. This is unlike ceramics and other brittle material.

The aluminum C355 used is heat treated to T6 specifications. This process increases the strength of the material by as much as 30%. The alloy is heated to 500 degrees, quenched and aged which causes a crystalline structure to form which increase the strength of the alloy. Therefore the material properties of the C355 greatly increase through this heat treatment process, as does the fatigue strength of the material.

Fatigue analysis often starts at cracks/stress concentrations. During regular static structural analysis, most stress concentration regions were eliminated therefore reducing the risk of fatigue failure.

A S-N (Stress vs number of cycles) graph was generated using a CES model. The detailed model can be found [here](#). This model is based on tensile load rather than fatigue condition due to the lack of available data. Fatigue data also displays large variations even when actual tests are performed.

530 CHAPTER 12 CYCLIC STRESS AND STRAIN FATIGUE

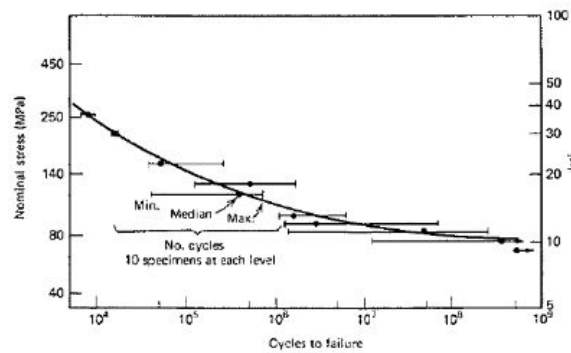


FIGURE 12.10 Constant load amplitude fatigue data for 7075-T6 aluminum alloy notched specimens (0.25-mm root radius).⁶ (Reprinted from Hardrath et al., NASA TN D-210.)

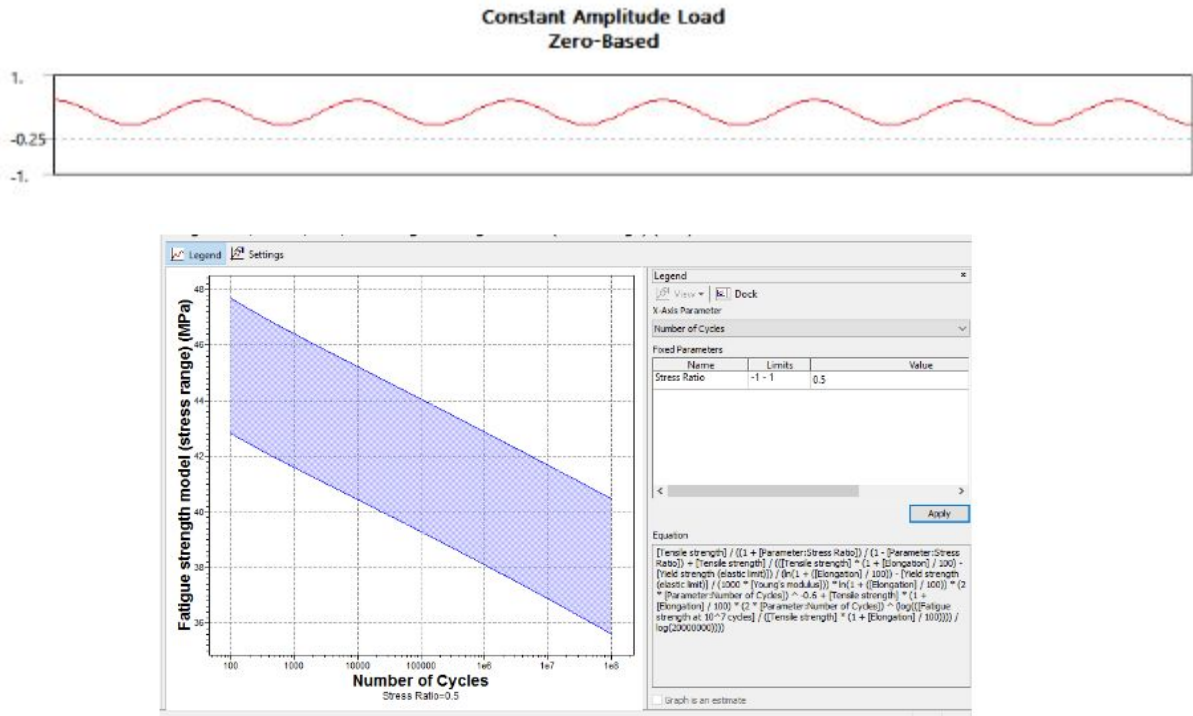
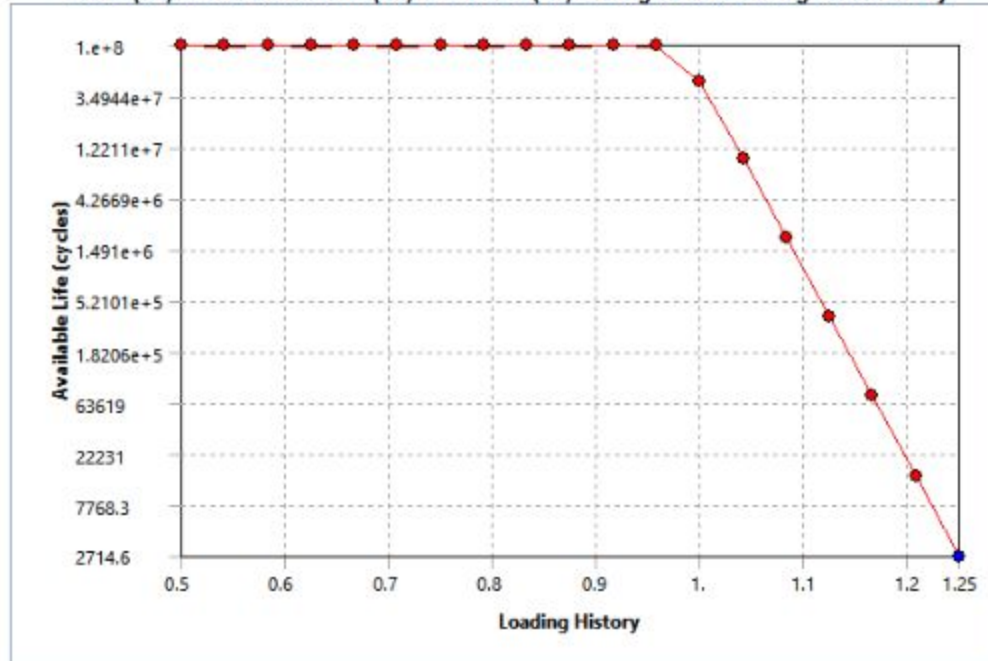


FIGURE 15
 Model (A4) > Static Structural (A5) > Solution (A6) > Fatigue Tool > Fatigue Sensitivity



A dramatic drop in available cycles occurs by only increasing the load factor by 10%-20%. Conversely, slight improvement on the design can dramatically improve fatigue life. For future analysis, the following improvements will be made to the model:

- Fatigue scale factor K_f , based on Surface finishing etc. to be inputted into Ansys
- Generate a MATLAB code based on the Coffin-Manson model, modify the calculation so it is based on Gerber instead of Goodman criteria.
- Introduce variable load cycles.

3.4. Shock and Springs

The front and rear suspension have been designed to house a shock and spring system with the properties shown in Table X and Table X. A Cane Creek DBcoil IL will be used on all wheels; it is shown in Figure X.



Figure 3.3.1 Shock and Spring combo

Table 3.3.1: Front Shock and Spring

Parameter	Value	Units
Extended Shock Length	9.02	in
Neutral Shock Length	8.19	in
Compressed Shock Length	6.81	in
Shock Travel	2.29	in
Bump Suspension Travel	2	in
Droop Suspension Travel	2	in
Wheel Frequency	2.21	Hz
Installation Ratio	3.08	/
Spring Rate	172	lb/in
Spring Preload	158	lb

Table 3.3.2: Rear Shock and Spring

Parameter	Value	Units
Extended Shock Length	10.87	in
Neutral Shock Length	9.95	in
Compressed Shock Length	8.968	in
Shock Travel	1.90	in

Bump Suspension Travel	2	in
Droop Suspension Travel	2	in
Wheel Frequency	2.45	Hz
Installation Ratio	4.34	/
Spring Rate	226	lb/in
Spring Preload	206	lb

The goal of spring calculation is to ensure a good pair of extended shock length and shock travel when the car undergoes 2 inches of bump and droop (4 inches in total), at the same time, as a part of the team constraint, the spring will have a preload larger than 50lb. This calculation is only done for the left wheels because the car is symmetric about the y-axis and the geometry which may influence the shock performance are the same for front and rear respectively.

Using the 2D geometry in CATIA we can acquire the shock length at extended, neutral and bump state, and calculate the shock travel as the extended length minus the bump length.

For each wheel, the sprung weight is calculated based on the weight distribution. Then we find the value of wheel rate using the formula

$$\omega = \frac{1}{2\pi} \sqrt{\frac{K_w \cdot 12.32.2}{W}}$$

where ω (Hz) is the natural frequency, K_w (lb/in) is the wheel rate and W (lb) is the sprung weight on each wheel.

Also using the 2D geometry in CATIA, we calculate the installation ratio using the following formula

$$IR = \frac{\Delta Z}{\Delta S}$$

where ΔZ is a very small wheel displacement in z-axis and ΔS is the corresponding decrease in spring length.

The spring rate follows the formula

$$K_s = K_w \cdot IR^2$$

Minimal spring length follows the formula

$$L_{s \min} = \frac{W \cdot IR}{K_s} + L_{s \text{ neutral}} - L_{s \text{ bump}}$$

where $L_{s \text{ neutral}}$ and $L_{s \text{ bump}}$ are the length of the spring at neutral and bump states. Another safety factor of 0.375 in is added to this value when choosing spring products.

3.5. Steering

The steering system of Viridian is a parallel steering mechanism that utilizes a Rack and pinion to turn the wheels. The amount of steering needed is based on the figure 8 course of WSC as it is the smallest turn radius that the car has to navigate. A simplified formula was used to determine the steering angle needed:

$$\text{Steering angle } (\alpha) = [(W/R) * (180/\pi)] + 5^\circ$$

Where W = wheelbase (1.727m), R = turn radius (6.5m), and 5 is an additional 5 degrees of safety factor added to the value. A steering angle of 20.2 degrees is therefore calculated and used.

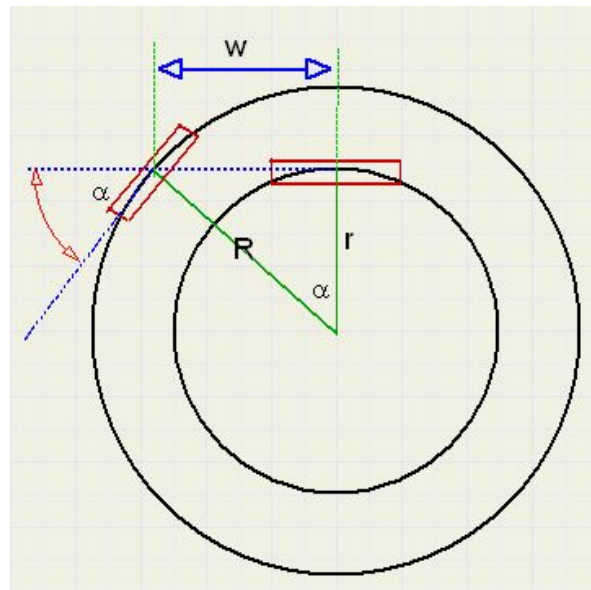


Figure 3.4.1 Steering angle diagram

The steering system is comprised of the following components:

- Steering wheel
- Steering wheel shaft: 0.75" OD 0.065" ID 4130 Steel tube
- Two bolt flange bearing
- Base mounted bearing
- Collapsible steering shaft
- 2 U-joints
- Rack and Pinion
- Custom made tie rods

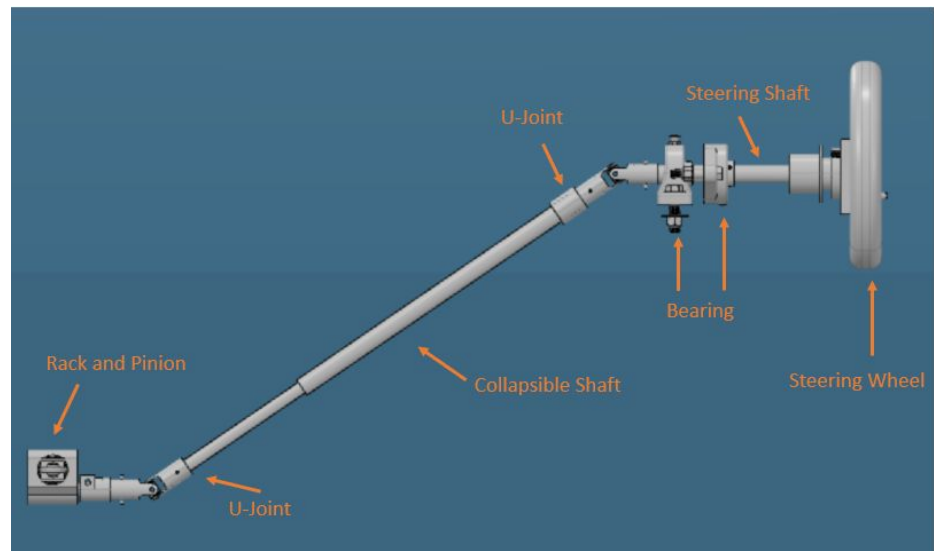


Figure 3.4.2 Steering Components



Figure 3.4.3

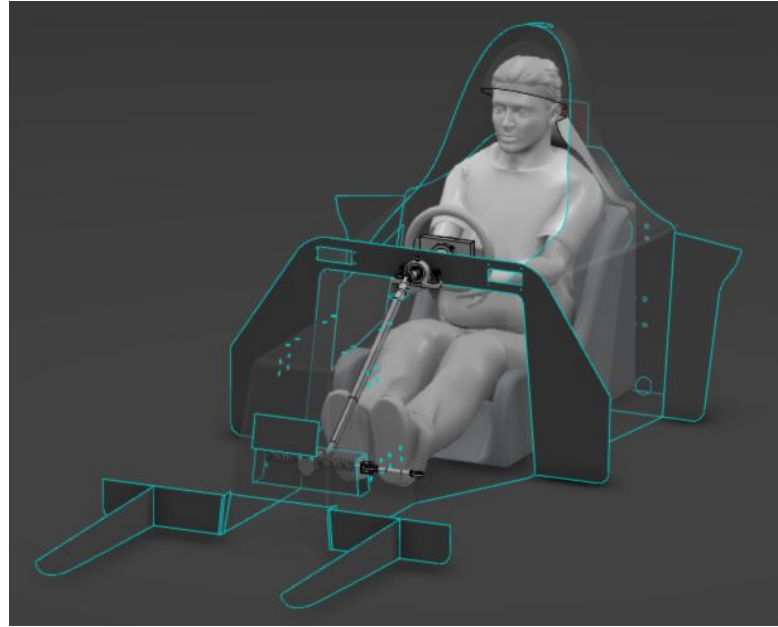


Figure 3.4.4

A more detailed explanation on the critical components is given below.

- **Rack and Pinion**

A 20:1 rack and pinion with an original length of 11.25" will be modified to have a length of 12.8" by welding additional pieces of steel to either side. This is done in order to achieve a steering ratio of 15:1, meaning that every 15 degrees of rotation in the steering wheel results in 1 degree of wheel rotation. The following formulas are used to calculate the steering ratio:

$$\text{Steering Ratio} = 1 / \arcsin \left(\frac{c\text{-factor}}{\text{arm length}} \right) / 360$$

$$c\text{-factor} = \text{rack travel} / \text{pinion rotation}$$

The c-factor of the rack remains constant at 1.68 as the rack travel and pinion rotation increase proportionally. The modified rack will also ensure a minimal bump steer is experienced, as explained in the 2D suspension section. The length of the steering arm will be 4.32" to achieve the ratio as well.



Figure 3.4.5 Rack and Pinion

Using these values, a steering ratio of 15.72 will be achieved, which is very close to the desired 15:1 ratio. This steering ratio is believed to give the driver the ability to complete a figure 8 course without difficulty, and will ensure the steering system is stable enough when driving on a straight course to prevent driver fatigue.

- **Collapsible Shaft**

A collapsible steering shaft with an extended length of 27" and a collapsed length of 21" is used. This will ensure that in case of a frontal collision, the collapsible shaft will absorb some of the impact and the steering shaft/wheel will not pierce through to the driver.



Figure 3.4.6 Collapsible Shaft

- **U-Joints**

Two military certified aerospace grade universal joints with misalignment angle of 35 degrees will be used to connect the steering components. The u-joint allows the rotation of the steering wheel to reach the rack and pinion which is installed at a lower height. It also acts as a safety component in case of a frontal collision. The u-joint will cause the steering shaft to rotate away from the driver in case of an accident, protecting him/her from any piercing (fig XXX)

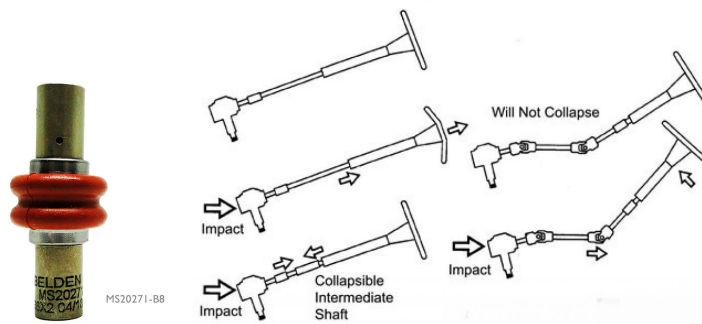


Figure 3.4.7 U-Joint and U-joint collapse

- **Bearings**

Sealed steel bearings with plastic housing are used to support the steering shaft. The plastic housing adds weight saving advantages while the steel bearing still provides the rigidity needed.

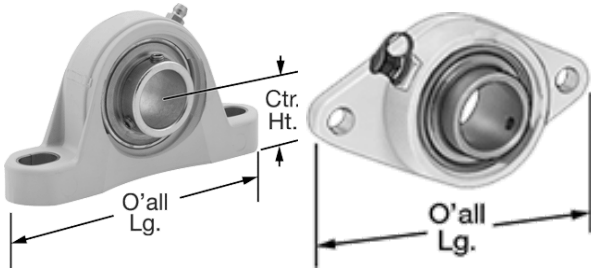


Figure 3.4.8 Plastic Housing bearings

- **Torsional Calculations**

Torsion of steering rods calculation: Ensuring the steering rod is able to handle 100 N.m of torque (based on benchmarks)

$$\tau = Tr/J$$

$$J \text{ for a hollow cylindrical shaft} = \pi(D^4 - d^4)/32$$

$$D = 3/4" = 0.019m \quad d = 0.62" = 0.0157m$$

$$J = 6.829 * 10^{-9} m^4$$

$$r = D/2 = 0.009525 m$$

$$T = 100 N.m$$

$$\pi = 139.48 MPa$$

$$F.O.S = 1.5 \Rightarrow \pi_{max} = 209.22 MPa$$

$$\text{Material used} = 4130 \text{ Steel with a } \sigma_{yield} = 435 MPa$$

$$\text{Using Von Mises Yield Criterion} \Rightarrow \tau_{yield} = 307.6 MPa$$

Therefore as $209.22 < 307.6$, the shaft passes the analysis

Shear calculations for rivets or spring pins used: Ensuring the rivets or spring pins used to connect the steering elements will not fail due to shear

$$T = 100 N.m \quad r = 0.01905 m$$

$$F = T/r = 5249.3 N \text{ with } F.O.S = 1.5 \Rightarrow 7873.9 N$$

A spring pin goes through the entire tube therefore the tensile force is divided into two areas :

$$7873.9 / 2 = 3936.975 N$$

$$\text{Shear Strength of spring pins used (420 steel)} = 1,400 \text{ lbs.} = 6227.51 N$$

Therefore $3936.975 < 6227.51$ so one spring pin is enough

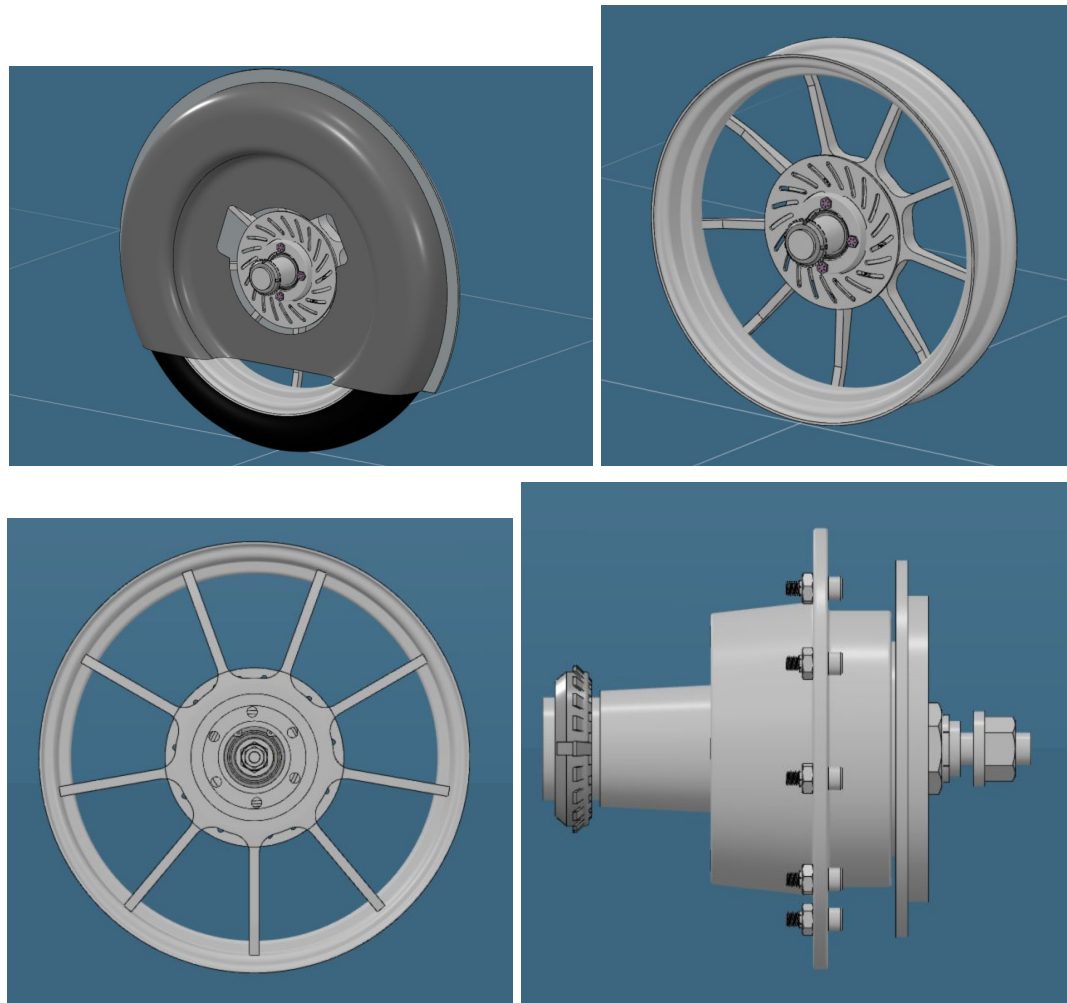
A rivet experiences the full tensile force.

$$\text{Shear Strength of rivets used (5/32" steel rivets)} = 370 \text{ lbs.} = 1645.84 N$$

$$7873.9 / 1645.84 \approx 5 \text{ Therefore 5 rivets are needed}$$

3.6. Wheel System

The wheel system is hub centric and consists of the hub, axle, and inner fairing.



The loads on each wheel were calculated by the following equation

Assuming weight of vehicle = 300kg, using 6 given load conditions for bump, brake, turn

$$(300\text{kg})(9.81\text{m/s}^2)(G)(\%\text{ of load on wheel})$$

The worst case scenarios were the following:

Table 3.5.1 Forces for each case

Bump (Gs)	Brake (Gs)	Turn (Gs)	Brake (N)	Turn (N)	Normal (N)
6	0	0	0	0	5000
2	1	-1	2122	2123	4246

- Hub

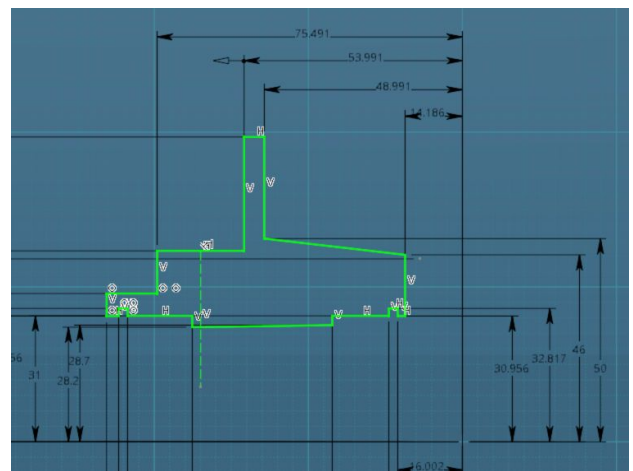
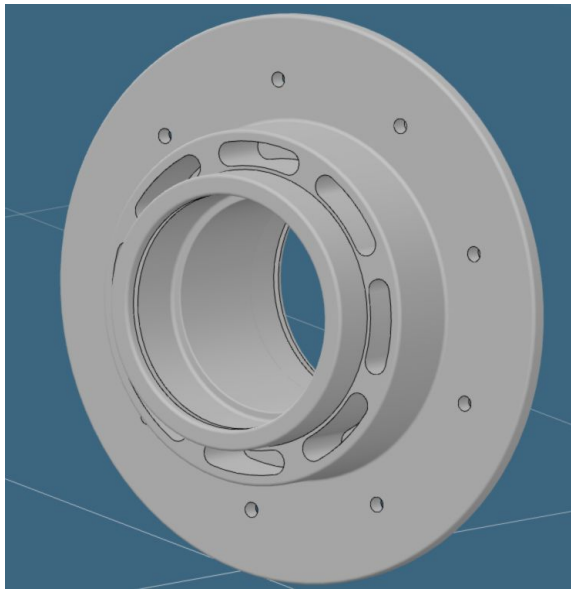
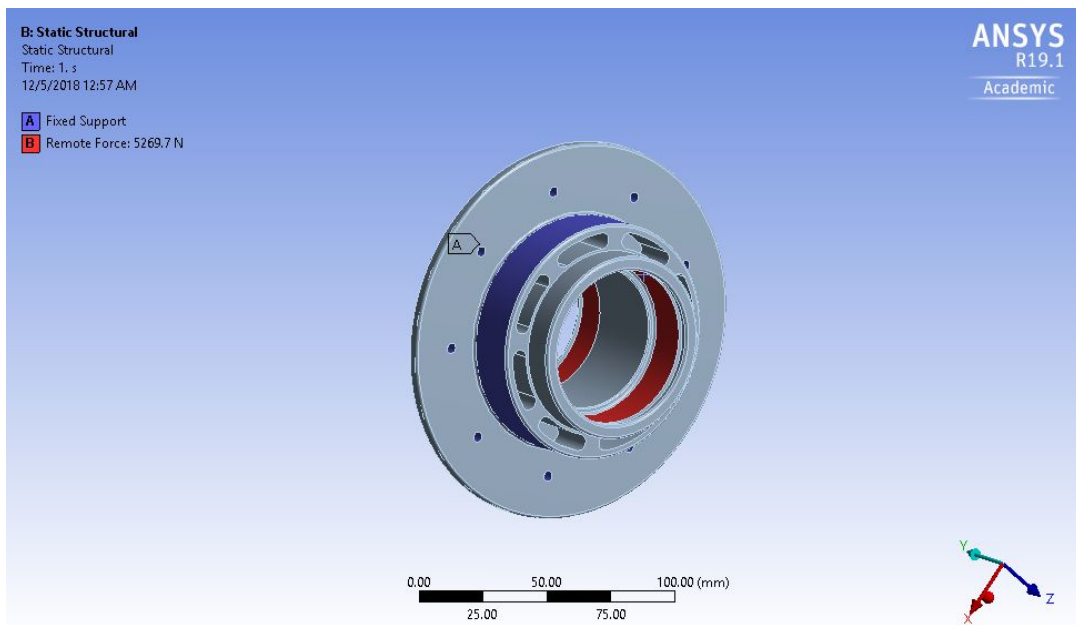


Figure 3.5.1 Hub 3D and 2D

Simulation Summary



Case	Safety Factor	Stress (MPa)	Deformation (mm)
2,1,-1	12.075	41.658	0.006266

- **Axle**

The axle will be machine out of 4340 steel. It will consist of two bearings and will be fitted into the upright by the tapered section.

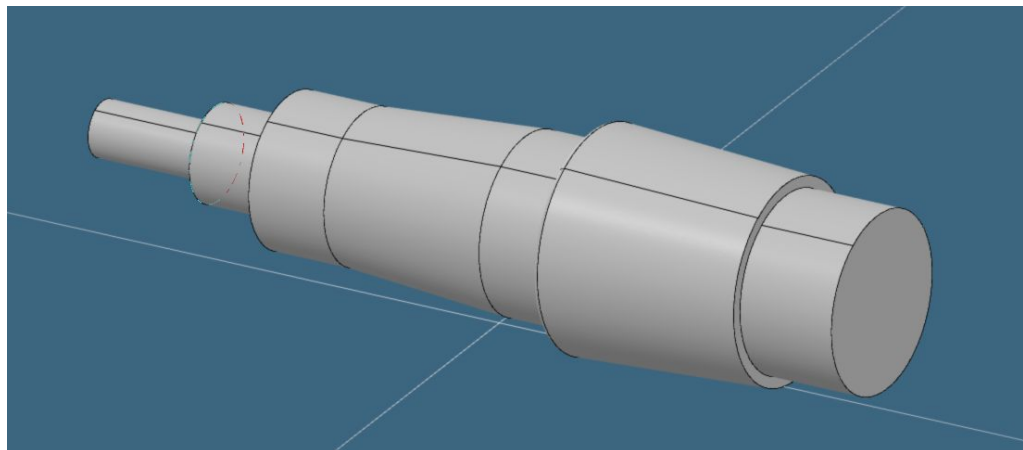


Figure 3.5.2 Axle 3D

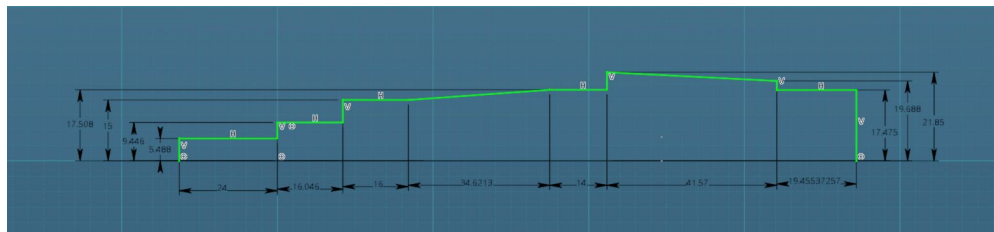
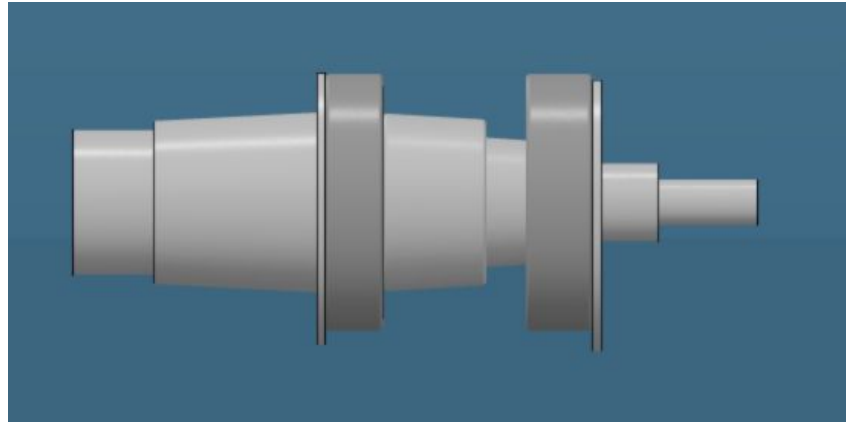


Figure 3.5.3 Axle 2D Sketch



Simulation Summary

The diagram below shows the forces acting on the axle

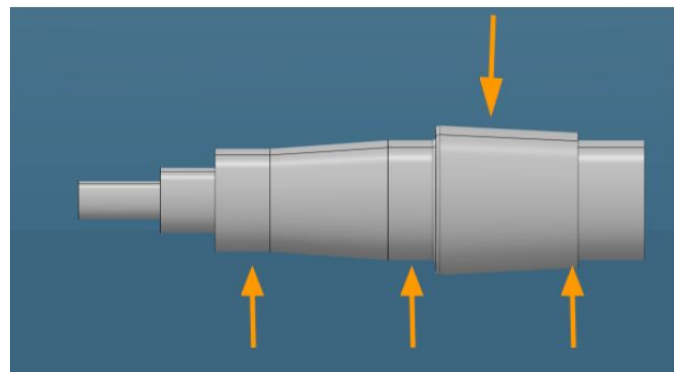


Figure 3.5.4 Forces on Axle

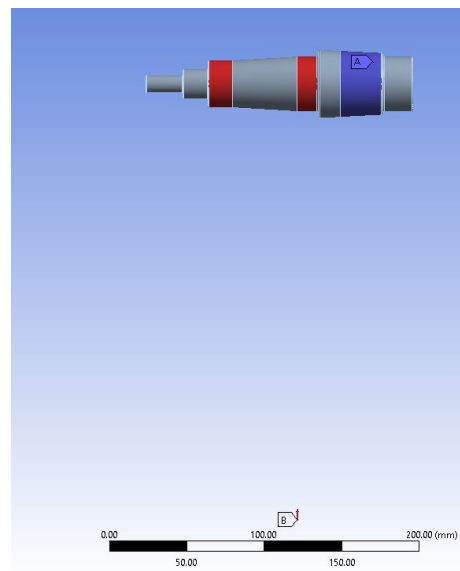


Figure 3.5.5 Remote Force

Table 3.5.1 Forces for each case Axle Simulation Summary

Case	Safety Factor	Stress (MPa)	Deformation (mm)
2,1,-1	1.5035	472.22	0.18252
6,0,0	3.1091	228.36	0.018052

- **Inner Fairing**

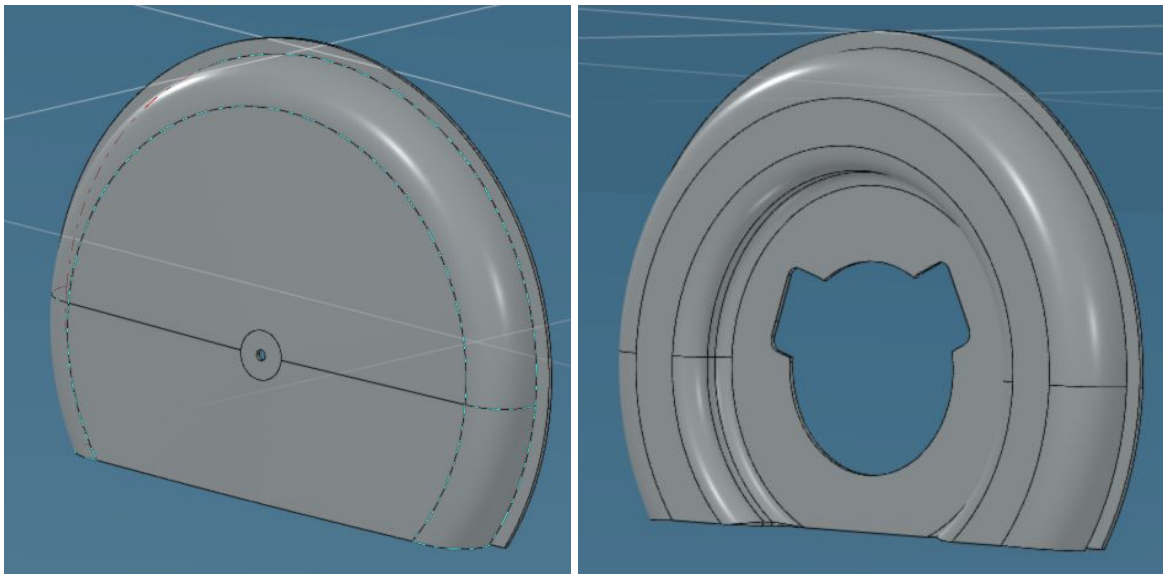


Figure 3.5.6 Outer Fairing and Inner Fairing

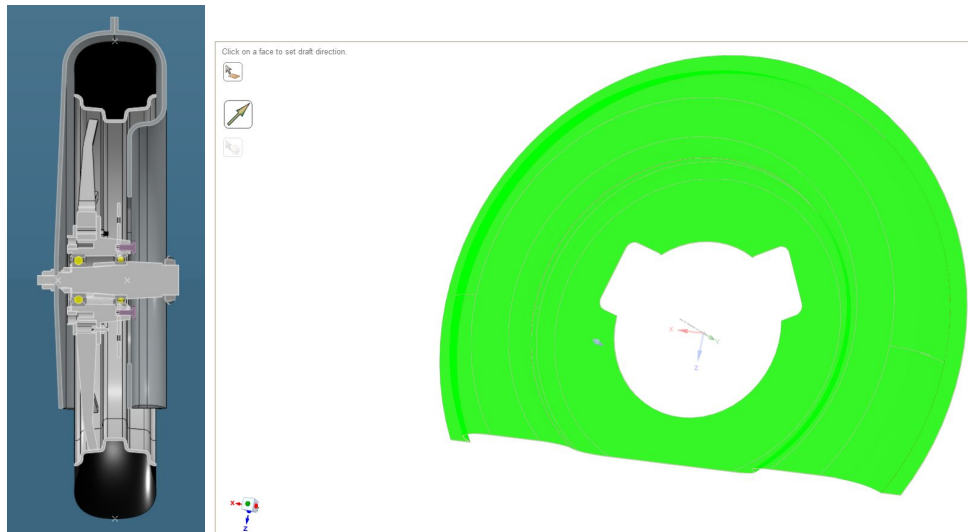


Figure 3.5.7 Draft Analysis

3.7. Brakes

The WSC regulations state that the solar car must have a primary and secondary brake systems that operate independently. The primary system must operate on all four wheels while the secondary is only applied to one pair of wheels (the front wheels). This is due to the fact that as the car brakes, the weight of the vehicle is shifted forward causing the front tires to take more load and therefore require more force to stop. The primary system is also adjusted such that more of the braking pressure is distributed to the front wheels.

The brake system is consisted of the following components:

- Brake Calipers and pad assembly
- Brake Disc
- Master Cylinders
- Brake Hoses
- Proportioning Valve
- Brake Pedal

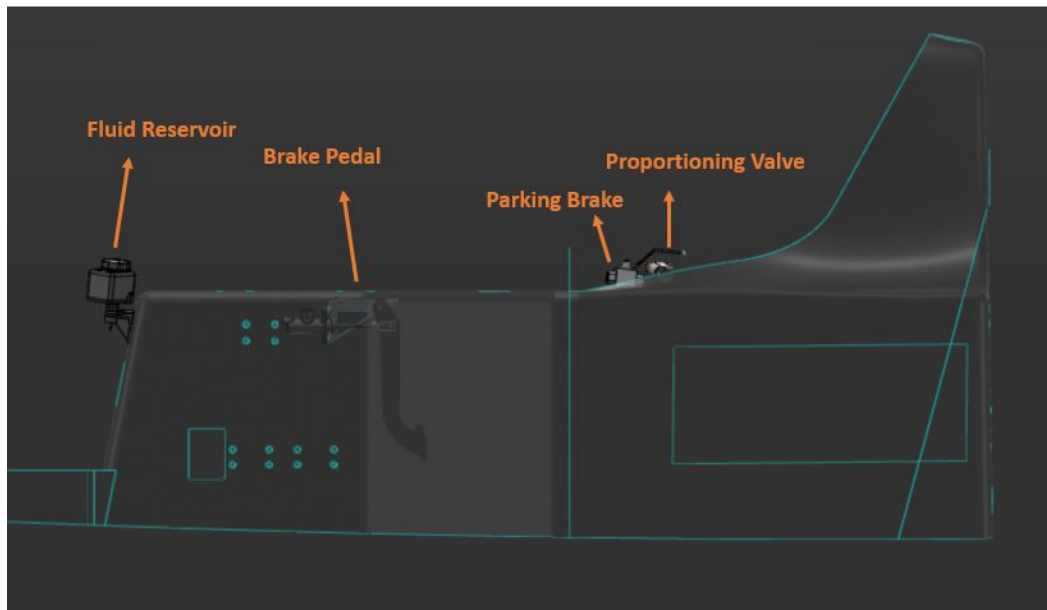


Figure 3.6.1 Brake Components

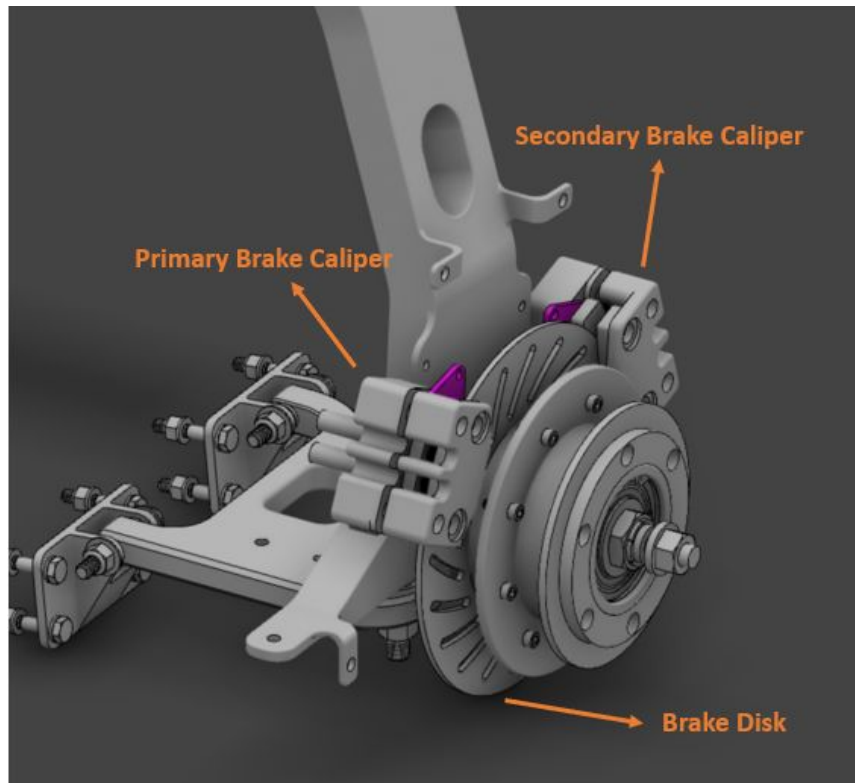


Figure 3.6.2 Front Brake Components

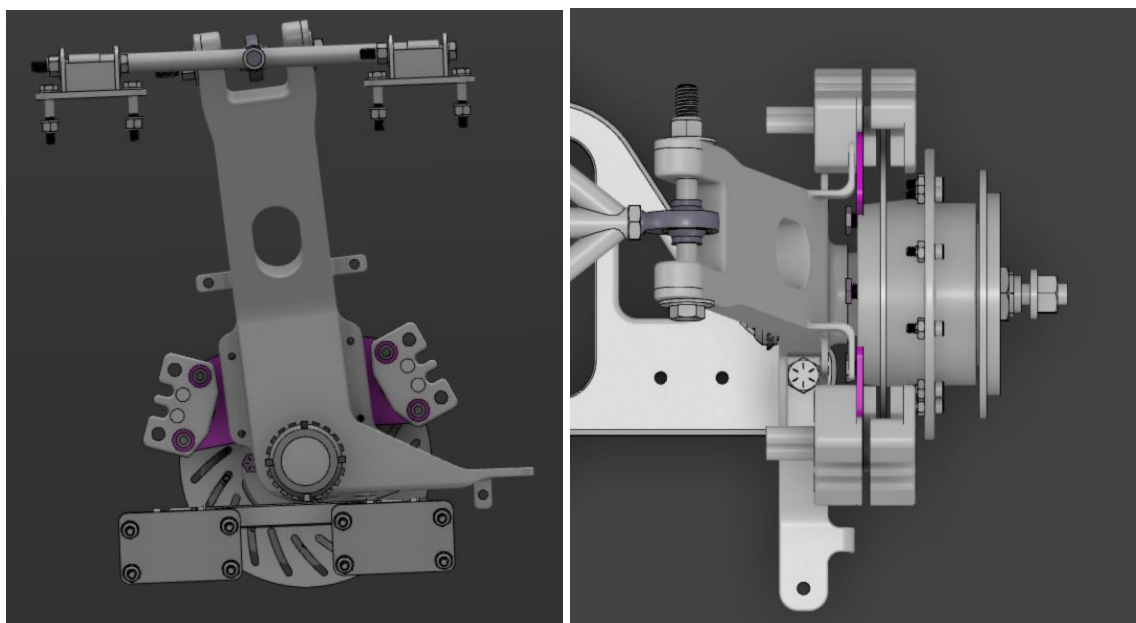


Figure 3.6.3 Brake Components

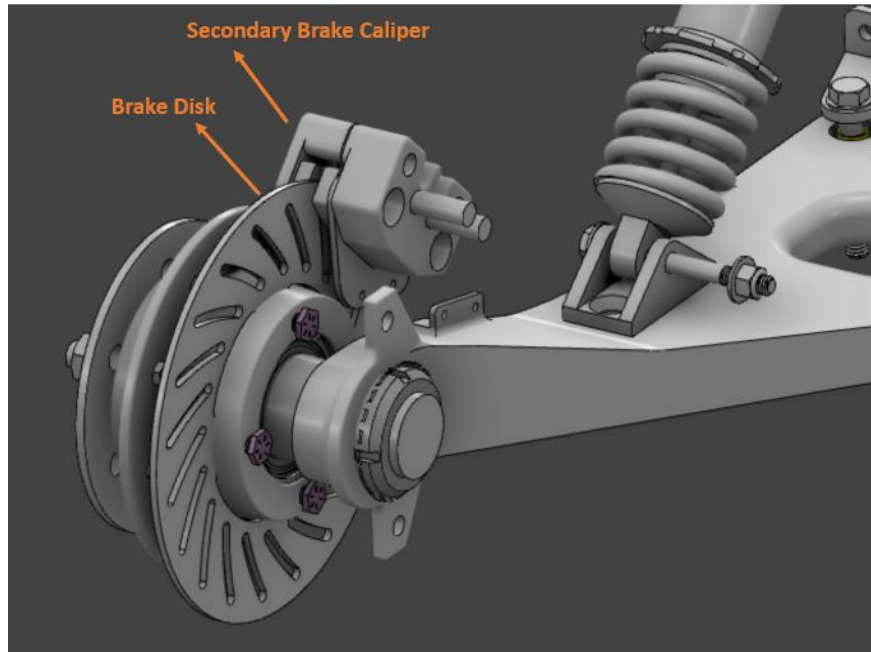


Figure 3.6.4 Rear Left Brake Components

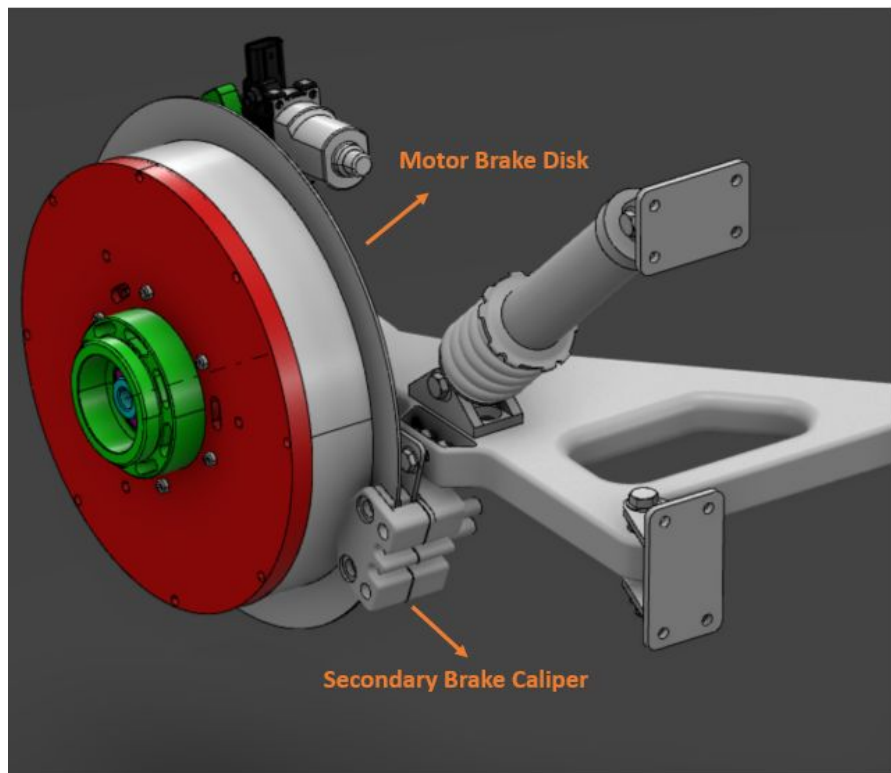


Figure 3.6.5 Motor Brake Components

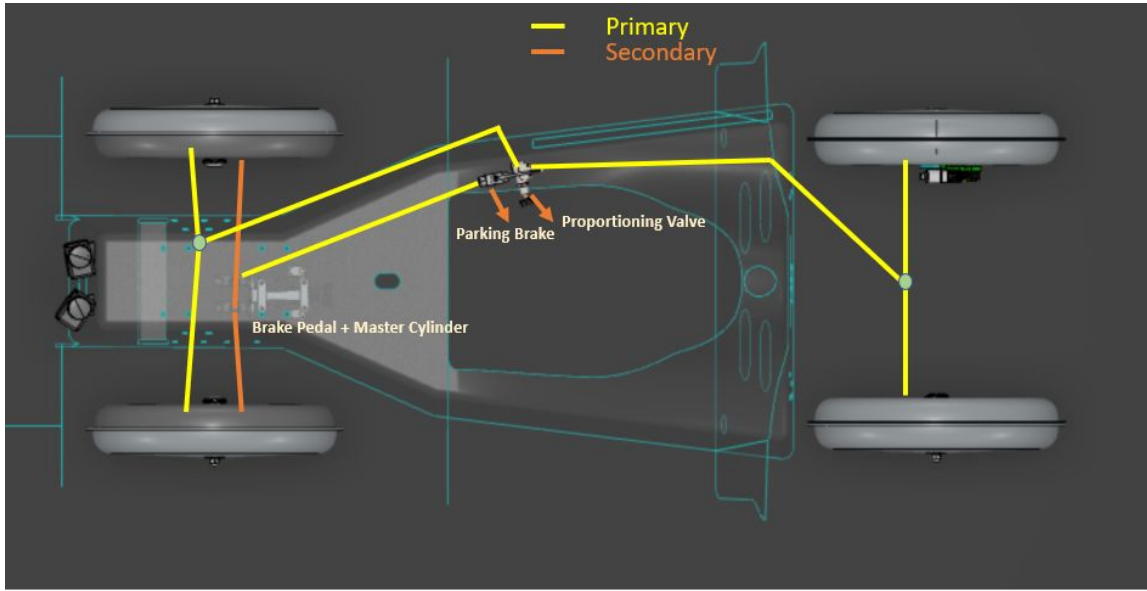


Figure 3.6.6 Brake Hose Layout

Preliminary Brake Calculations

Pressure: Calculating the pressure required to operate the brake systems

$$p = F * \frac{r_{tire}}{\#calipers * A_c * \mu_{pad}}$$

$$R_{pedal} = p * \frac{A_{mc}}{F_{foot}}$$

$$F_{foot} = p * \frac{A_{mc}}{R_{pedal}}$$

Where:

$$F = 1G = 661.4 \text{ lbs} \quad r_{tire} = 11" \quad r_{brake disc} = 3.55"$$

$$A_c = \text{Area of calipers} = (1"/2)^2 * \pi = 0.785 \text{ inch}^2$$

$$\mu_{pad} = \text{coefficient of friction of brake pads} = 0.3$$

$$R_{pedal} = \text{pedal to foot ratio} = 7$$

$$A_{mc,1} = \text{Area of master cylinder} = (7/16)^2 * \pi = 0.6013 \text{ inch}^2$$

$$A_{mc,2} = (5/16)^2 * \pi = 0.3068 \text{ inch}^2$$

Primary System :

$$p_1 = 661.4 * \left(\frac{11}{4 * 0.785 * 0.3} \right) = 2175.51 \text{ psi}$$

$$F_{foot,1} = \frac{(2175.51 \text{ psi} * 0.6013 \text{ inch}^2)}{7} = 186.8 \text{ lbf}$$

Secondary :

$$p_2 = 661.4 * \left(\frac{11}{2 * 0.785 * 0.3} \right)^{\frac{1}{3.55}} = 4351.02 \text{ psi}$$

$$F_{foot,2} = (4351.02 \text{ psi} * 0.3068 \text{ inch}^2)/7 = 190.7 \text{ lbf}$$

Volume: Calculating the volume needed in the master cylinders to properly supply the calipers

$$V_{mc} = A_{mc} * \text{Piston Travel}$$

$$\text{Piston Travel} = 1.12"$$

$$V_{caliper} = (A_c * \text{Rotor Spacing} * 2) * 4$$

$$\text{Rotor Spacing} = 0.079" (2mm)$$

$$V_{mc,1} = 0.6013 * 1.12 = 0.673 \text{ inch}^3$$

$$V_{mc,2} = 0.3068 * 1.12 = 0.344 \text{ inch}^3$$

$$V_{caliper,1} = (0.785 * 0.079 * 2) * 4 = 0.496 \text{ inch}^3$$

$$V_{caliper,2} = (0.785 * 0.079 * 2) * 2 = 0.248 \text{ inch}^3$$

Therefore the safety factor for primary system = $\frac{0.673}{0.496} = 1.36$

Secondary system = $\frac{0.344}{0.248} = 1.38$

Parking Brake Calculation

Parking brake has to hold the solar car at a 20% incline/decline

$$\text{Force} = 1G * \text{Sin} (20) = 0.342 G$$

The parking brake is connected to the primary brake system which is designed for 1G of force based on the above calculations. Therefore the parking brake meets regulations

with a safety factor of $\frac{1}{0.342} = 2.9$

3.8. Connection Methods

Due to their weakness when experiencing bending loads, rod ends are only used in one location in the suspension, the top control arm. This is to allow adjustability when performing alignment on the car as the rod end allows changes to camber and caster. Other connections in the suspension are done using spherical bearings or bushings.

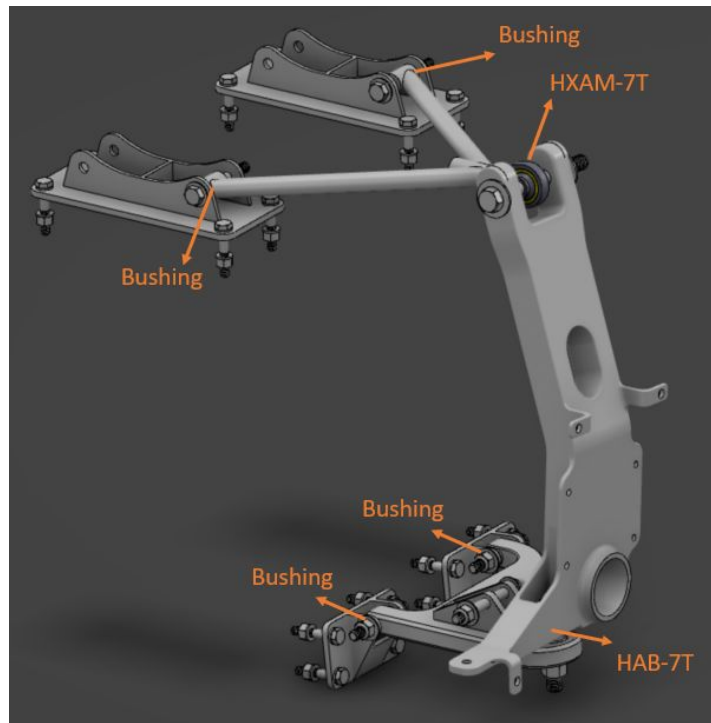


Figure 3.7.1 Chassis Connection Methods

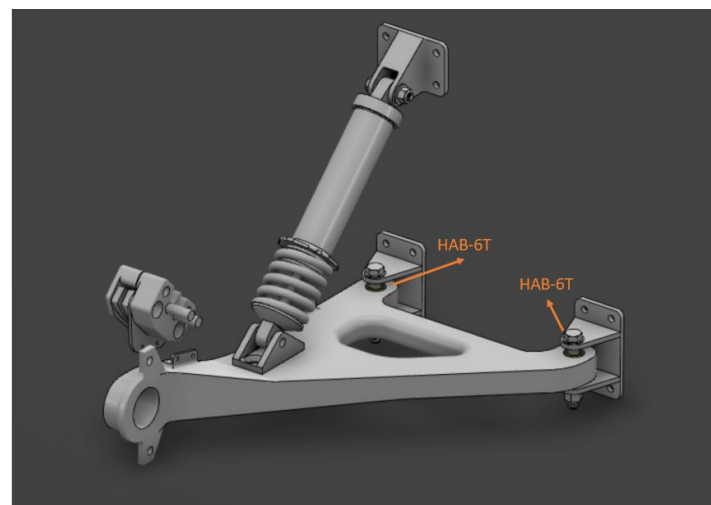


Figure 3.7.2 Bottom AARM connections

- **Bushings**

Bushings are currently manufactured in house using 4130 steel. They are press fit into the suspension arms and include an ear to keep them inside the hole. Other off the shelf plastic bushings are being researched and might replace these components in the future.

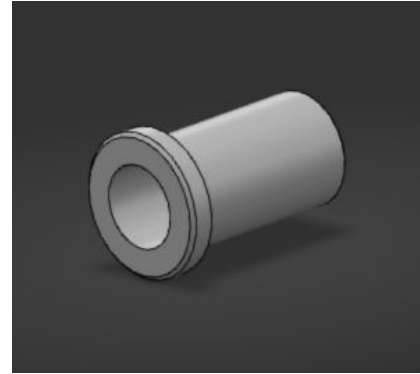


Figure 3.7.3 Steel Bushing

- **Rod Ends:**

The only rod end used is at the connection of the upright to the top arm. This rod end is a HXAM-7T high misalignment rod end with 21 degrees of available misalignment. The following procedure is followed to determine the size of the rod end:

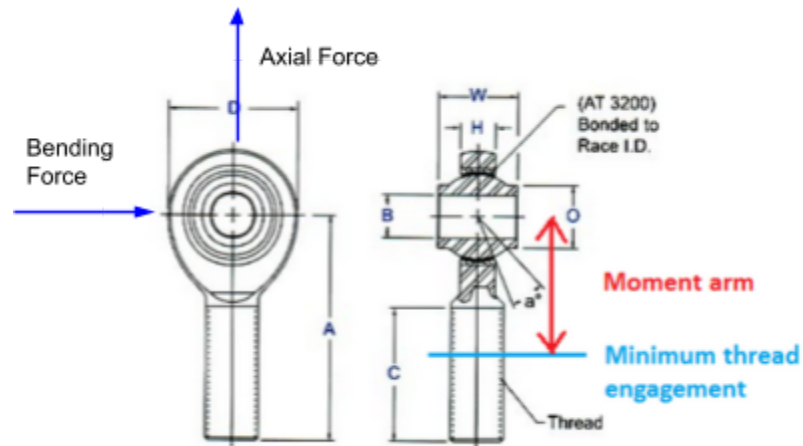


Figure 3.7.4 Rod End Diagram

$$\sigma = \frac{F}{A} + \frac{32M}{\pi d^3}$$

σ = Total Stress on the rod end

F_A = Axial Force

F_B = Bending Force

d = minor diameter

A = Area = $\pi * (\text{Minor diameter}/2)^2$

M = $F_B * \text{moment arm}$

Rod Ends are from Aurora Bearings company : 4340 Steel with Rockwell Hardness RC 39 – 42

Root radius of UNJ thread = 0.18

Corresponding stress concentration factor = 2.5

Corresponding yield strength = 102,000 psi = 703.265 MPa

Jam Nut width = 0.25"

Table 3.7.1 Calculations for HXAM-7T

Parameter	Value
F_A	969 N
F_B	2092 N
Minor Diameter	0.4387 " = 0.01114298 m
Tensile stress area	0.160 in ² = 1.0322 * 10 ⁻⁴ m ²
Moment arm	$A - C + \text{Jam Nut} = 1.22" = 31 \text{ mm} = 0.031 \text{ m}$
Moment	64.852 N.m
Bending Stress	477.44 MPa
Axial Stress	9.34 MPa
Total Stress	486.78 MPa
Safety Factor	486.78/312.56 = 1.44

Although the safety factor is slightly below 1.5, the assumptions in the calculations are that the force is being directly exposed to the threads, however in this setup the rod end is inserted all the way in the top AArm such that no threads are exposed.

- **Spherical Bearings:**

Calculations:

For spherical bearings, a radial load limit is provided by the manufacturer. The axial load limit is 20% of the radial load limit. Spherical Bearings are utilized for the connection of the bottom aarm to the upright, and the trailing arms to the rear clevises.

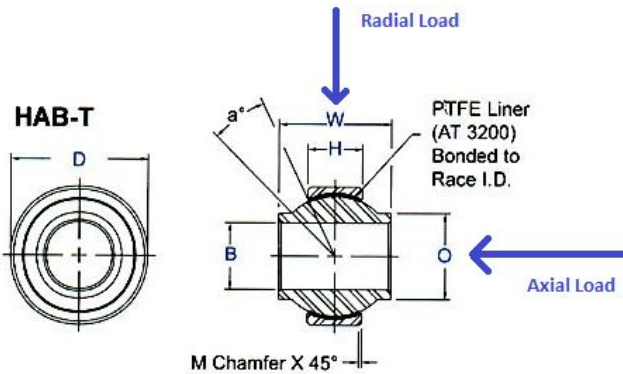


Figure 3.7.5 Rod End Diagram

Table 3.7.2 Calculations for HAB Bearings

Location	Bottom AARM	Trailing Arm
Bearing	HAB-7T	HAB-6T
Radial Load Capacity [N]	84,596.3	75,508.6
Max Radial Load Applied [N]	5,227.5	6391.6
Safety Factor	16.2	11.8
Axial Load Capacity [N]	16,919.3	15,101.7
Max Axial Load applied [N]	4999.37	2542.3
Safety Factor	3.38	5.94

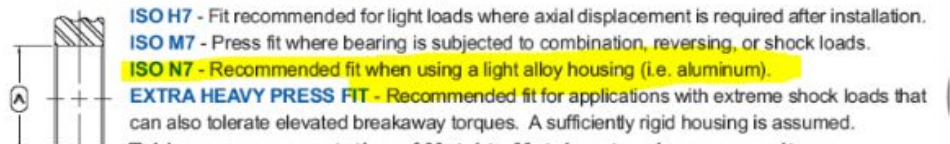
The safety factors are very high, however these size bearings were picked due to the bolt calculations done in the next section.

Installation:

The variables of the standard fit range and mechanical specifications of various bearing configurations along with other variables such as housing stiffness, make it very difficult to make standard recommendations for housing size for PTFE lined Bearings such as the HAB series. In actuality machining tolerances and economics often result in a wider housing size range. But research into bearing housing sizes yielded the following tolerance suggestions.

According to the ISO N7 standard, MIL-HDBK-1599A and the *“Department of Defense handbook: bearings, control system components, and associated hardware used in the design and construction of aerospace mechanical systems and subsystems”*, a tolerance of 13 micrometers is suggested when using a light alloy housing such as aluminum.

Suggested Housing Bores



Therefore the following housing dimensions are used:

- HAB 7-T in Bottom AARM:
 - Actual OD: 25.4 mm
 - OD of Housing: 25.387 mm
- HAB 6-T in Trailing Arm:
 - Actual OD: 23.012 mm
 - OD of Housing: 22.99 mm

A small chamfer on the entrance of the housing hole is included for ease of staking. See the following figure:

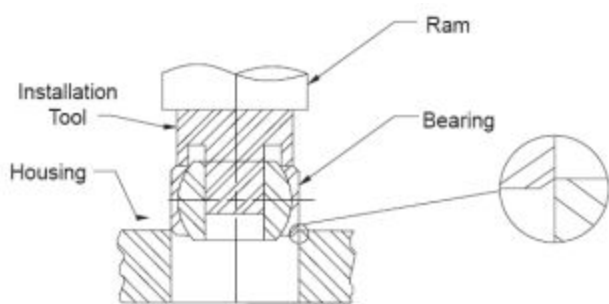


Figure 3.7.6 Chamfered Bearing Housing

For securing the bearing inside the housing, a shoulder is placed in the hole that the bearing is pushed against. A retaining ring in a groove is placed on the other side to secure the bearing and prevent it from exiting when axial load is applied.



Figure 3.7.7 Bearing Support

- **Bolts:**

Size/diameter of the bolts used when connecting the control arms to clevises was determined using shear/bending stress calculations.

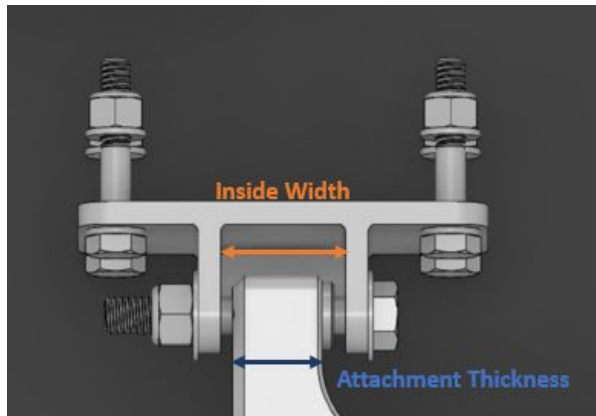


Figure 3.7.8 Bolt Dimensions

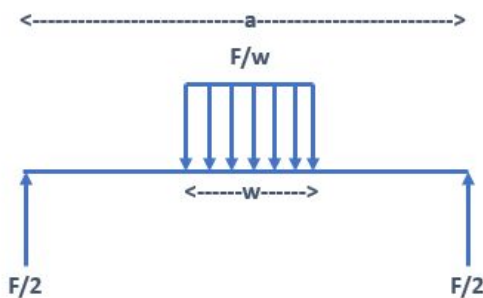


Figure 3.7.9 Bolt Forces

$$d = \sqrt[3]{\frac{32F(a/4 - w/8)}{574.53 * \pi}}$$

Where:

- D = diameter of the bolt
- A = inside width
- W = attachment thickness
- 574.53 MPa = 125,000 psi / 1.5 F.OS

A stress concentration factor of 2.0 was used to account for load applied on the threaded portion of the bolts. However in many cases, partially threaded bolts are used such that the force is only applied to the unthreaded portion.

Table 3.7.3 Calculations for Bolts

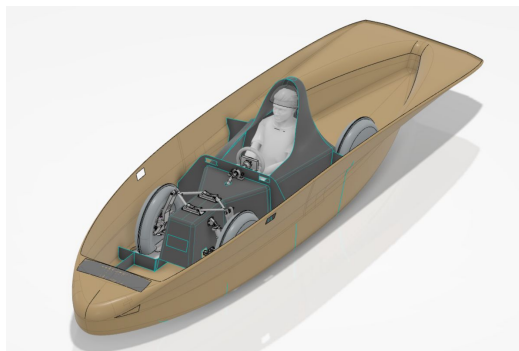
Location	F [N]	a (mm)	W (mm)	d (mm)	d (in)	Bolt Size - Chosen [in]	AN Equivalent
Top Left	1232.2	26.52	20.32	4.47	0.177	1/4	AN5
Top Right	1232.2	26.52	20.32	4.47	0.177	1/4	AN5
Bottom Left	4433.4	26.52	21.4376	6.77	0.26	5/16	AN5
Bottom Right	4433.4	26.52	21.4376	6.77	0.26	5/16	AN5
Rear Left	6391.6	34.93	20.96	8.85	0.35	3/8	AN6
Rear Right	6391.6	34.93	20.96	8.85	0.35	3/8	AN6
Front Shock - Top	7604.9	17.600	12.70	7.25	0.285	5/16	AN5
Front Shock - Bottom	7604.9	18.00	12.70	7.32	0.288	5/16	AN5
Rear Shock	9039	17.80	12.70	7.71	0.303	5/16	AN5
Bottom AARM	5227.96	-	-	9.84	0.387	7/16	AN7

4. Chassis

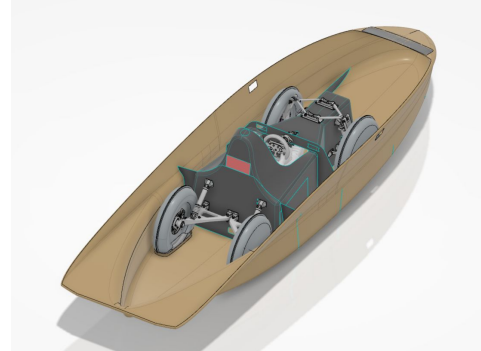
This chassis is assembled by bonding together:

- The bottom aerobody shell
- The moulded monocoque chassis
- Flat sandwich panels

The objective of the new chassis is to make best use of the composite materials and minimize the installation mass of assembling sandwich panels as we have done in the past.



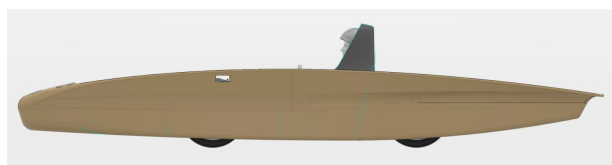
Front Isometric



Rear Isometric



Top View



Side View



Front View

Figure 4.1 Chassis

Material Selection

The moulded chassis design is manufactured using the Zoltek PX35 Biaxial Fabric prepreg with a total fabric and epoxy weight of 500 gsm. Zoltek is used due to its ease of draping which is a huge contributor towards manufacturability. A hybrid approach is used for the core material in the chassis. Rohacell HERO 71 and HERO 110 foam core is used for the parts of the chassis which experiences high loads. Rohacell HERO 200 is used for the suspension mounts (hard points) while the high curvature parts of the chassis (rollcage, fillets, etc.) will be made out of honeycomb core which gives us the flexibility to go around sharp curves and corners providing stiffness to those areas.

The aerobody itself will be made out of Axiom-5201M twill carbon fabric prepreg. The total weight of the fabric and epoxy to be used is ranging between 258–362 gsm. As for the core material, the bottom and the top aerobody will have Rohacell HERO 71 foam core while the sides will be manufactured using honeycomb core to optimize the performance and structural integrity of the whole structure while still keeping manufacturability in perspective.

To provide further torsional rigidity, the backrest board is extended up to the aerobody on either side and an extra board is added where the steering bearing is mounted. These boards will be made of sandwich panels and added after the main chassis is made. To secure the Tracker Box and part of the charge stand mechanism, a “Blue Sky Beam” made of sandwich panels is also added to the front and rear part of the aerobody.



Figure 4.2 Extra Chassis Boards

Performance:

Some ANSYS simulations have been conducted on the chassis design as shown in Table 2.12 and Table 2.13. Currently the front suspension load cases are still being conducted and will be updated in a later revision.

Crash Cases:

- Frontal Impact:

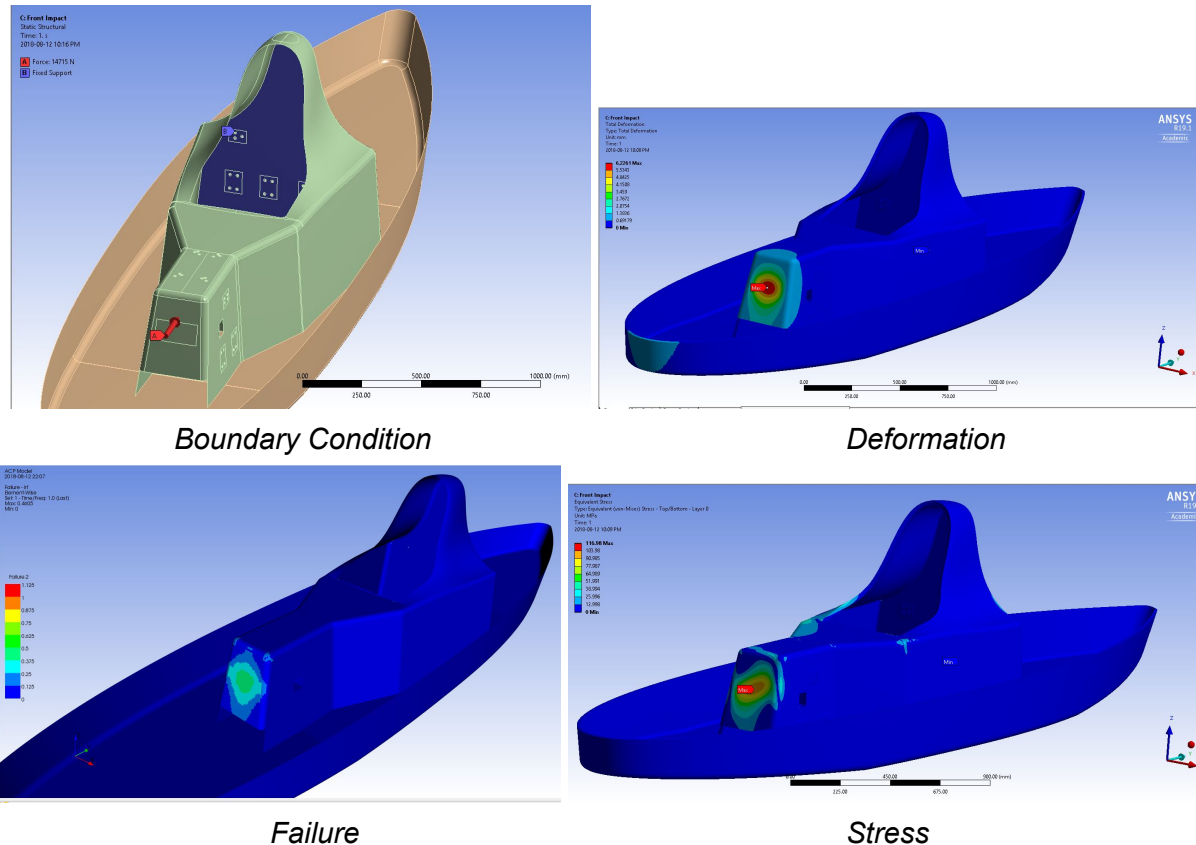


Figure 4.3 Frontal Impact Cases

- Side Impact:

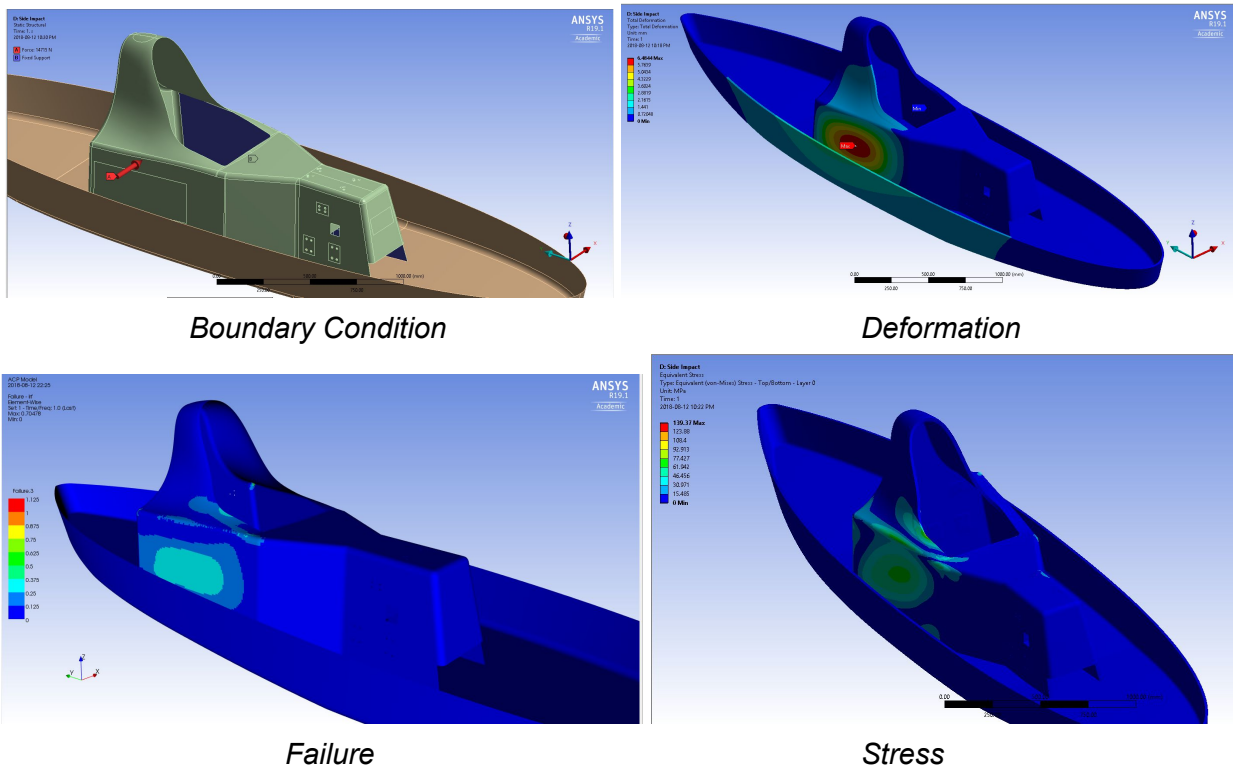


Figure 4.4 Side Impact Cases

- Top Impact:

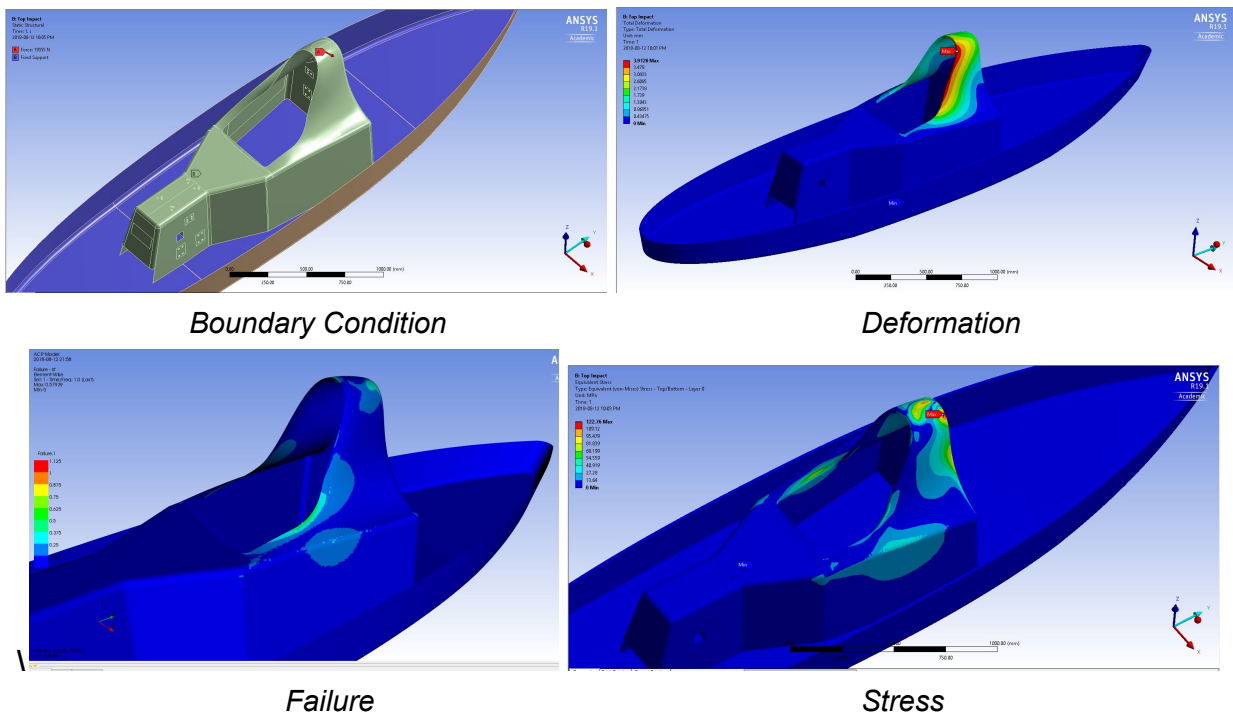


Figure 4.4 Top Impact Cases

Simulation Results

Case	Safety Factor	Stress (MPa)	Deformation (mm)
2,1,-1	1.5035	472.22	0.18252
6,0,0	3.1091	228.36	0.018052

Rear Suspension:

- 2,0,1:

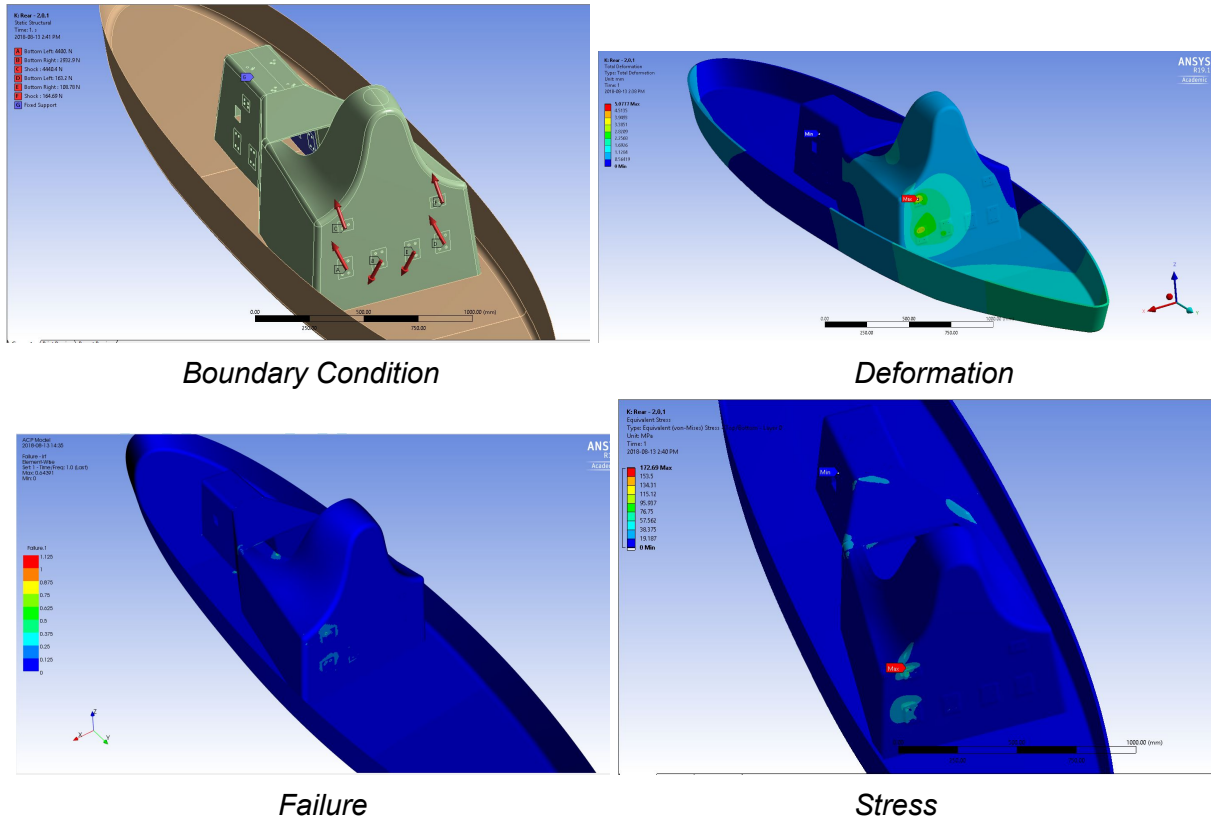


Figure 4.5 Rear Case 1

- **2.0.-1:**

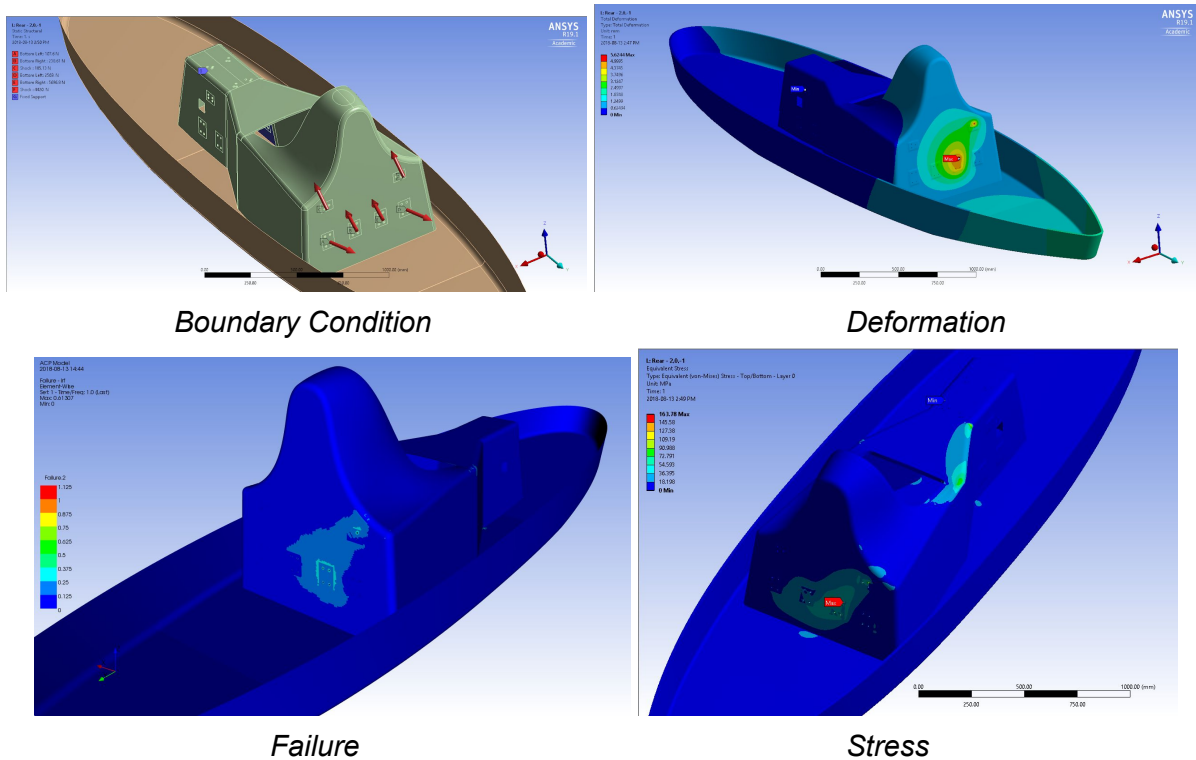


Figure 4.6 Rear Case II

- **6.0.0:**

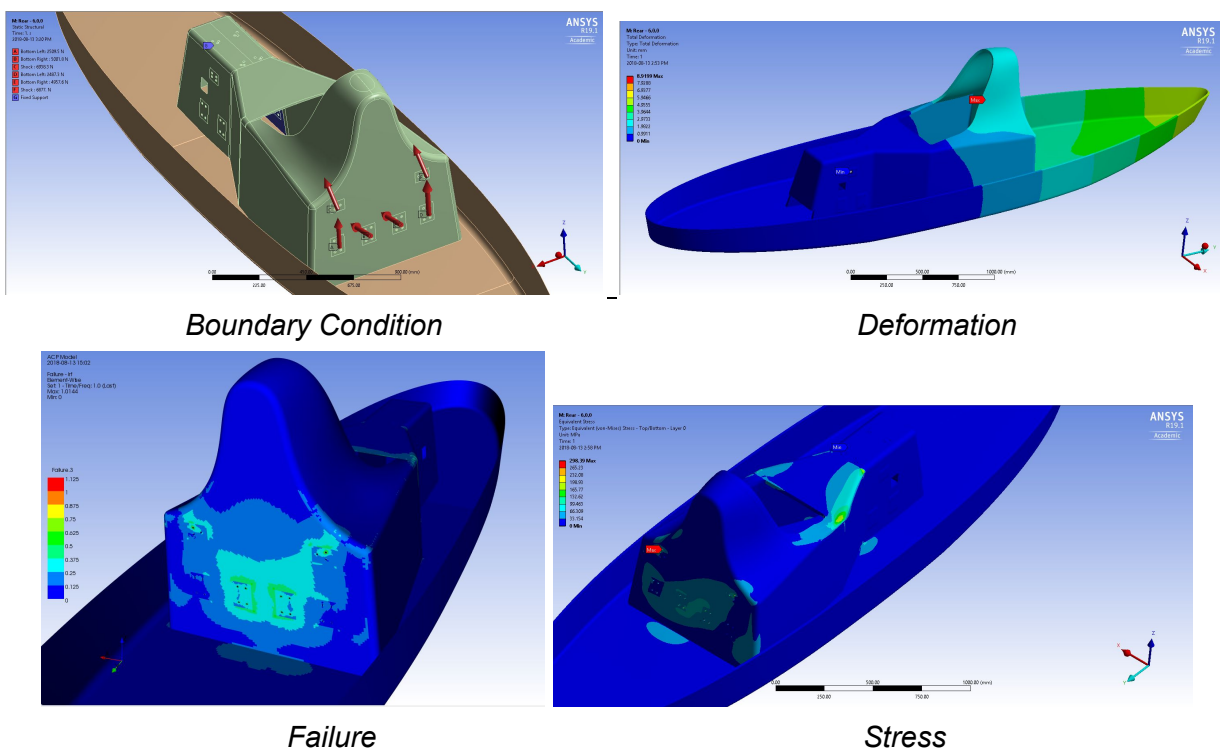


Figure 4.7 Rear Case III

Ergonomics:

Vision

According to the regulations: Each driver, when seated in the normal driving position with safety-belt and helmet on, must be able to identify 75 mm high letters at every point of forward travel that is:

- 4m from the driver's eyes, and
- Between 0.4m below eye level and 0.7m above eye level, and
- Between 100 deg left and 100 deg right of the direction of travel

Our compliance with the regulation is shown in Figure 2.23.

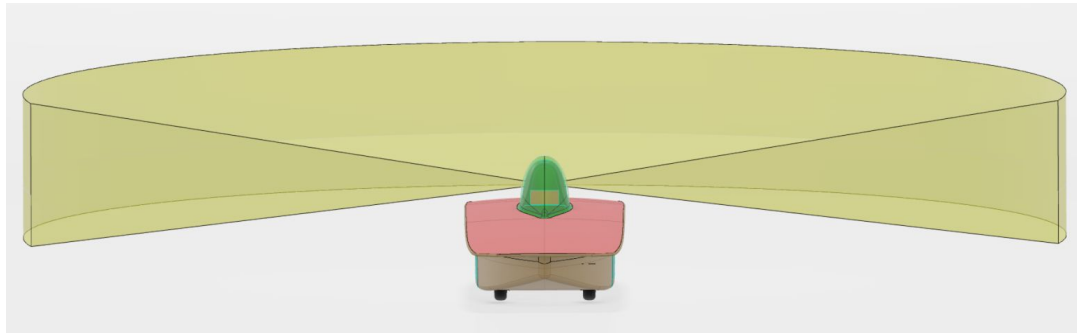
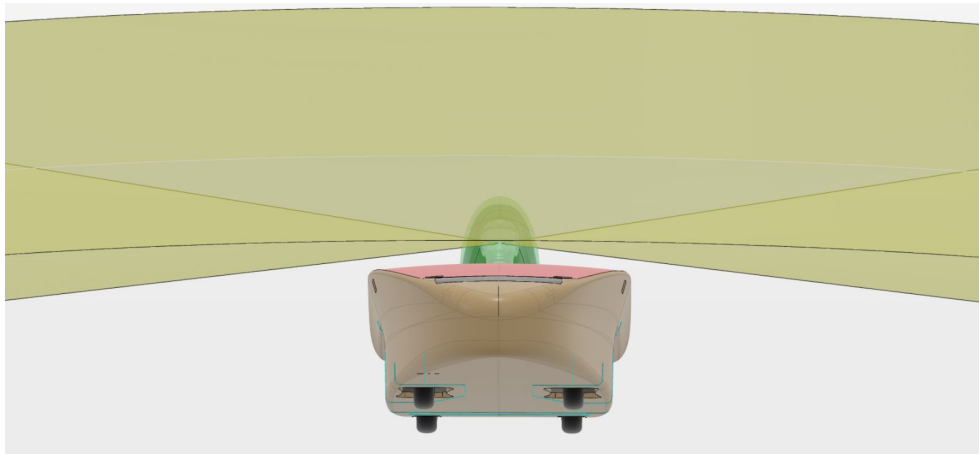


Figure 4.8 Front and Side Vision

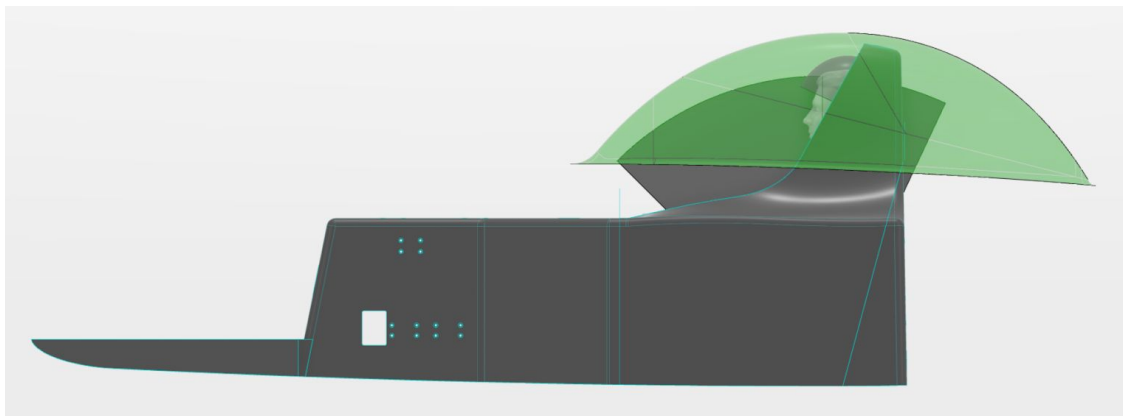


Figure 4.9 Occupant Space Check

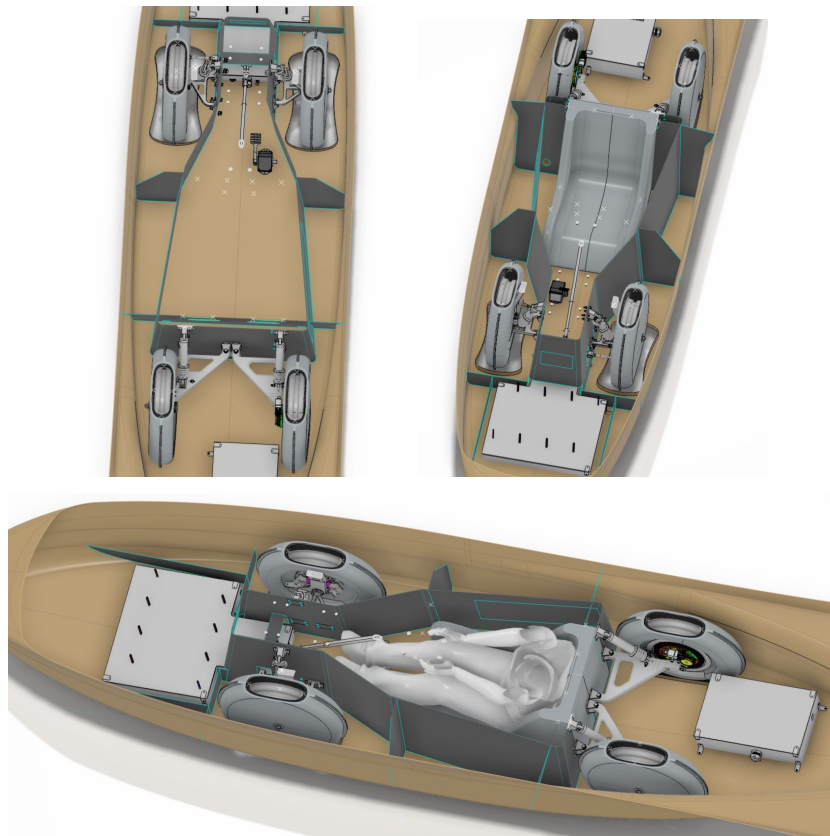


Figure 4.10 Driver Space

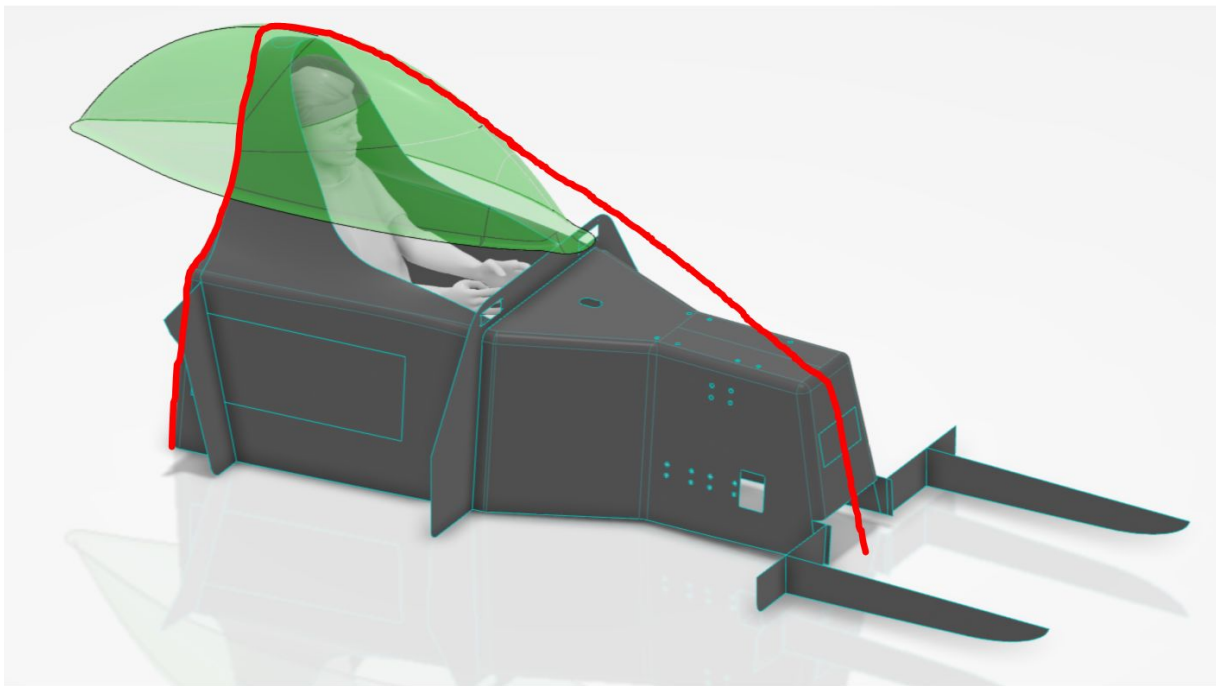


Figure 4.11 Occupant cell & Convex hull definition

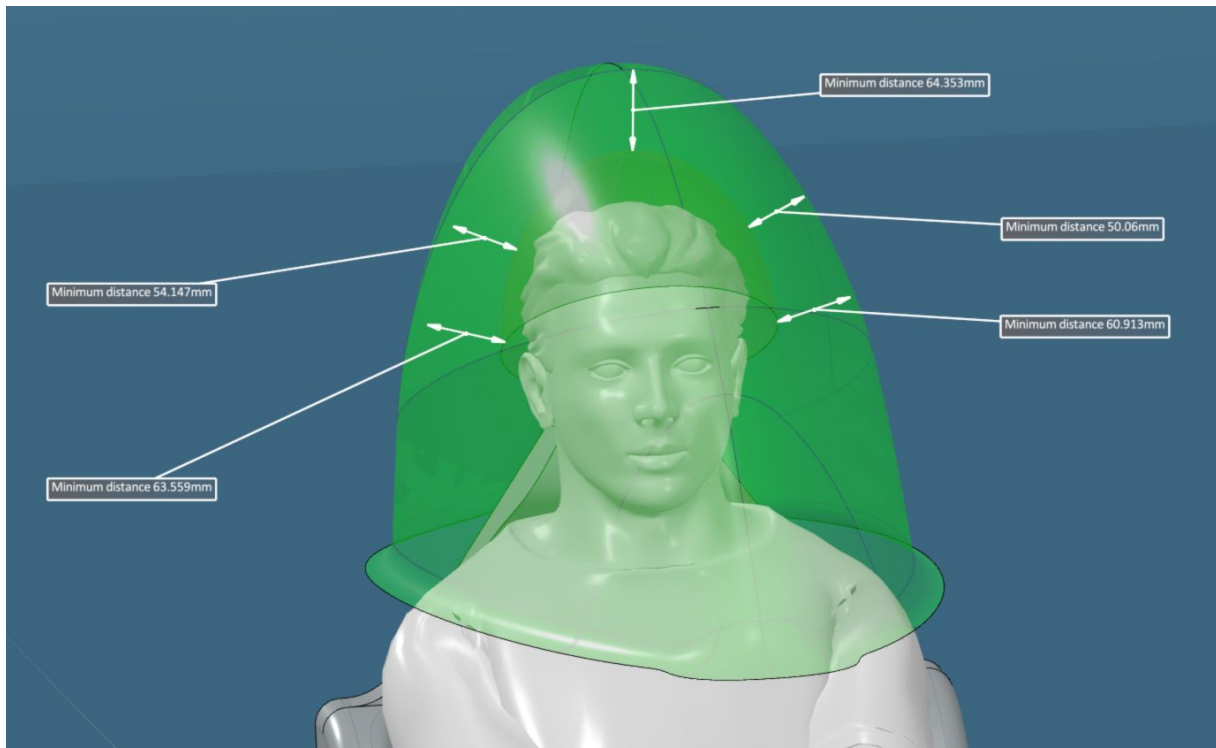


Figure 4.12 Head Clearance Requirement

Driver Jig

The driver jig started as a prototype used to test the occupant space and driver ergonomics. Due to the uniqueness of the chassis design, it was vital to test the design with a prototype like the driver jig. The jig now includes many other components and can be used to test many other systems of the car. Some of the features include:

- **Steering:** full steering with rack and pinion, u-joint, bearings and collapsible boss are installed. The location of the steering wheel from the driver was optimized using the setup.
- **Brakes:** The brake pedal, reservoirs, master cylinders, parking brake, proportioning valve and brake hoses were all installed in the jig. This helped to determine how far the pedal should be installed from the driver. The jig also helped with hose routing.
- **Driver Control Panel:** The location of the driver controls and buttons as well as the rearview screen and other panels was determined in the jig.
- **Charge Stand and Top Aerobody:** The charge stand mechanism which is a 6-bar linkage was installed and tested on the jig. A top aerobody was also added to test its opening and clearance with respect to the chassis. The installation location of the linkages was also determined using the jig.
- **Seat and Seat Belts:** Seat belt clevises and seat belts were installed to determine driver ergonomics. A seat prototype was also installed to further check driver ergonomics.
- **Suspension:** Suspension clevises were installed on the chassis. Suspension component prototypes will be tested and installed on the jig as well as they are manufactured.
- **Electromech Enclosures:** The battery box and PPT boxes were prototyped. Their installation location and how they fit was tested on the jig.

The driver jig allowed for prototyping components, testing them and in case of issues, changing the design if needed. The feedback gained from the jig has been vital in optimizing the design of many systems of the car. It is also a good source for the safety board to view the progress of the team and approve designs.

Several pictures are included below:



Figure 4.13 Driver Jig

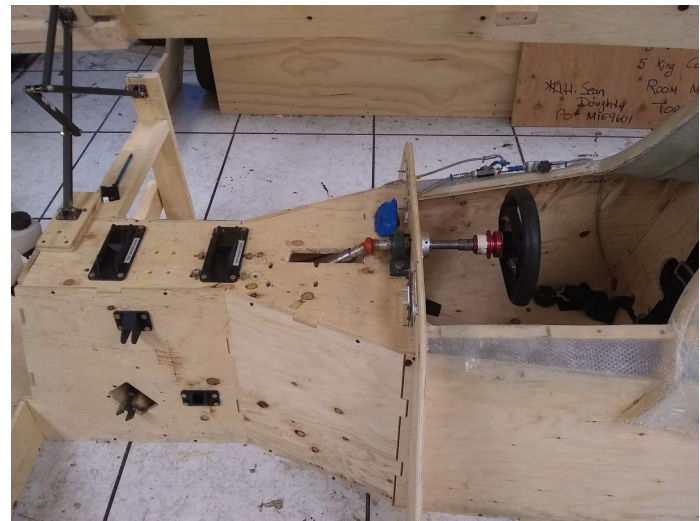
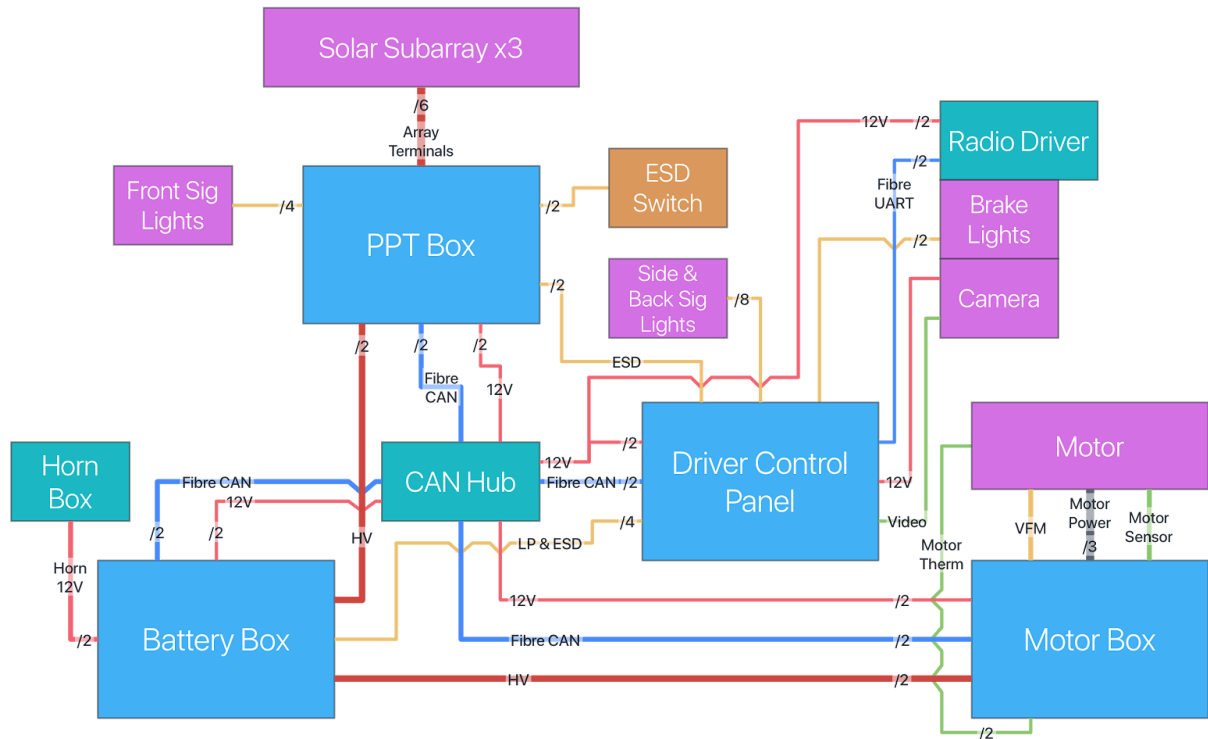


Figure 4.14 Driver Jig

5. Electrical/ Electromech

System Overview



The electrical system is composed of 4 main areas of control -- the boxes as described below -- connected by a CAN network. Low voltage is distributed alongside CAN and is isolated from high voltage. The high voltage power train connects the PPT Box, Battery Box, and Motor Box in parallel, and features 2 relays to completely cut off all 3 nodes from each other. The rest of this section will go over the high level features and functionality of each part of the system.

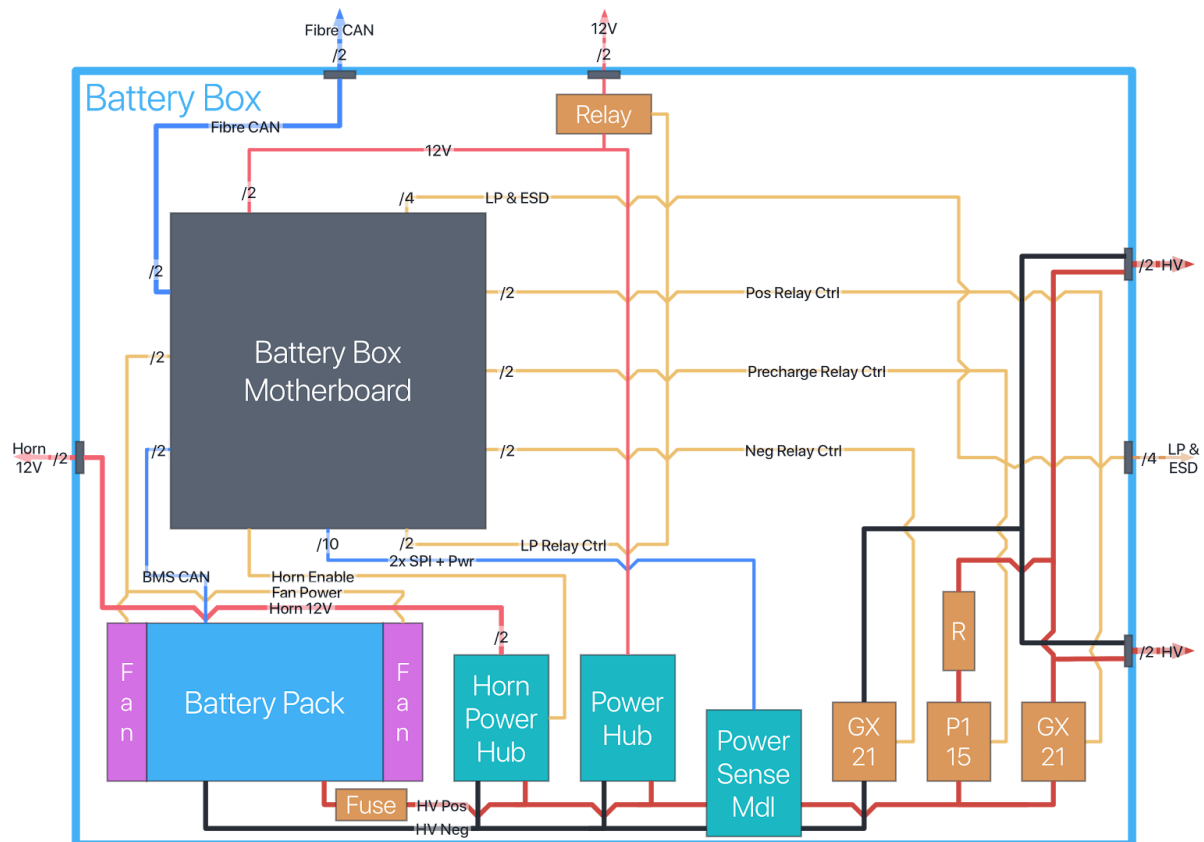
Motherboards

Each major enclosure (such as the Battery Box, PPT Box and the Driver Control Box) will contain a motherboard which will serve as the main routing point for all power, communications and signals. All communication between an enclosure and the others will be handled by the local STM32H743BI microcontroller. The motherboard will also route all wiring on the board, eliminating the need for running wires between parts of the enclosure.

In enclosures where needed, the Motherboards will also have an isolated power sense module, which will measure voltage in the connected system using an analog to digital conversion, and current on the wires using a Hall effect sensor. Due to the isolation requirements, the power sense module will have its own isolated DC-DC converter and an isolated SPI communication link. The aim of the PCB team is to place the measurement modules on the motherboard, but at locations with multiple Hall effect sensors (such as the PPT Box), some components may have to be moved off-board due to size constraints.

All modules in the enclosure will be managed by the local microcontroller, with their operation principle being active-high; unless the Microcontroller is in control, no system can be activated.

Battery Box



The battery box systems are managed by a central motherboard, and have the following functions:

- Providing 12V power access to every other part in the car's electrical system (through CAN bus)

- Handling communication with systems in other enclosures
- Managing a distributed BMS system
- Controlling the high voltage relays based on user input
- Powering the horn

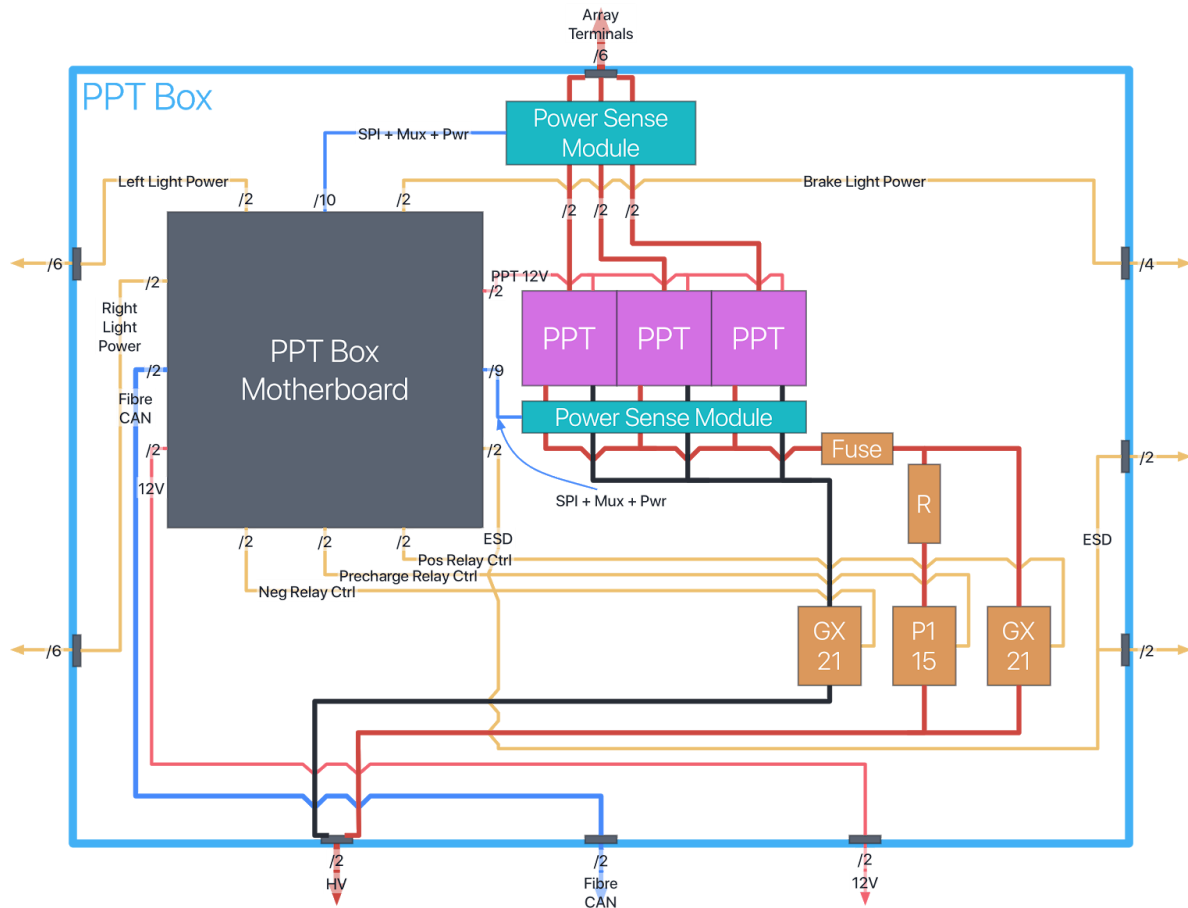
All systems will be controlled using a central controller, as described in the Motherboard section above.

Power measurement will be done on the Battery Box Motherboard, in an isolated power measurement circuit on the board.

The BMS will be in the module side of the Battery Box, but will act autonomously. The only values that the Battery Box Motherboard will get from the BMS will be the individual voltage and temperature readings. The BMS is described in further detail in [Batteries and BMS](#).

The powerhub on the Battery Box will have 2 Vicor DC-DC converters instead of 1, where one powers all critical and noise-sensitive systems on the car (including all systems connected to the CAN Hub), and the other will power all high-noise systems that are not affected by further noise, such as the Horn.

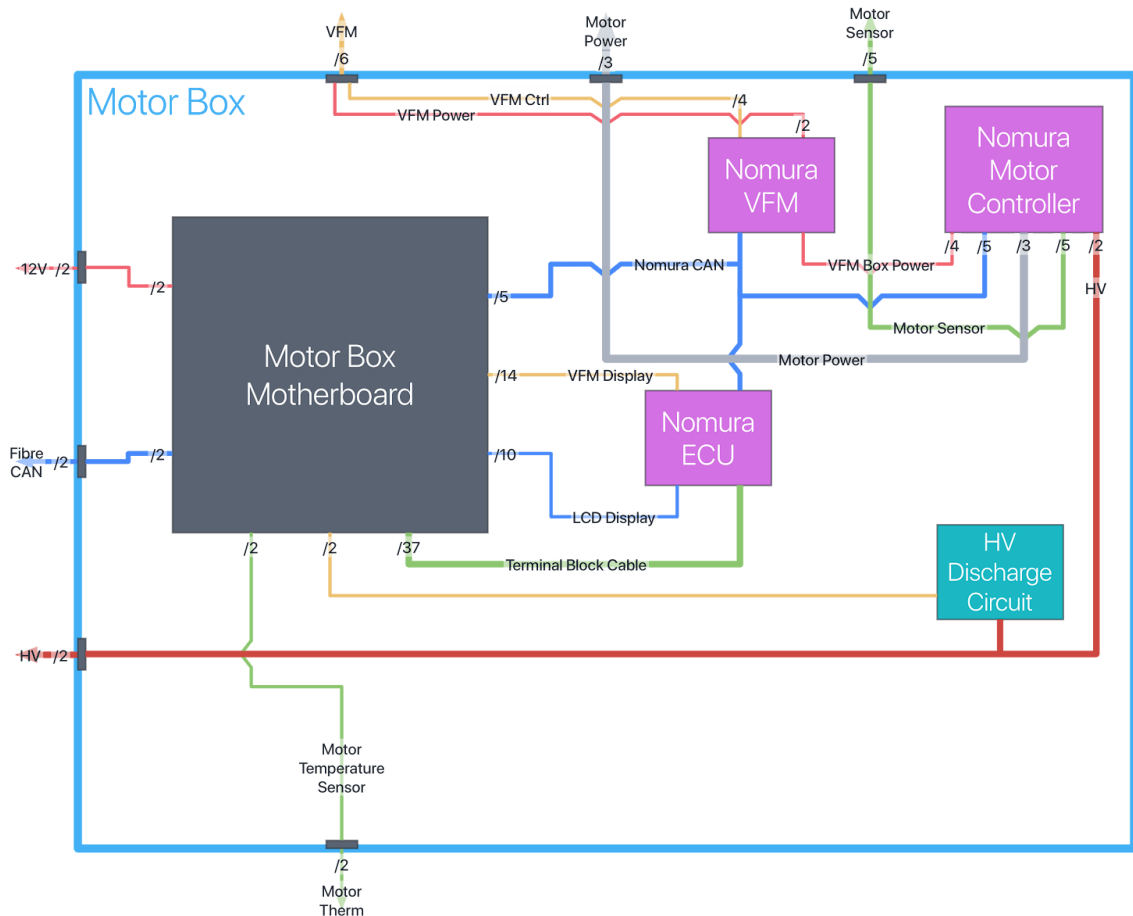
PPT Box



The PPT Box will have a similar architecture as Polaris, but rather than having distributed systems acting independently, the system will be managed by a centralized controller, as described in the Motherboard section above. The motherboard will determine the operating state of the high voltage relays depending on the user input and PPT-side measurements. The PPT Box is designed for use with 3 Nanoleaf (in-house) MPPT's, but it can accommodate up to 3 AERL Racemax MPPT's. Because communication with the MPPT's is not enabled, the motherboard is compatible with both MPPT types.

Lights on the top aerobody will also be driven by a local Lights Driver Board, rather than relying on a driver in a different enclosure.

Motor Controller Box



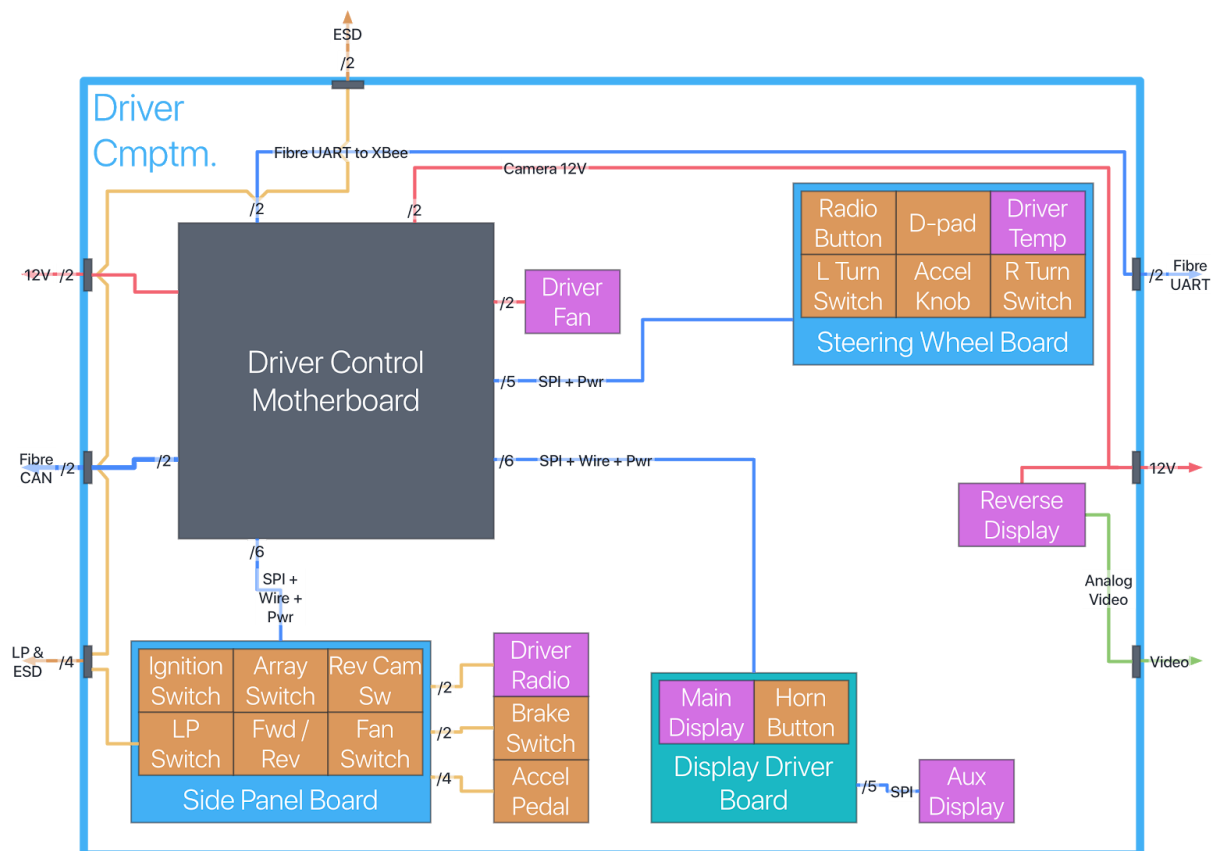
The purpose of the Motor Controller Box is to implement drive-by-wire. This is the solution to the problems we've been having last cycle with unmanageable wiring for all the switches stretching from motor controller to driver compartment, heavy cabling, and unsatisfactory robustness of the switches (and the difficulty of repairing them). We have implemented and tested drive-by-wire in the past with the Tritium motor controller, so not much will need to change on the software side.

The only thing novel about this design is that the microcontroller must emulate the analog interface to the Nomura ECU, because this motor controller only has analog.

To do that, we have designed what we call the motor controller controller. **It is a galvanically isolated domain full of solid state relays and digital potentiometers.** These will be wired directly into the Nomura controller's analog harness and emulate switches and potentiometers respectively. All control signals will arrive through digital isolators. Information the motor controller tries to send to the two displays normally required for operation will similarly be intercepted and parsed, and presented to the driver through our own system. This will essentially complete an abstraction layer for the Nomura motor controller, which can be built upon even further in future cycles.

The Motor Controller Box may also feature a high voltage bus discharge circuit, which will help us meet the regulation for discharging the high voltage bus capacitances to 60 V within 5 s of emergency shutdown. The details of this circuit is yet to be determined.

Driver Control Box



The driver controls have been divided into three enclosures: the Steering Wheel, the Side Panel and the Front Panel.

- The Steering Wheel has the most frequently used controls, such as the accelerator knob, screen display controls and button inputs. All inputs in the steering wheel are monitored by a local STM32L4A6RG microcontroller, and then communicated using SPI to the Driver Control Motherboard.
- The Side Panel has all the switches that are used less frequently than those that are placed on the steering wheel. Signals from these switches are handled the same way as in the Steering Wheel Board, and passed to the motherboard over a SPI channel.
- The Front Panel is the dashboard of the car, and only features displays. It will have a rear-view display, an OLED dot matrix screen and (optionally) the motor information display provided by Mitsuba. The data for the rear-view display will come in the form of analog data, but the remaining two displays will receive their data from the Driver Control motherboard.

The Driver Control motherboard will be located in the same enclosure as the Side Panel Board, and it will serve the following purpose:

- Following the status of all switches, as received on SPI lines
- Powering all connected low power systems
- Acting on new switch status, by either making local changes or sending information over the CAN Bus to other motherboards
- Driving all lights on the bottom aerobody using a local Lights Driver Board
- Providing data for the Radio, which will be located on the aerobody or the roll cage

The horn and ESD signals are the only two signals that are not passed from the Driver Controls side to the Battery Box over a communication line. Both signals are carried over a signal-ground pair between the enclosures over a D-Sub or a similar cable.

Batteries and BMS

Batteries

There is a new regulation limiting teams to a quantity of 420 instead of weight if the team uses 18650 cells. This regulation gives teams that use 18650 cells a potential advantage in cell mass, so this is what we decided to go with. Our main criterion for cell selection was efficiency, while the cell must also meet discharge current requirements and be of reasonable capacity.

The cell we have chosen is the Samsung INR18650-35E. The datasheet for this cell can be found in [Appendix H](#). Some of the manufacturer's parameters include:

- 3,350 mAh capacity
- 2.65 V to 4.20 V operation
- 3.60 V nominal voltage
- 2,000 mA peak charging current
- 13,000 mA peak discharge current
- 0 °C to 45 °C charging operating temperature
- -10 °C to 60 °C discharge operating temperature

- -20 °C to 60 °C storage temperature
- 50 g weight

Our battery pack consists of 7 electrically identical modules in series. Each module has 5 identical submodules in series, and each submodule is 12 cells in parallel. This adds up to the below battery pack parameters:

- 40,200 mAh capacity
- 92.75 V to 147 V operation
- 126 V nominal voltage
- 156 A peak discharge
- 24 A peak charge
- 5,065.2 Wh energy
- 21 kg of cells
- 241.2 Wh/kg energy density

This directly translates to our basic BPS parameters:

- 92.75 V pack under voltage
- 147 V pack over voltage
- -156 A pack over current
- 24 A pack over current
- 2.65 V cell under voltage
- 4.29 V cell over voltage
- -10 °C cell under temperature
- 60 °C cell over temperature

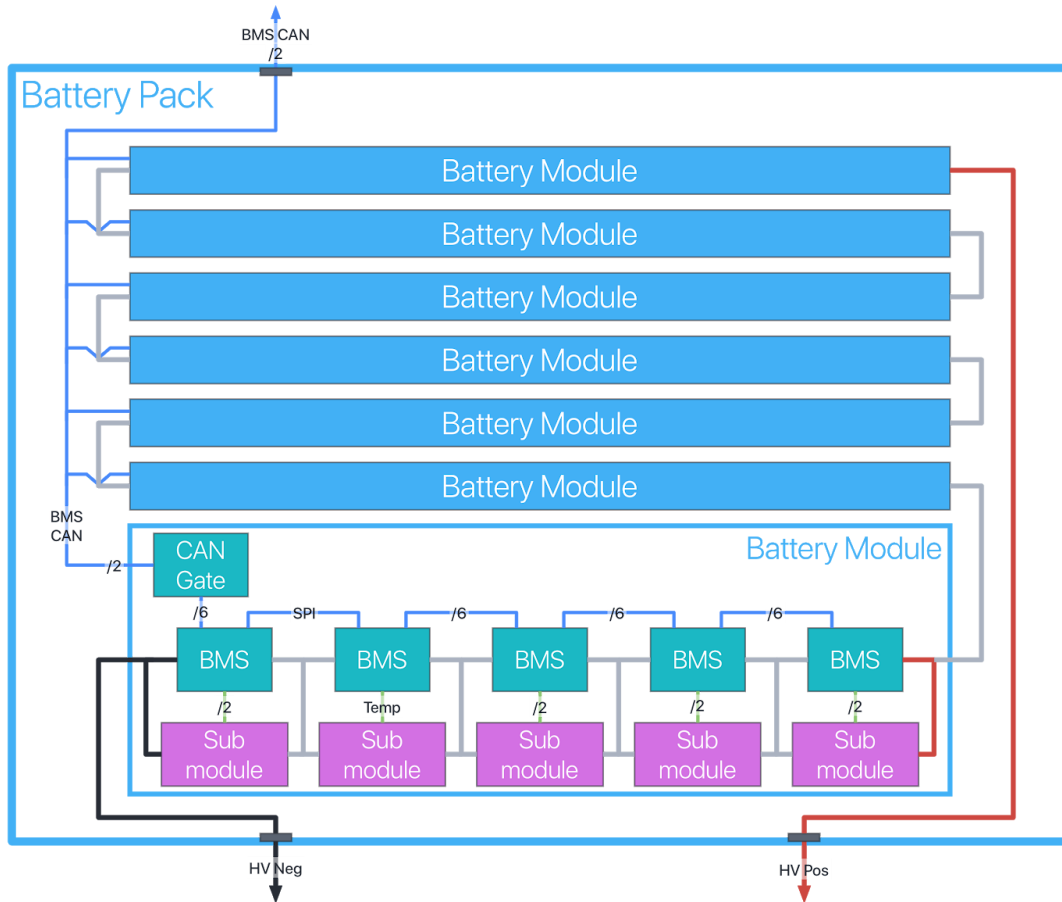
To prevent transients from shutting down the system sporadically, there will first be a low pass filter over the collected samples, then an error margin allowed for different levels of overage.

The filtering and triggering of BSD will be implemented in the Battery Box microcontroller. The proposed numbers for the error margins are currently:

- $\geq 0\%$ for 5 minutes
- $\geq 1\%$ for 1 minute
- $\geq 2\%$ for 30 s
- $\geq 5\%$ for 10 s
- $\geq 10\%$ for 1 s
- $\geq 15\%$ immediate shutdown

The percentages are relative to the operating range. The driver and crew will be notified of any level of BPS parameter violation immediately.

Modular BMS



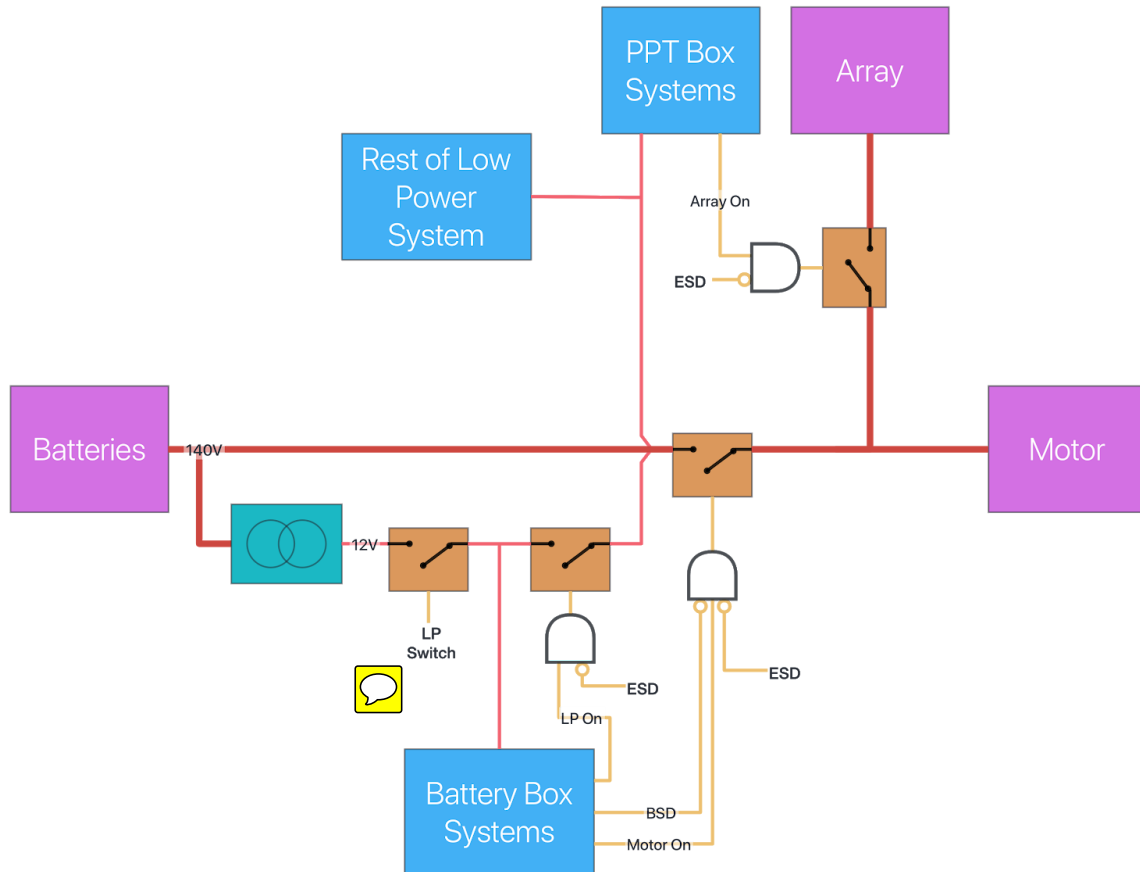
To address some of the problems we've had in previous cycles, we have designed a custom modular BMS system for the battery pack. There will be 35 modular BMS boards, 1 for each submodule or 12 cells in parallel. The modular BMS boards measure their respective submodule voltages and temperatures. They are powered off of the battery submodule itself, and feature isolated communications to each other. The 5 modular BMS boards on each module are daisy chained into a CAN gateway board, which connects the data bus on the module to the BMS CAN bus which is connected to the Battery Box motherboard and the rest of the modules.

The idea of this topology is to minimize the effect of a single point of failure. If any of the modular BMS boards fail, it would take down a minimum of 0 and a maximum of 4 other boards with it, and we will still have visibility into the rest of the cells instead of the whole system going dark.

However, we have also received feedback about the effect of glitches on the system and the general complexity of it. To address these points, we plan to test this system rigorously on a real

battery module, but not before we develop a fallback module-level design with off-the-shelf BMS ICs.

Powertrain



Above is a simplified diagram of the elec system, highlighting the topology of the powertrain. The dark red lines in the diagram are the high power. 2 sets of heavy duty contactors are used to isolate both rails of the high power bus from the components sitting on it. The one closer to the batteries is located within the battery box, while the one closer to the array is in the PPT box. These contactors are default off and controlled by the low power system. The low power system is powered off a 12V supply that is drawn directly from the batteries, regardless of the state of the contactors. The driver, however, has the ability to completely turn off the low power system as well. While the contactors are automatically controlled (see [the below section](#) for details on how it's done), the ESD and BSD signals bypass that control logic and shut down the system from a separate channel. ESD disconnects down all high power contactors immediately, while BSD cuts off the batteries immediately, while the motherboard sends a soft shutdown command to the PPT box. This topology satisfies both our desire to automate the operation of

the high power contactors to minimize driver error, and the regulations requirements on safety and battery protection.

High Voltage Relay Control

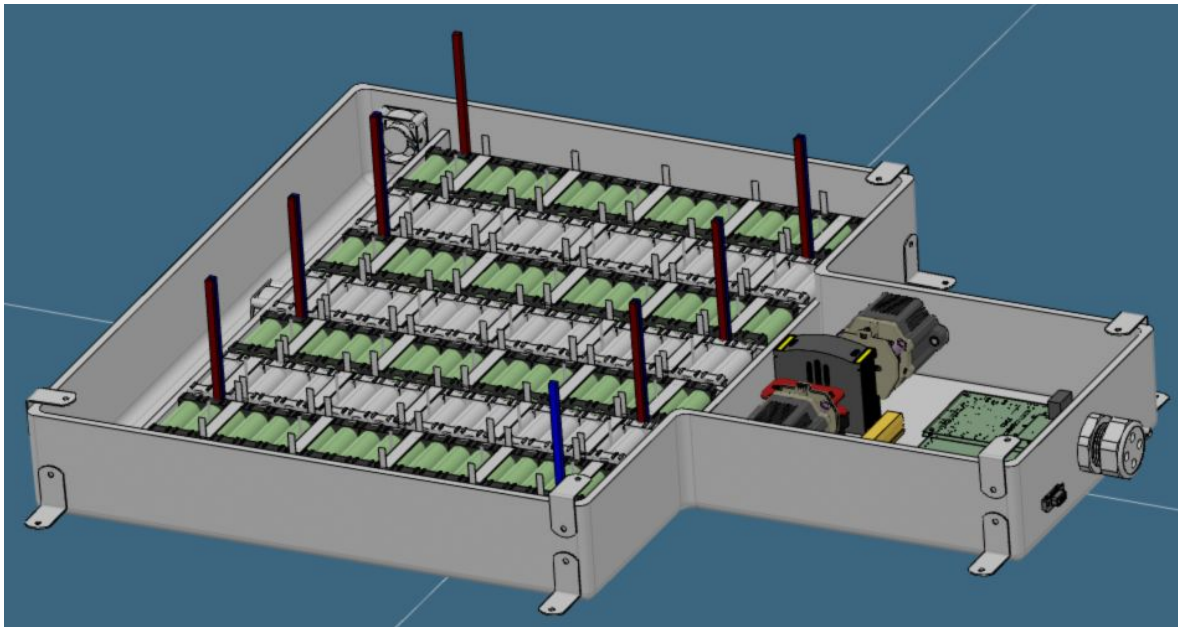
Unlike the relay controls of the previous cycles, which depended on manual operation using switches, the localized microcontrollers will handle the relay control depending on the operation mode indicated by the user. All operations such as activating precharge and determining which relays should be on will be automated. The relay control circuit (which will be based mostly on the precharge circuit of Polaris - Refer to [Appendix G](#)) will be reduced in scope to control only the local relays, and repeated across the Battery Box and the PPT Box to reduce system complexity.

In case of a CAN communication failure, the high voltage relays will be automatically opened after a certain interval (during which the driver will be warned), unless communication is reestablished. On the motor controller side, throttle can either be kept constant until the high voltage relays are turned off, or reduced linearly to 0%.

Communication

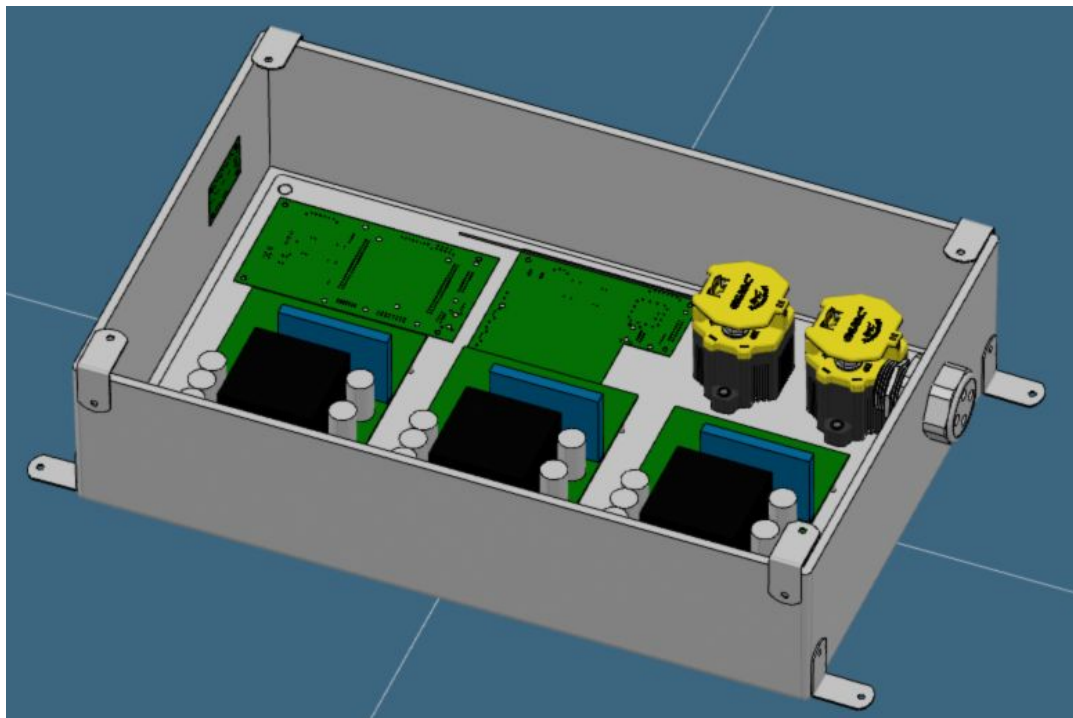
To mitigate issues we've had with CAN communication, to achieve maximum galvanic isolation between subsystems, and to create the most optimal environment for a potential switch to CAN FD, we are running CAN over fibre optic. Each CAN controller in the car will have 2 optic connections running to the CAN Hub, which is a miniaturization of the entire physical CAN bus. The fibre optic will carry the CAN Tx and CAN Rx signals to each CAN controller, while the differential bus exists only on the CAN Hub PCB. The CAN Hub will have ample shielding to protect data integrity, and the tighter control over the differential pair parameters will allow us to run CAN at higher data rates (CAN FD). The CAN Hub will also act as a power distribution board for the low power systems, enforcing a star topology and eliminating accidental ground loops.

Enclosures

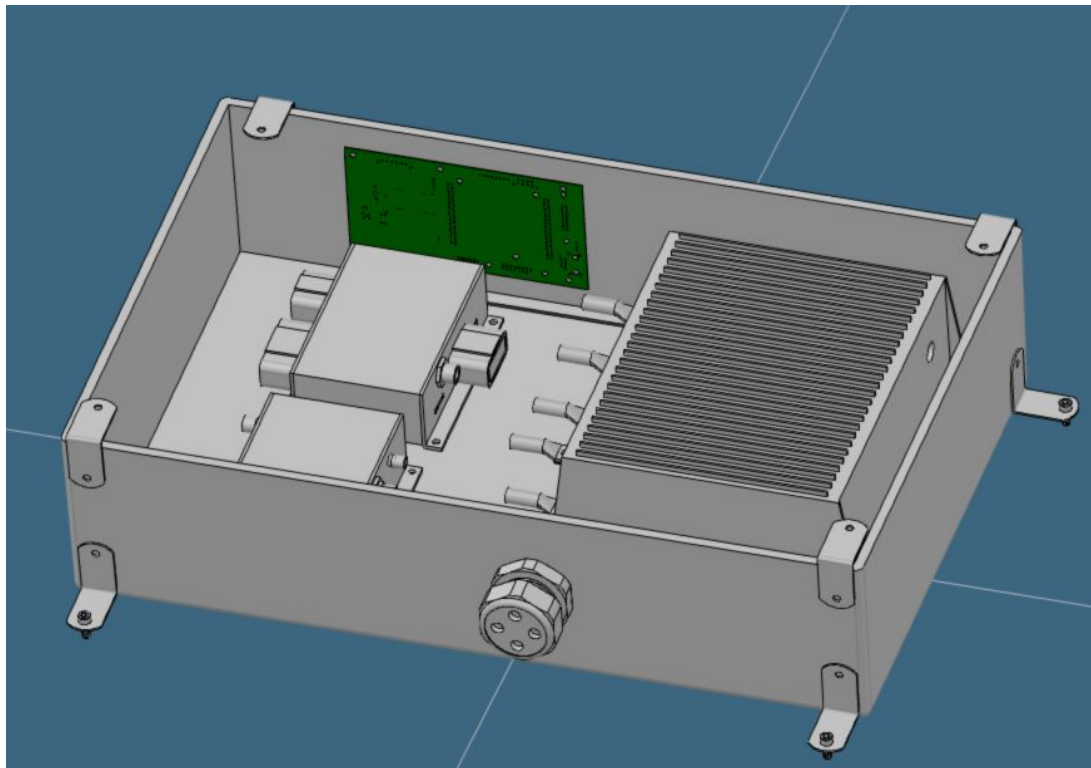


Battery Box with exposed contents

The red and blue blocks protruding out of the battery modules are simply the positive and negative terminal wires for each module. The smaller thinner grey rectangles extending vertically are the extended tabs meant to be folded over and attached to the BMS PCB's (the grey rectangles lying horizontally across the modules).



PPT Box with exposed contents



Motor Controller Box with exposed contents

The Battery, PPT and Motor Controller Box all have lids (hidden in the photos above) that are simple flat boards (composed of kevlar and core) cut out to match the geometry of the boxes. All

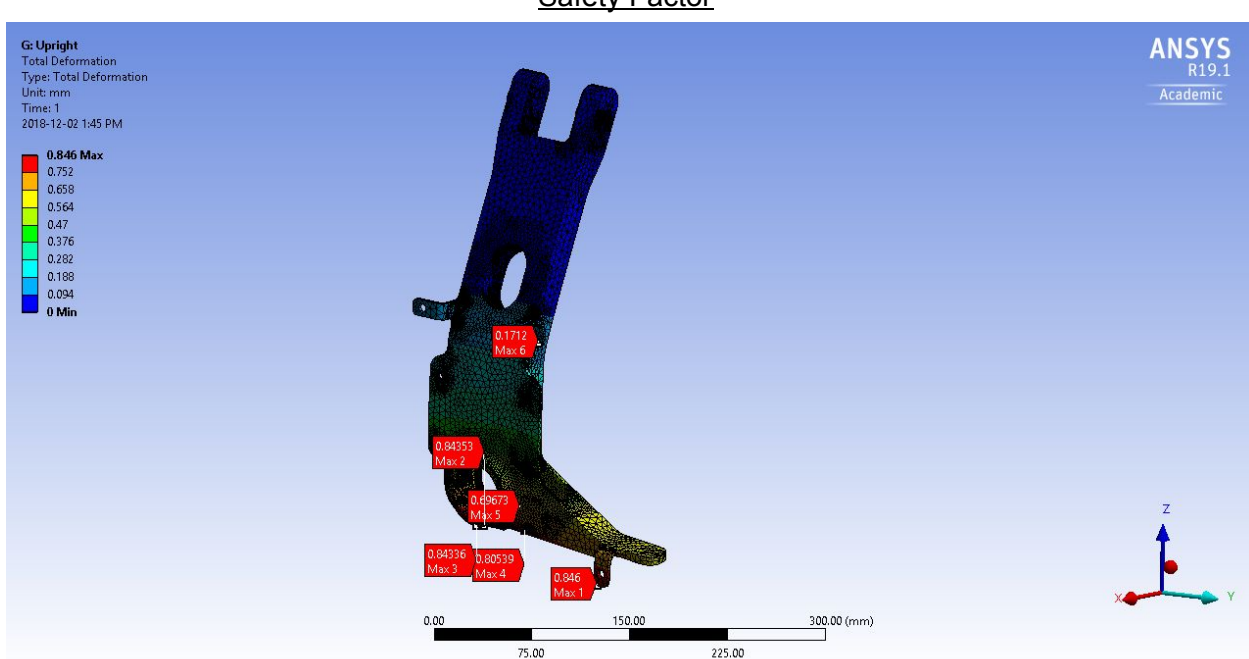
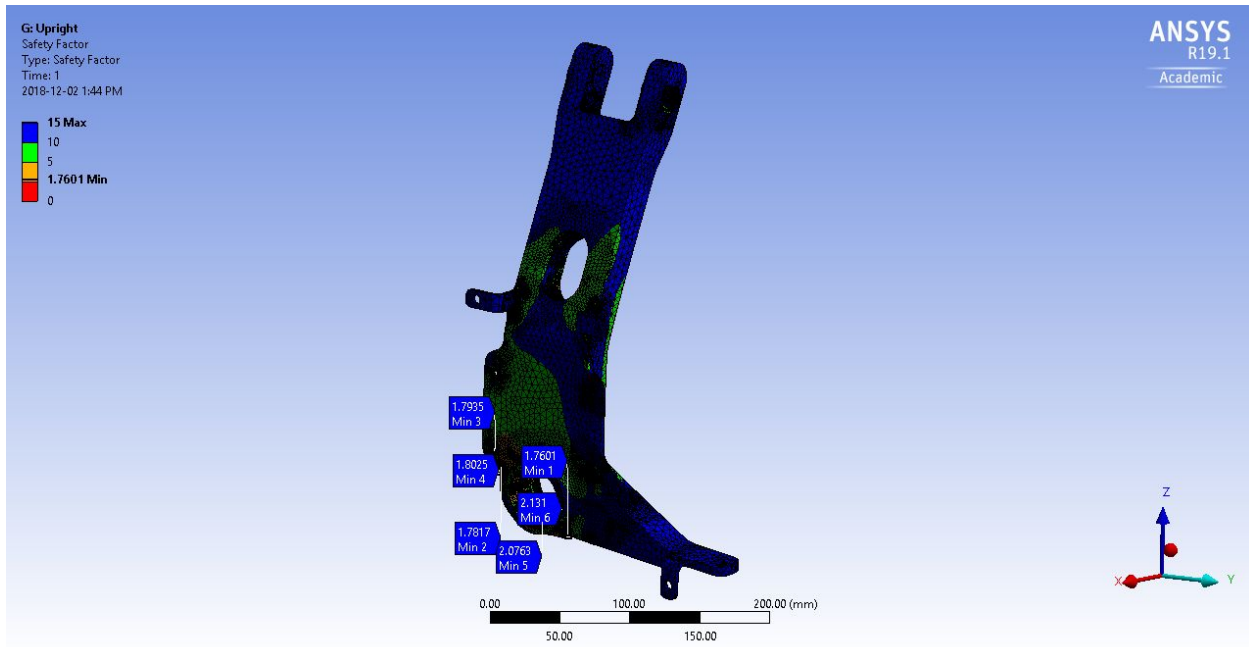
of them are secured using L-brackets and bolts, and this fastening method is also used to secure the boxes themselves to the car itself.

The Motor Controller Box lid has a rectangular cut out directly above the motor controller to allow for heat dissipation, and a meshed material is installed as a barrier for that cut out.

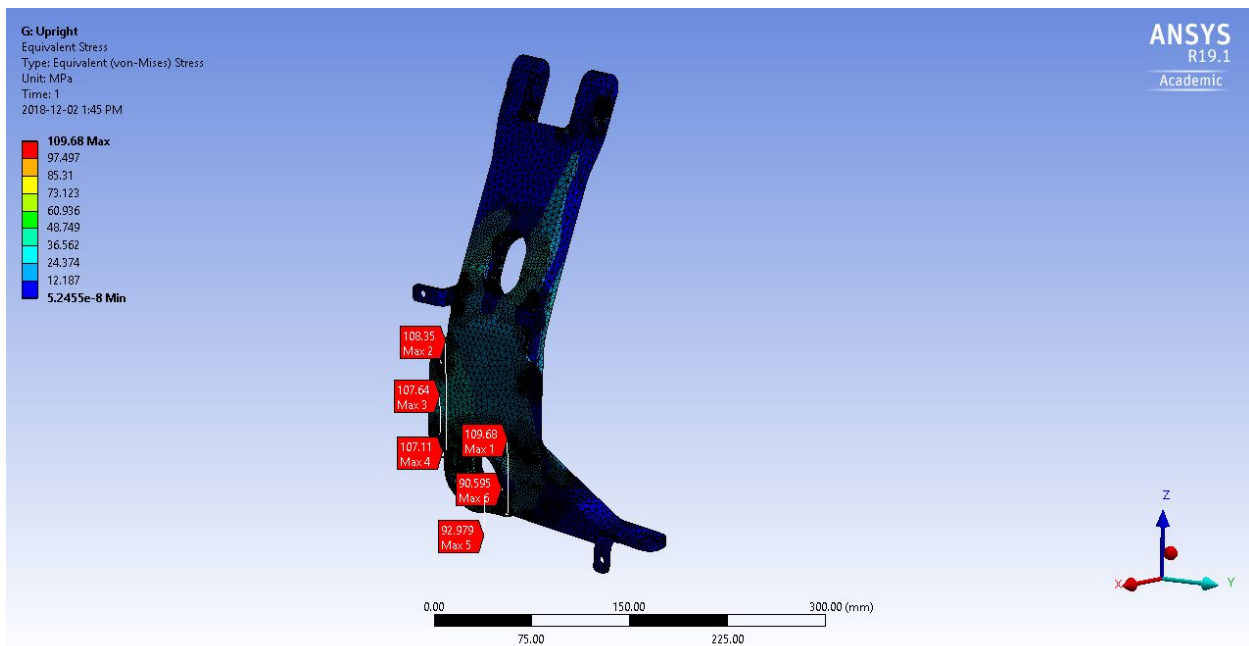
Appendix

Appendix A: Upright Simulation Results

CASE 1: 2,1,1

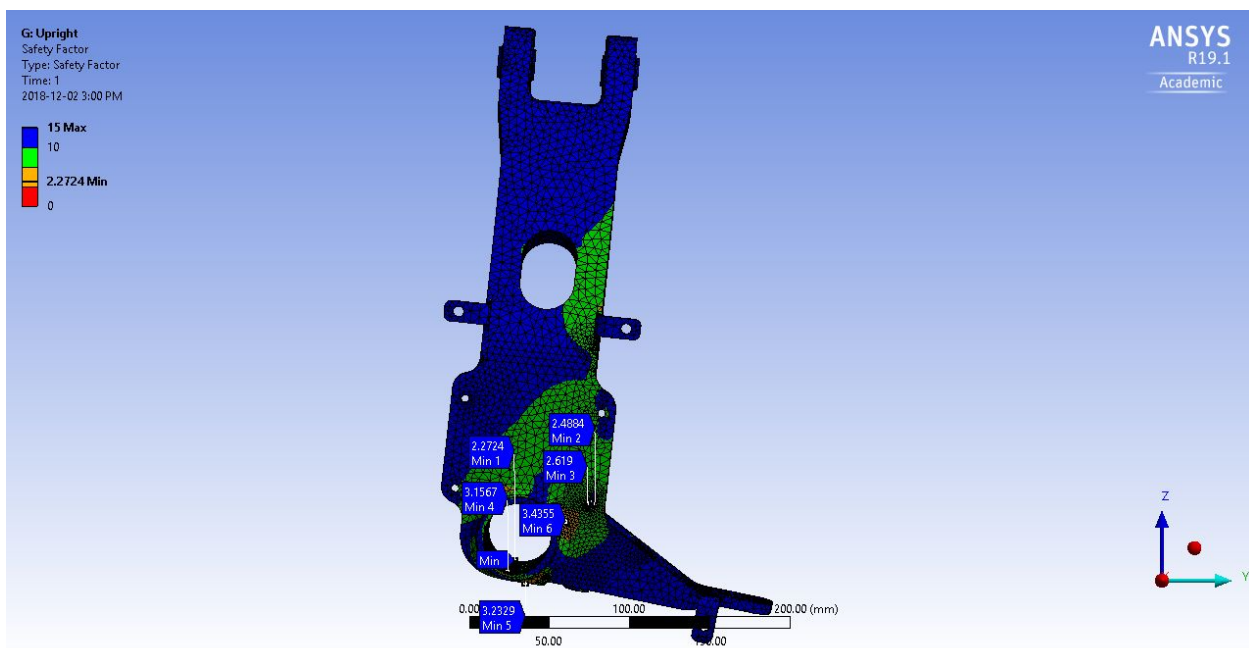


Deformation

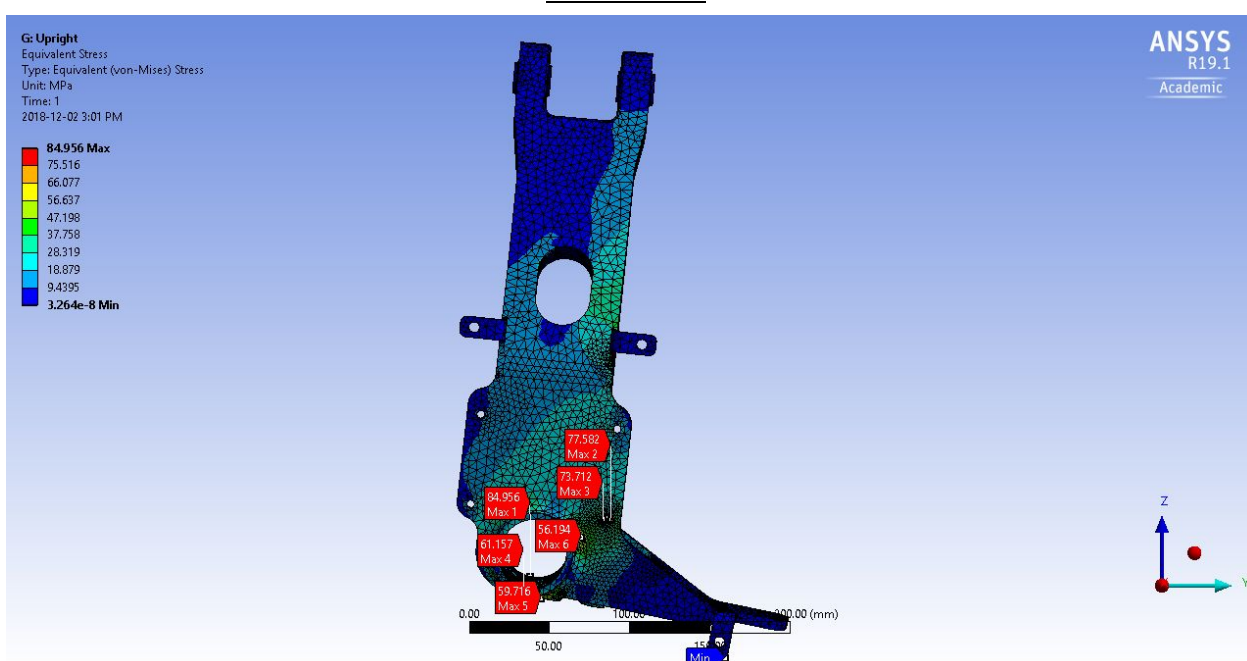
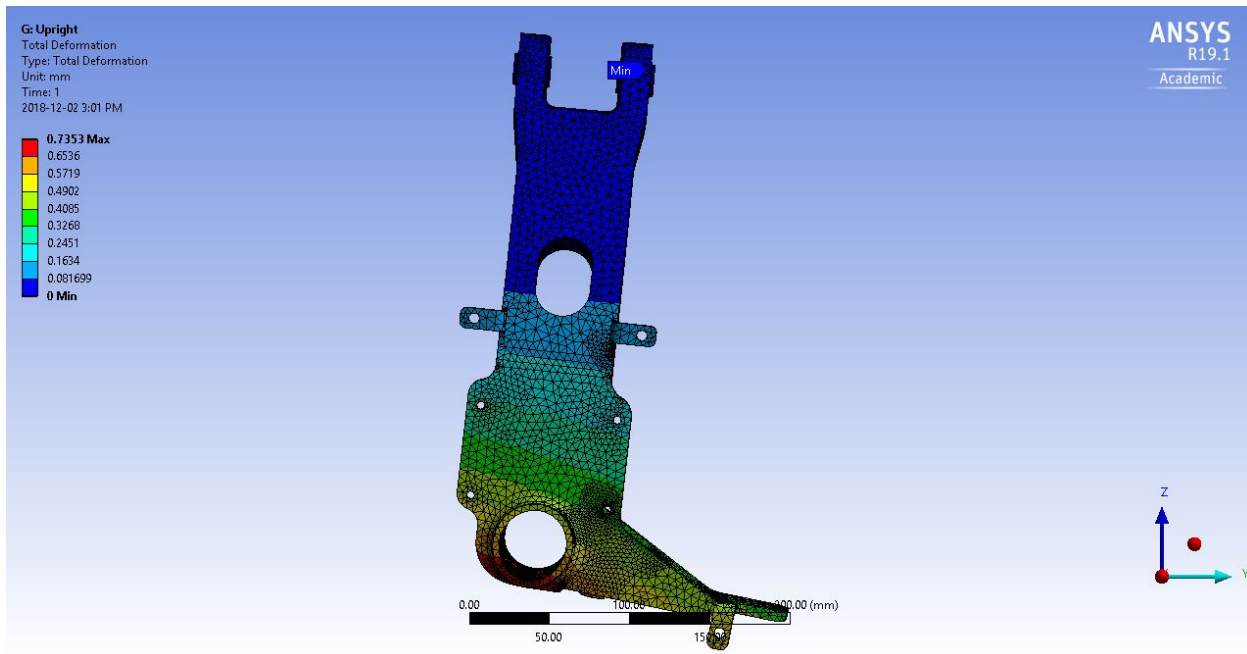


Equivalent Stress

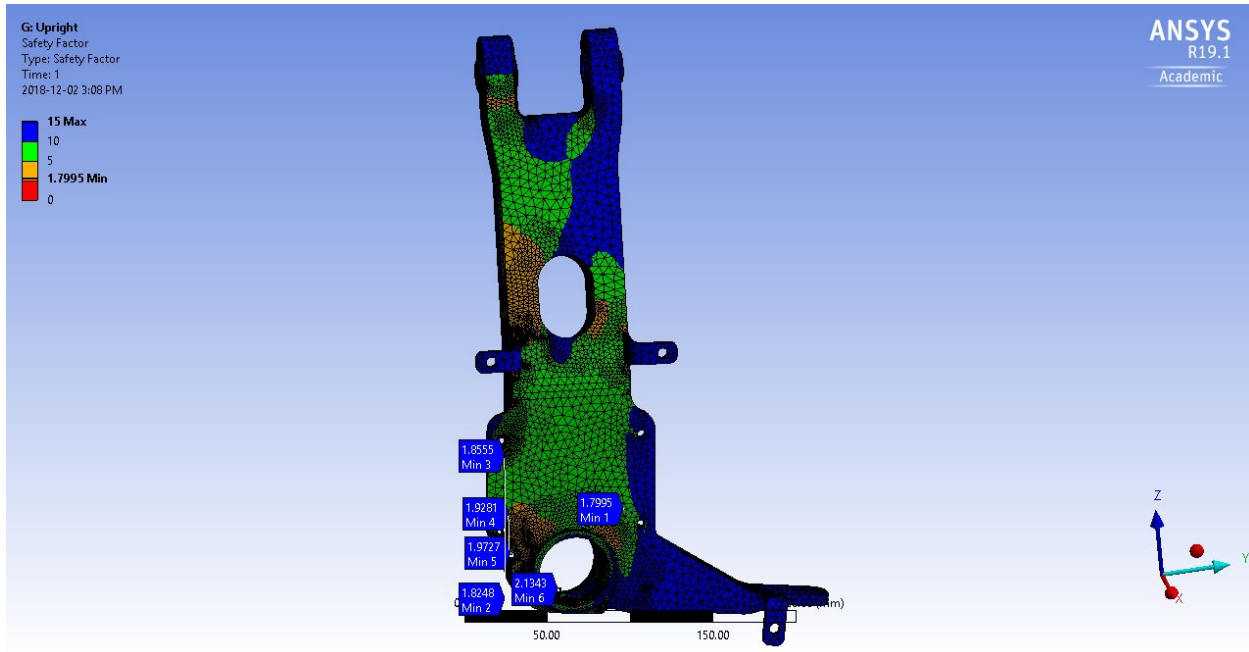
CASE 2: 2,0,1



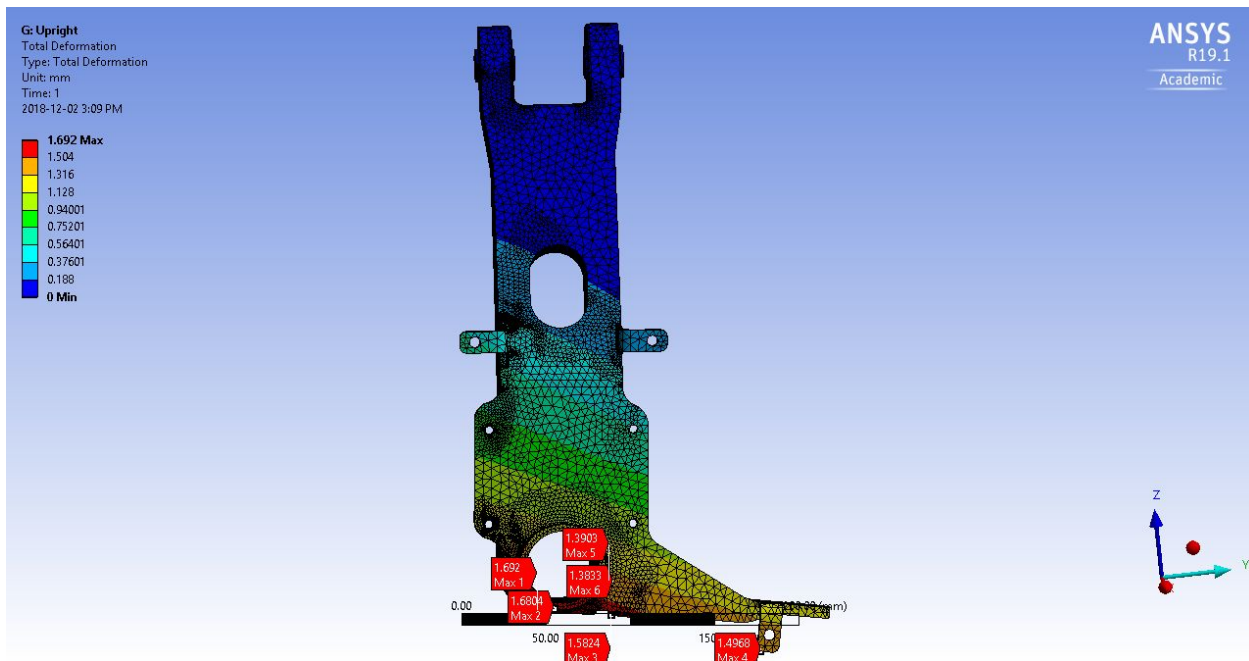
Safety Factor



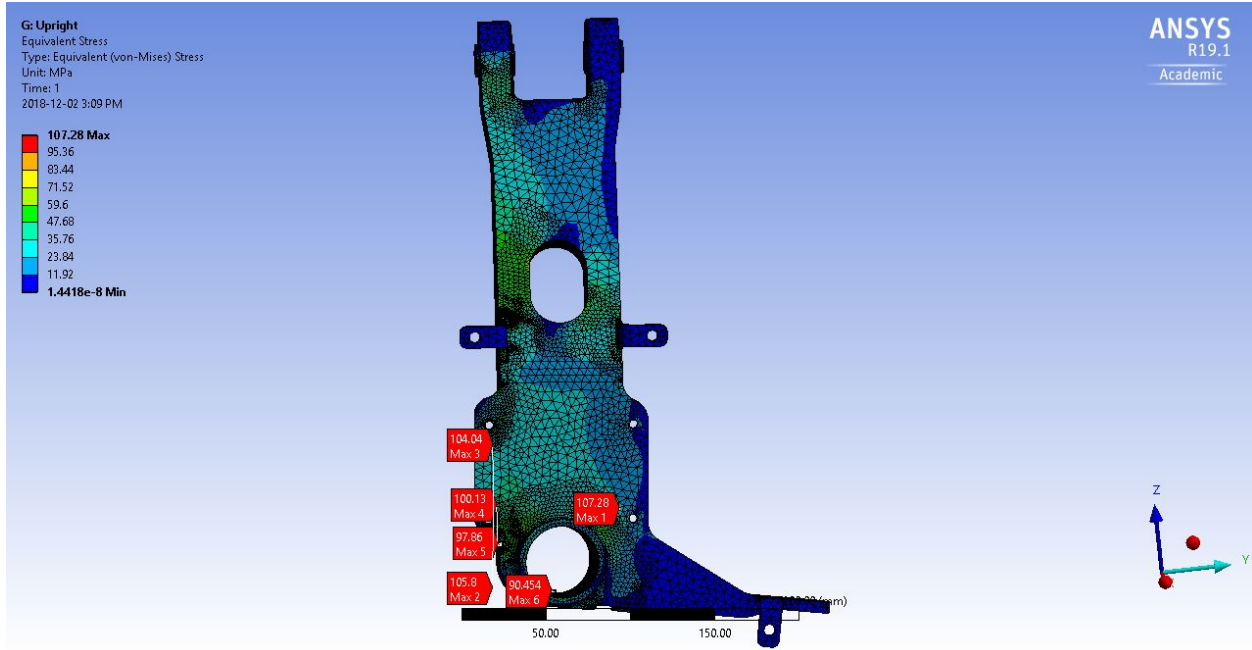
CASE 3: 6,0,0



Safety Factor



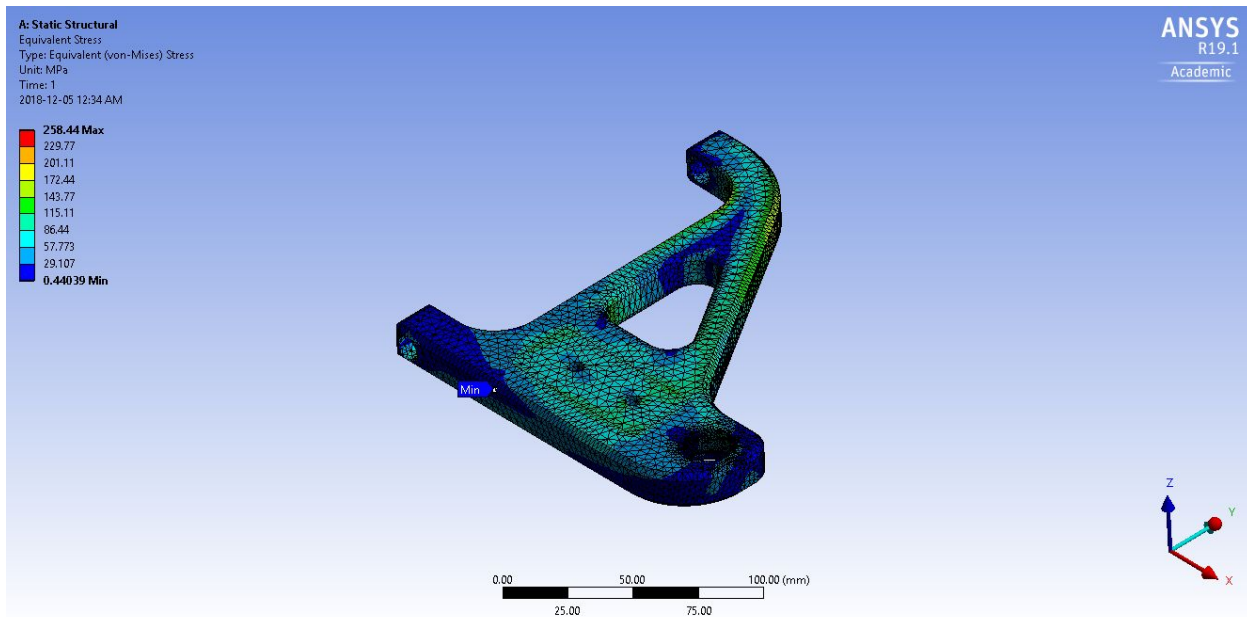
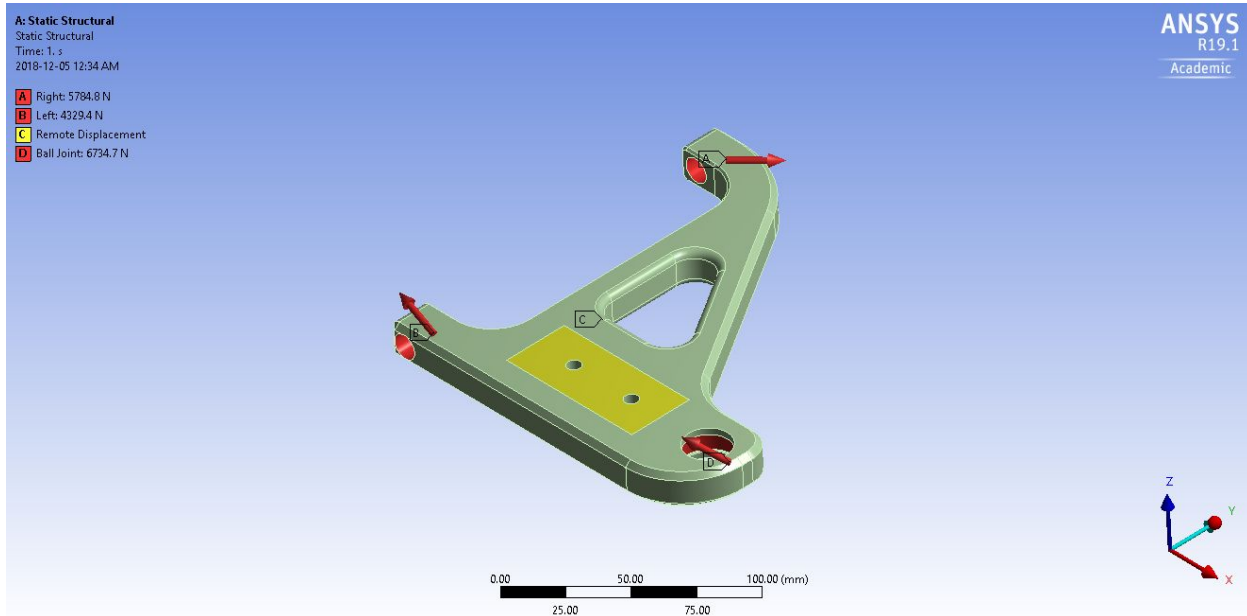
Deformation

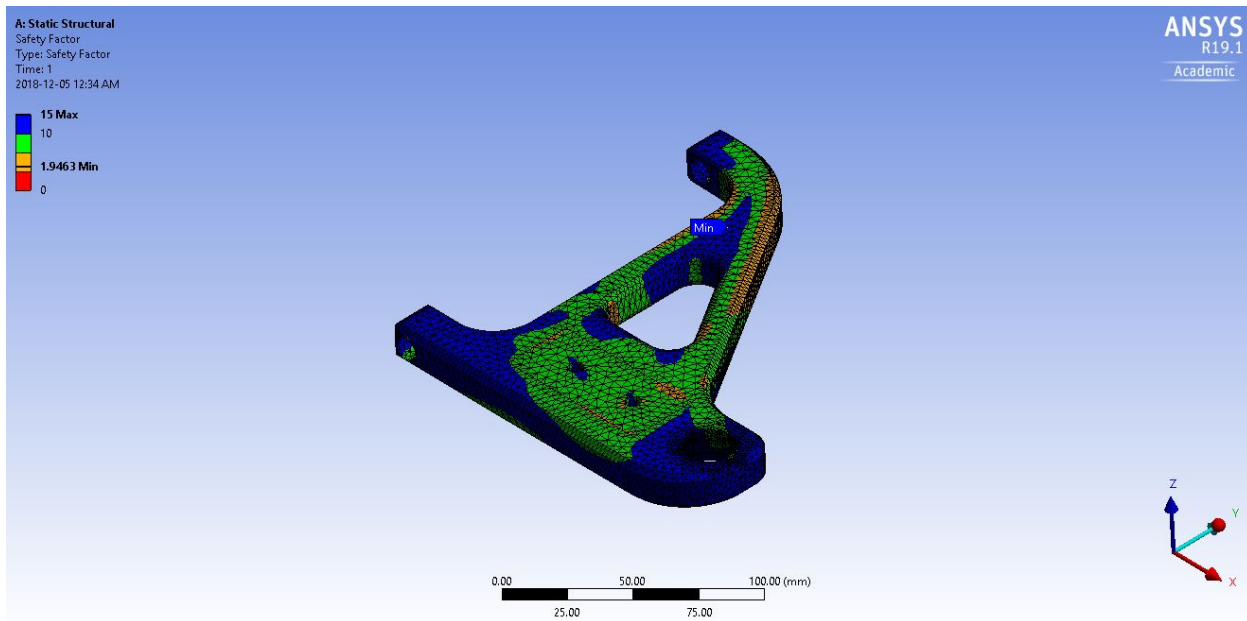
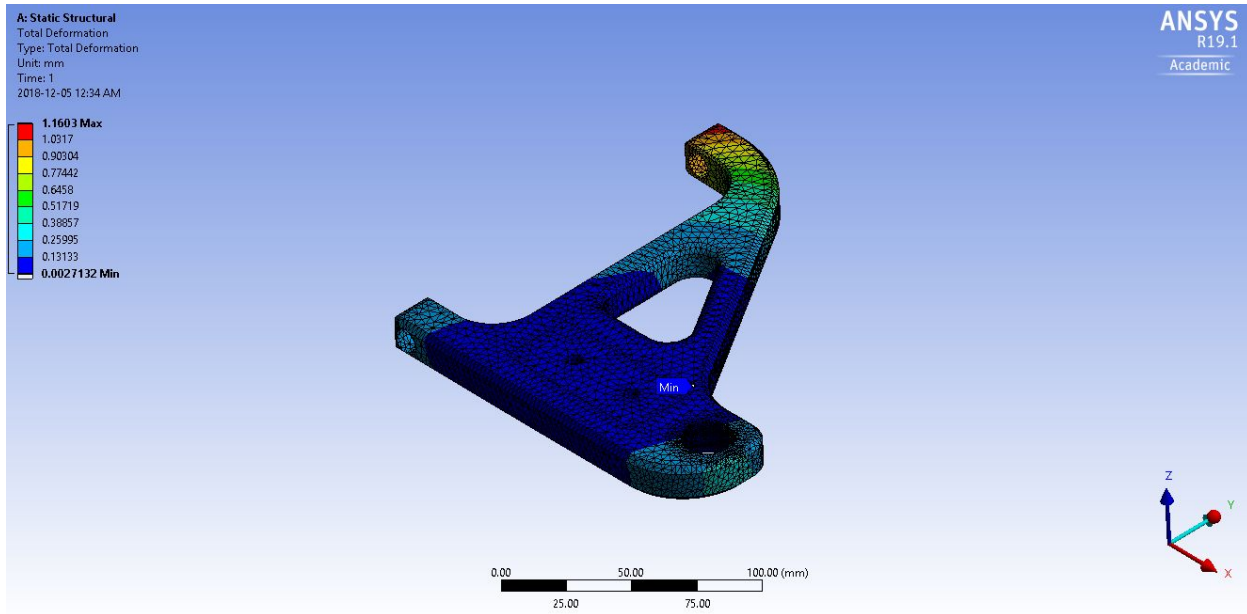


Equivalent Stress

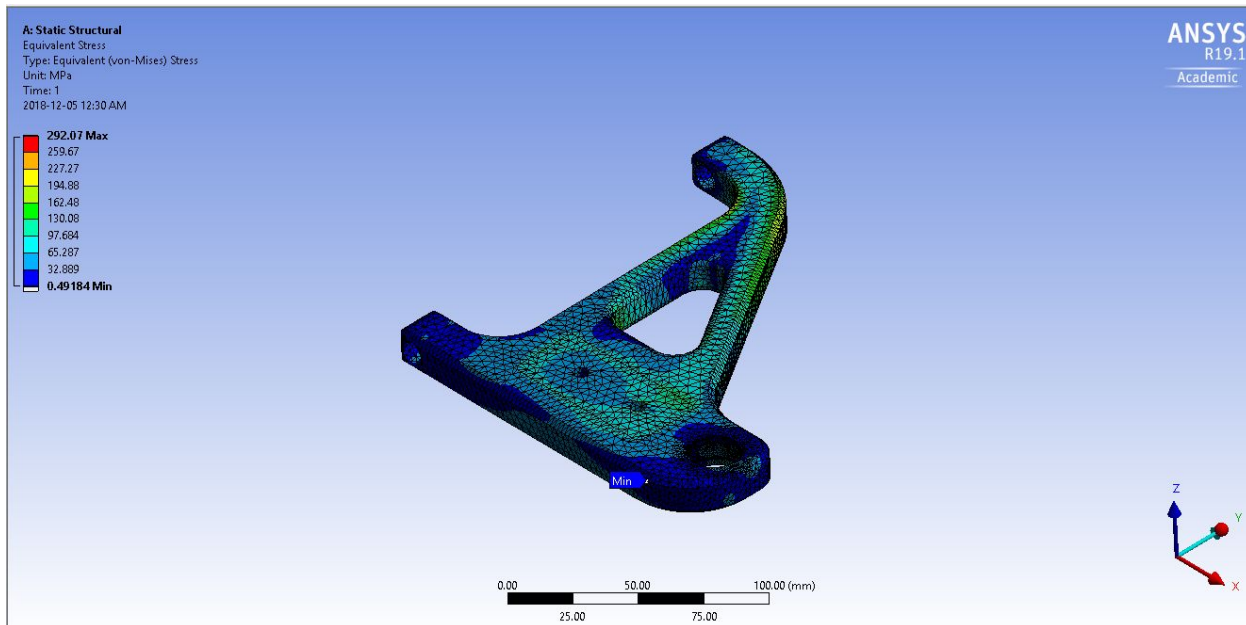
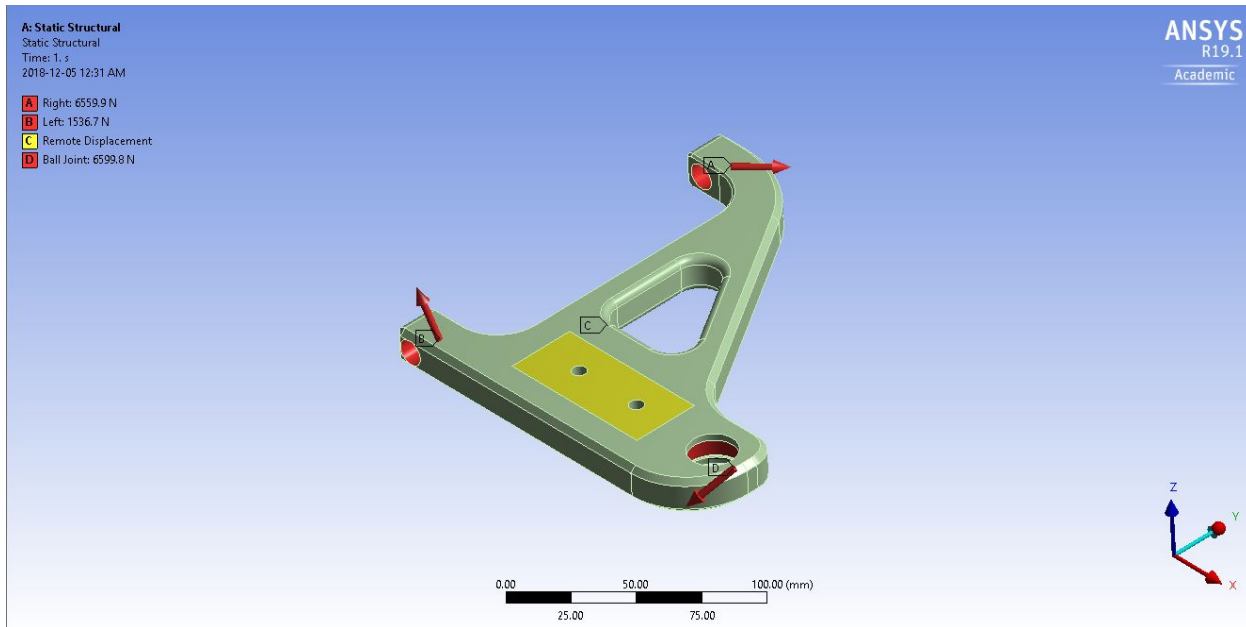
Appendix B: Bottom AARM Simulation Results

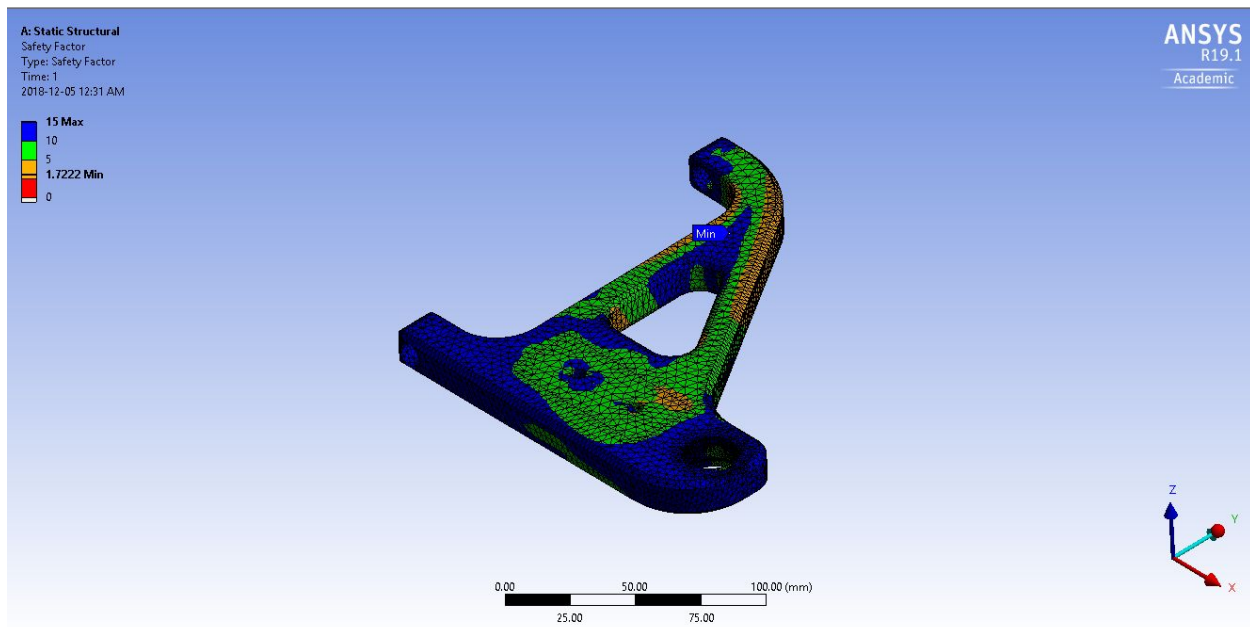
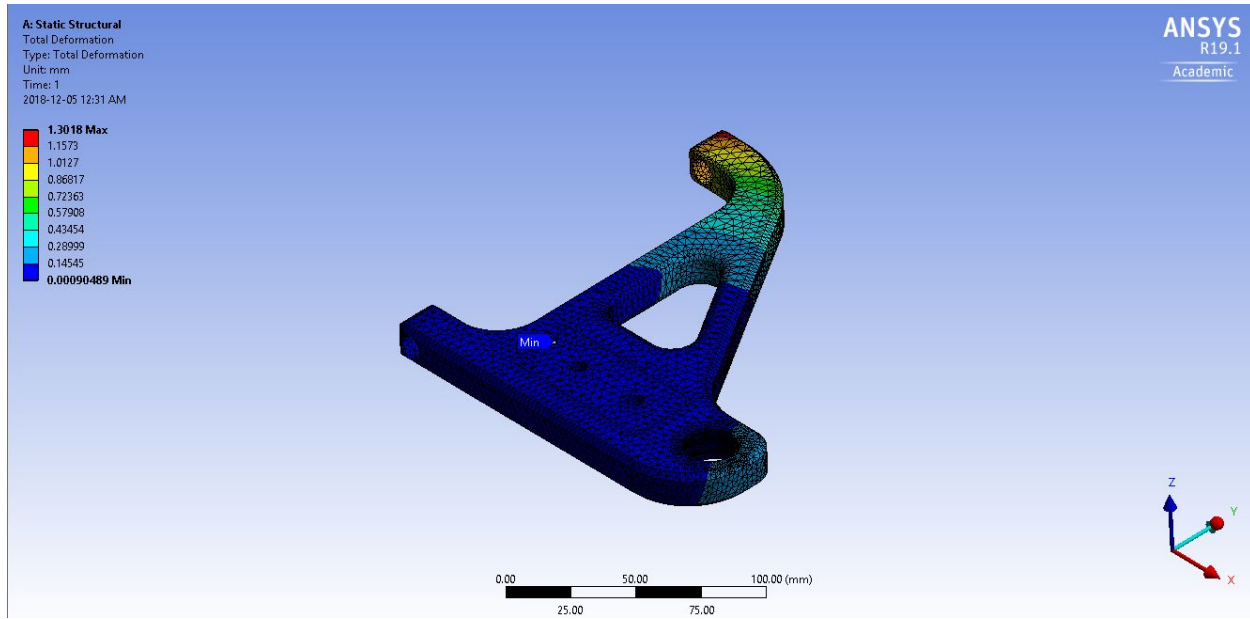
CASE 1: 2,1,1



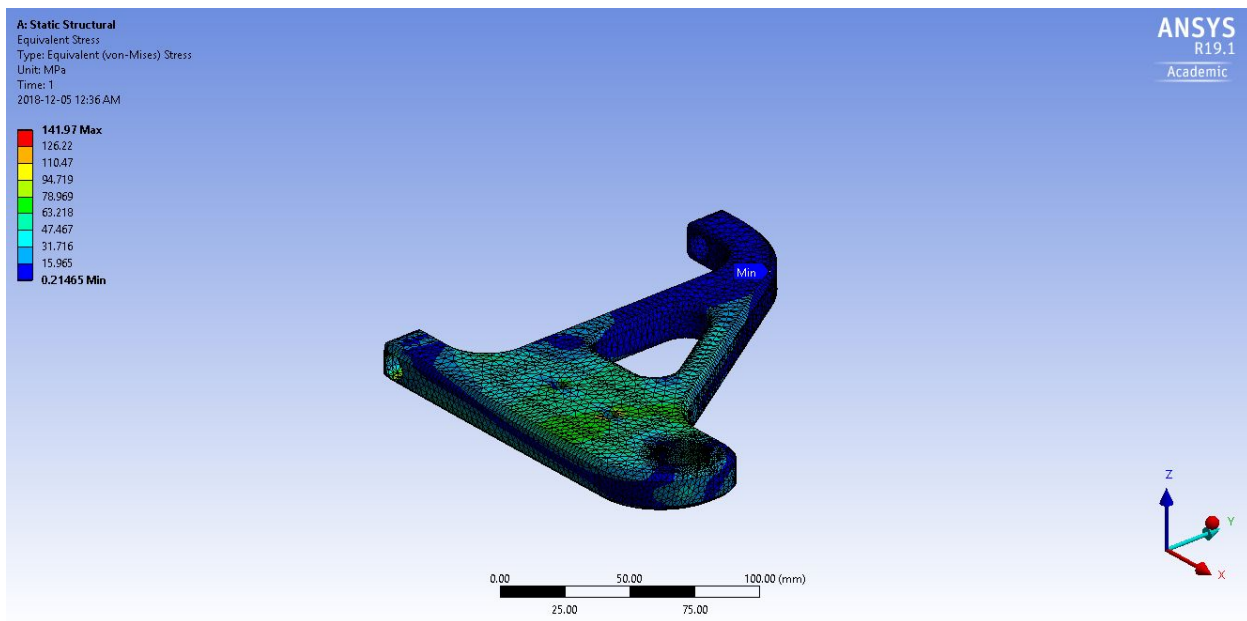
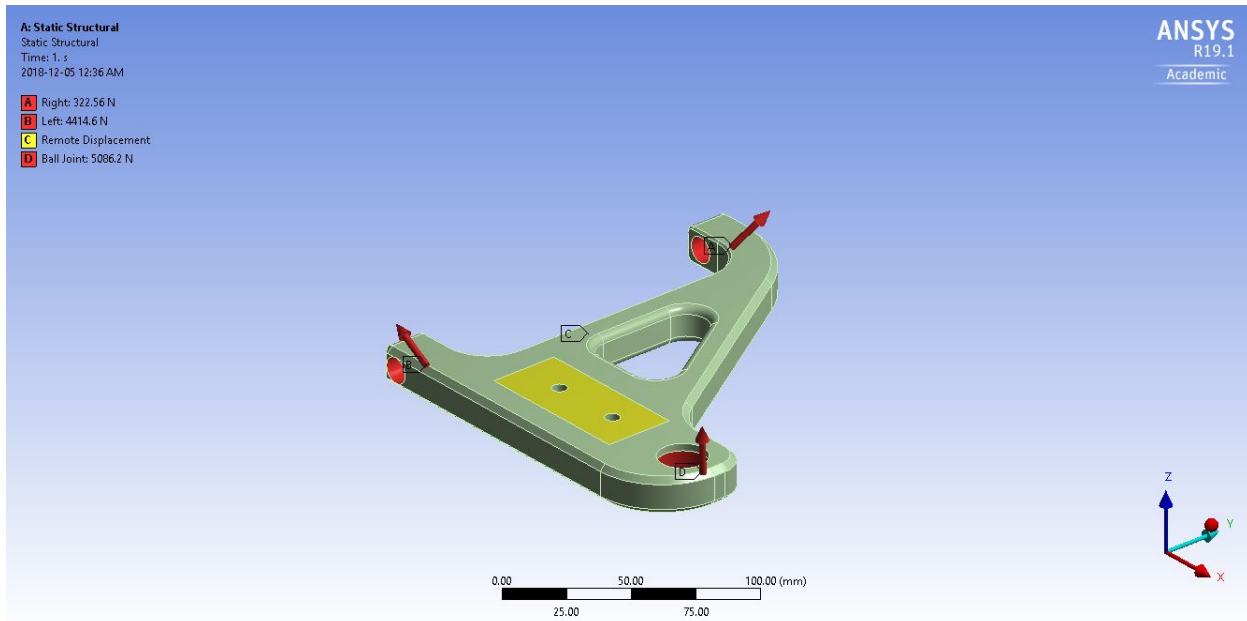


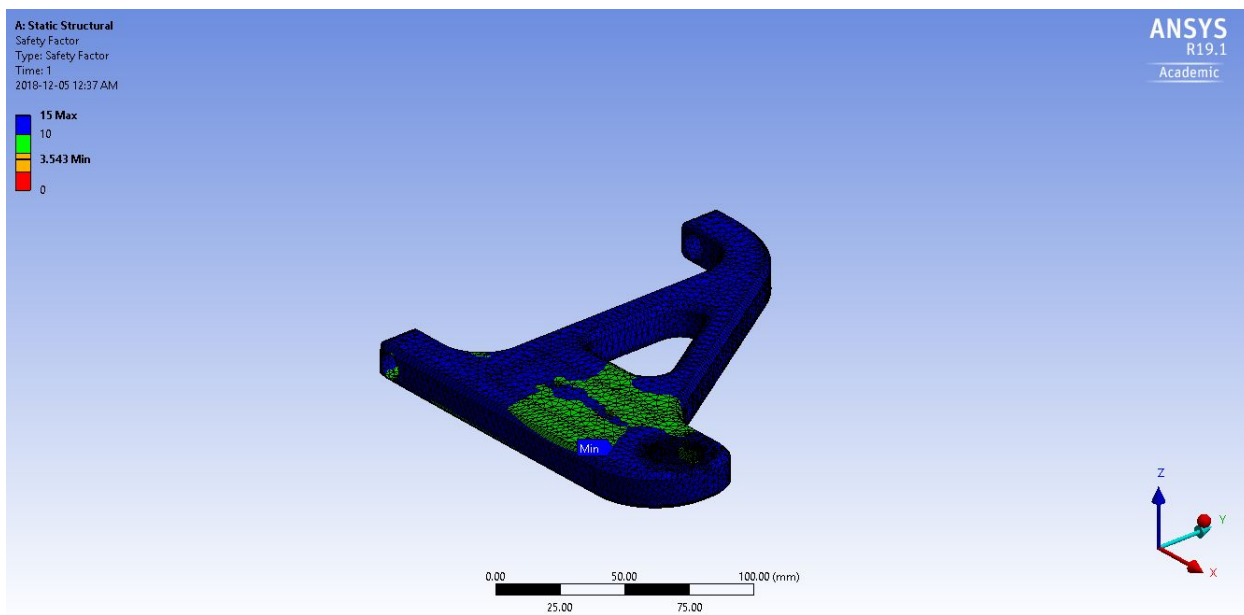
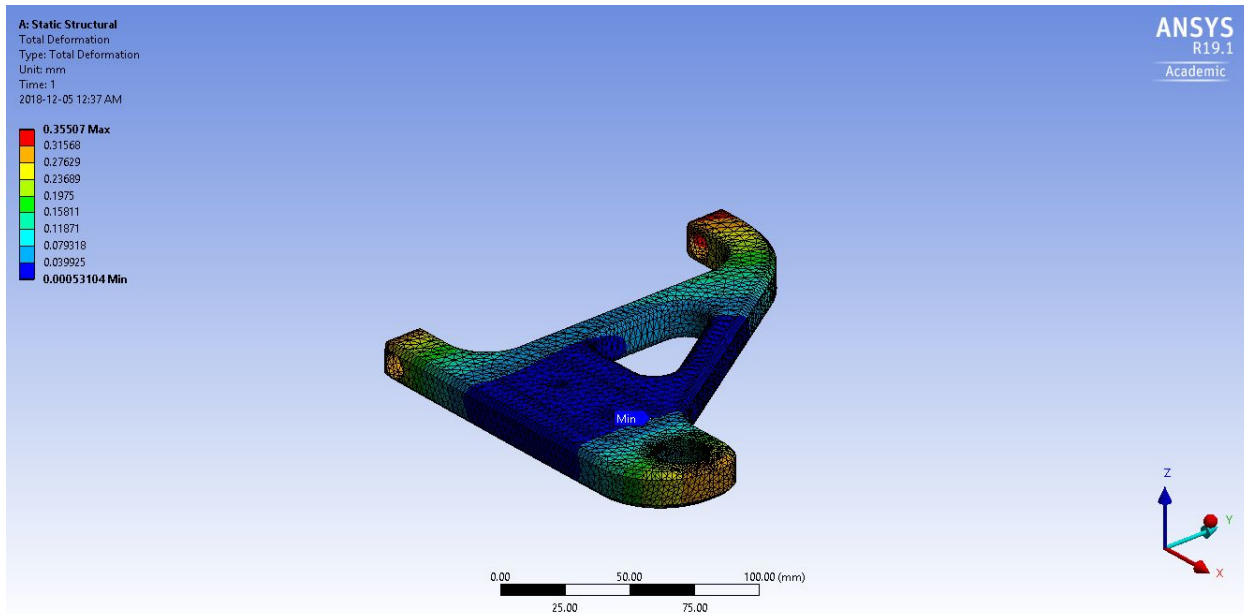
CASE 2: 2,1,-1





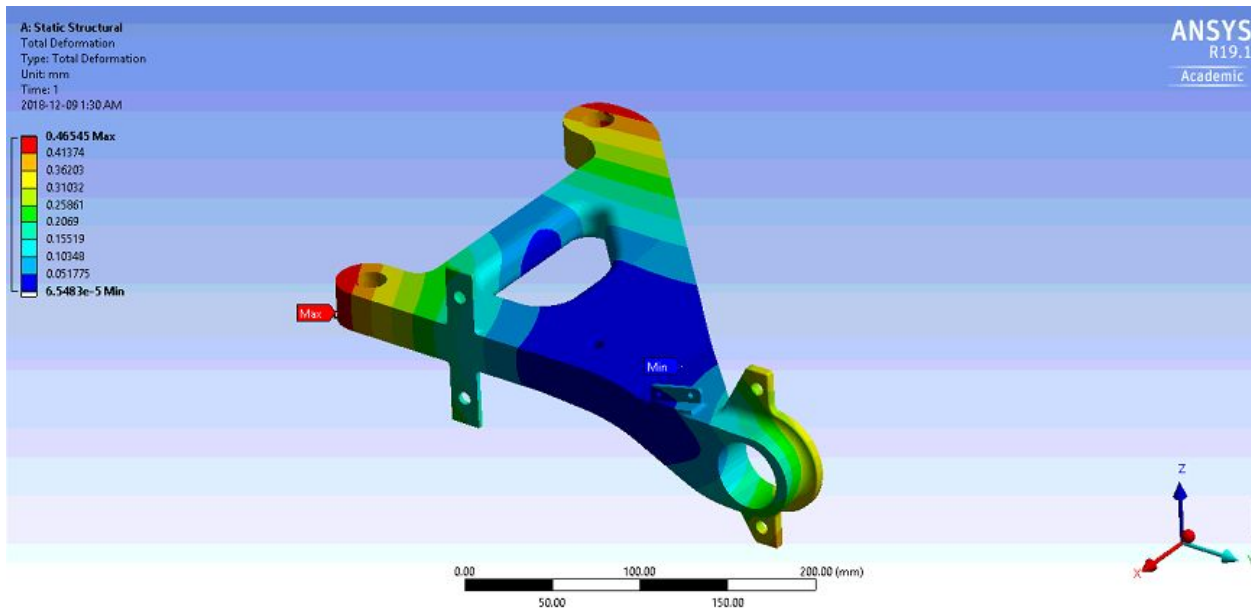
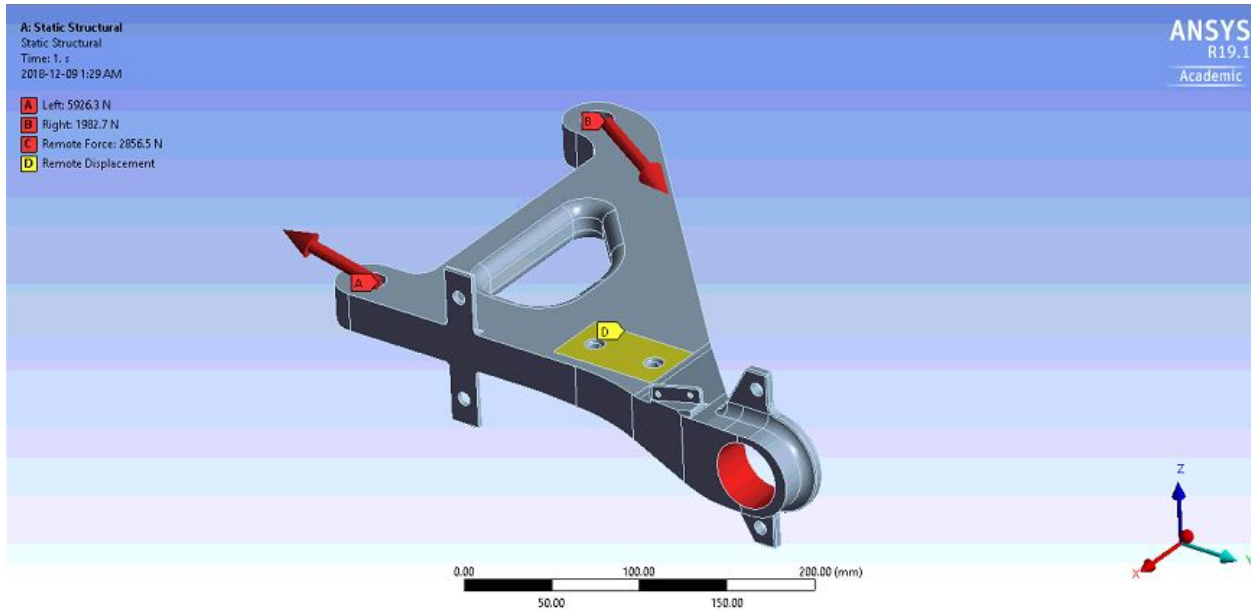
CASE 3: 6,0,0

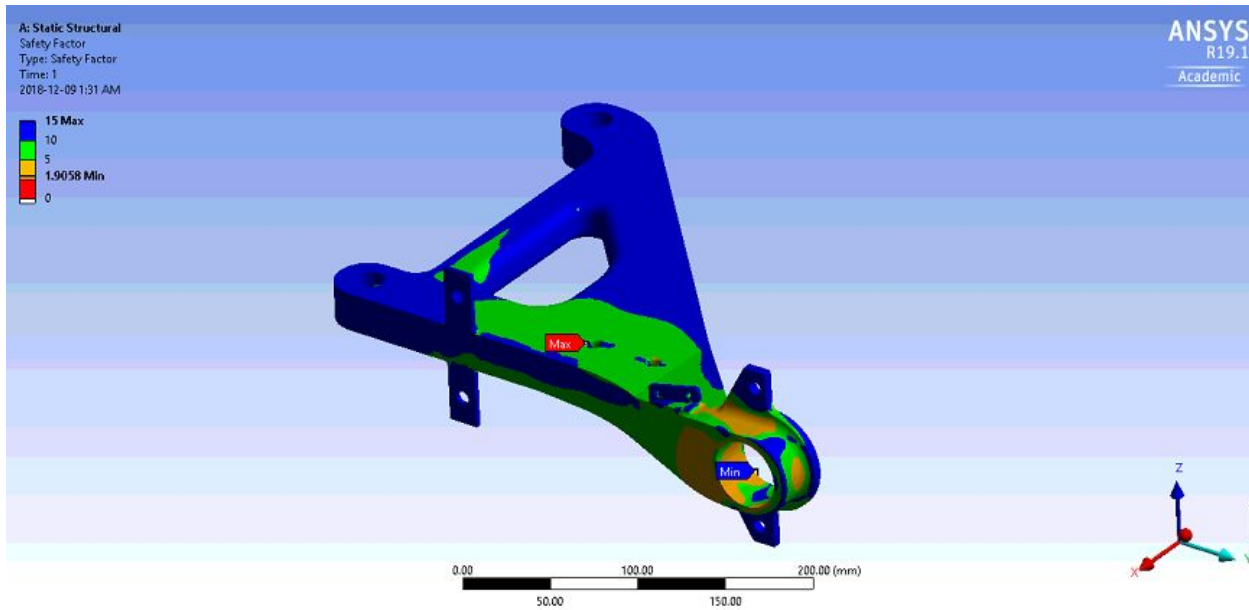
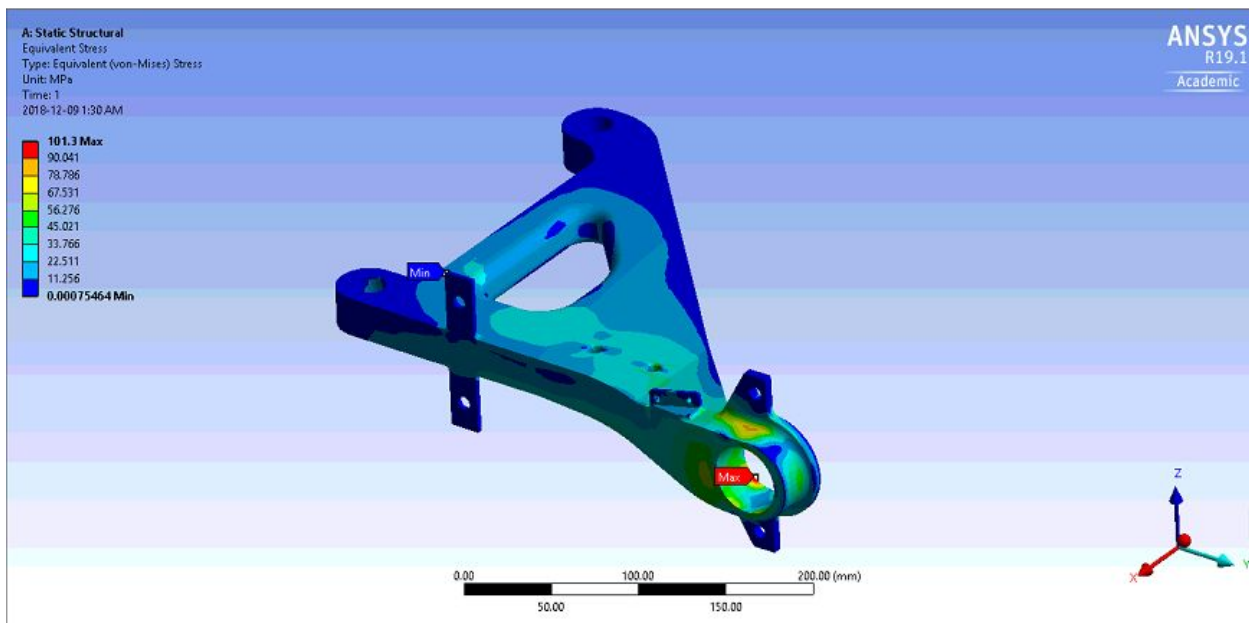




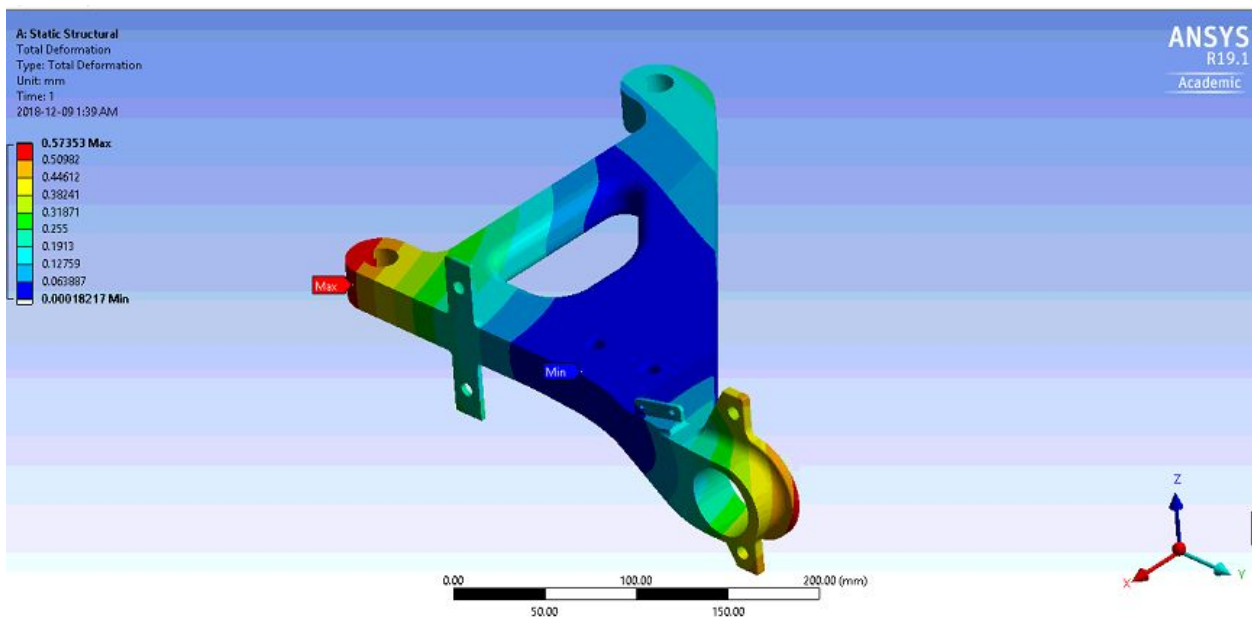
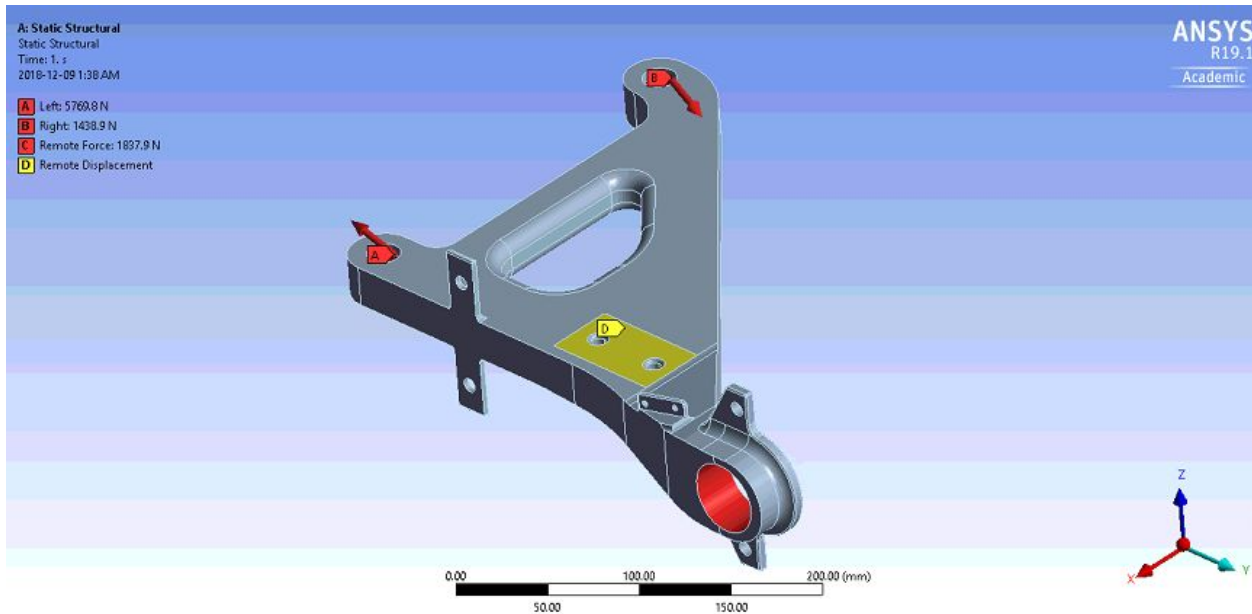
Appendix C: Trailing ARM (Rear Left) Simulation Results

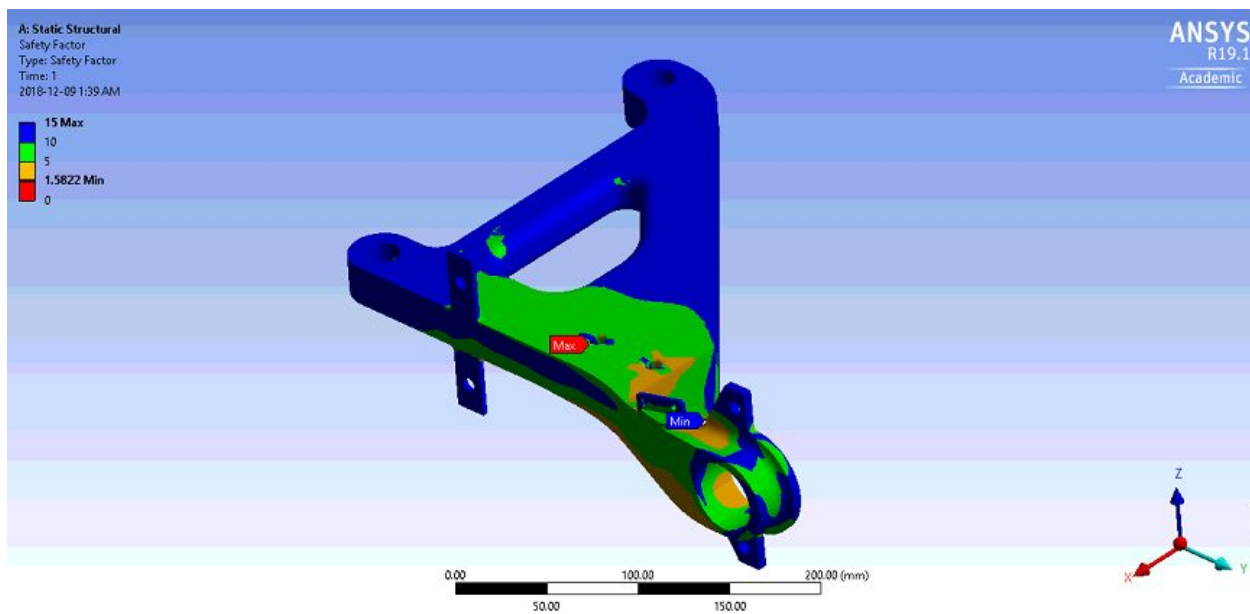
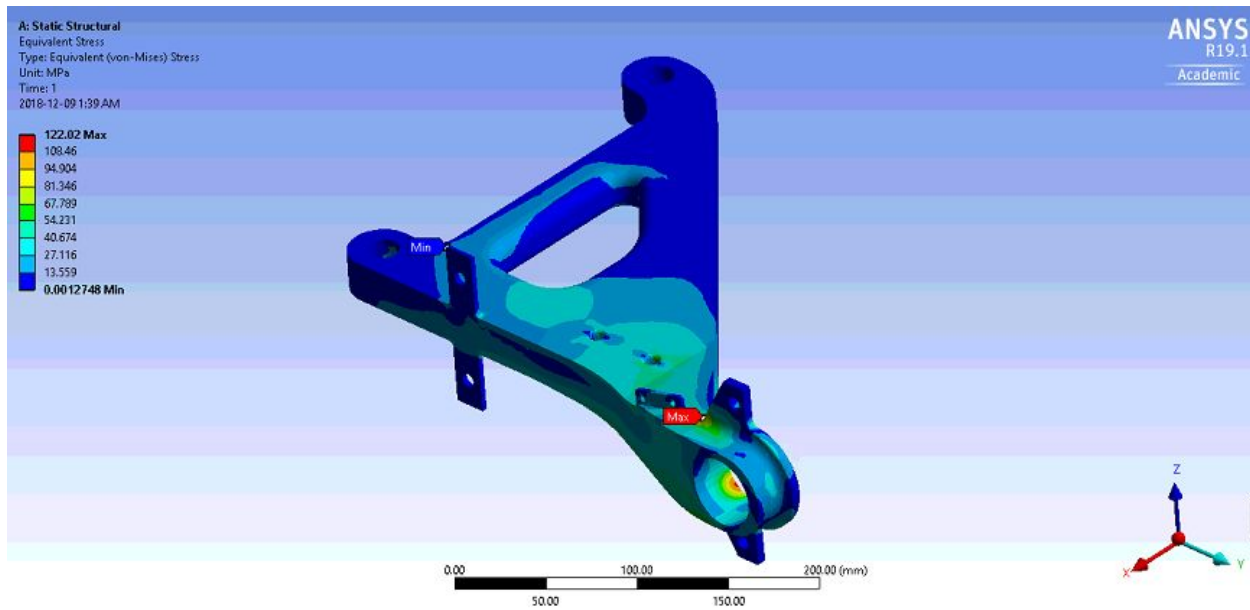
2,0,1



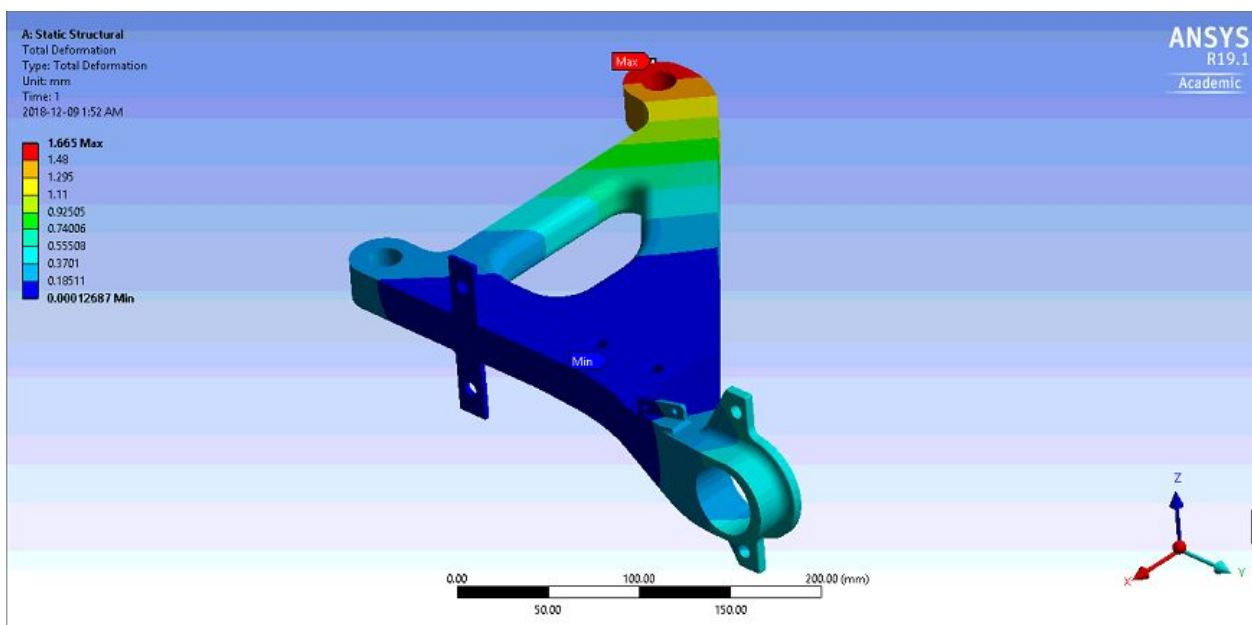
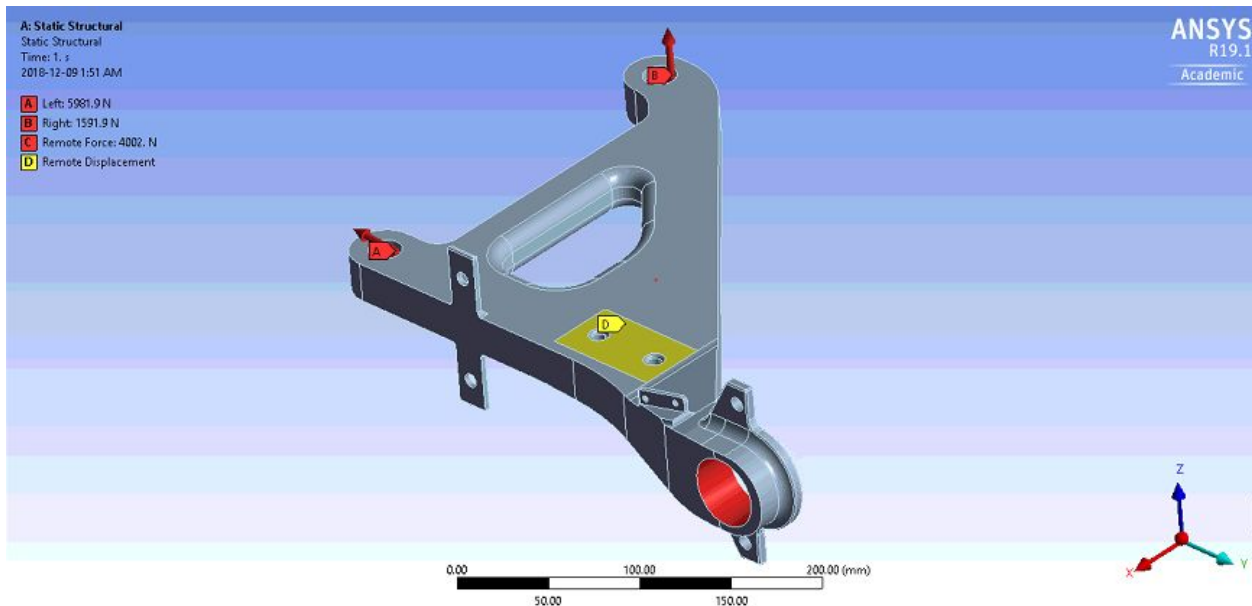


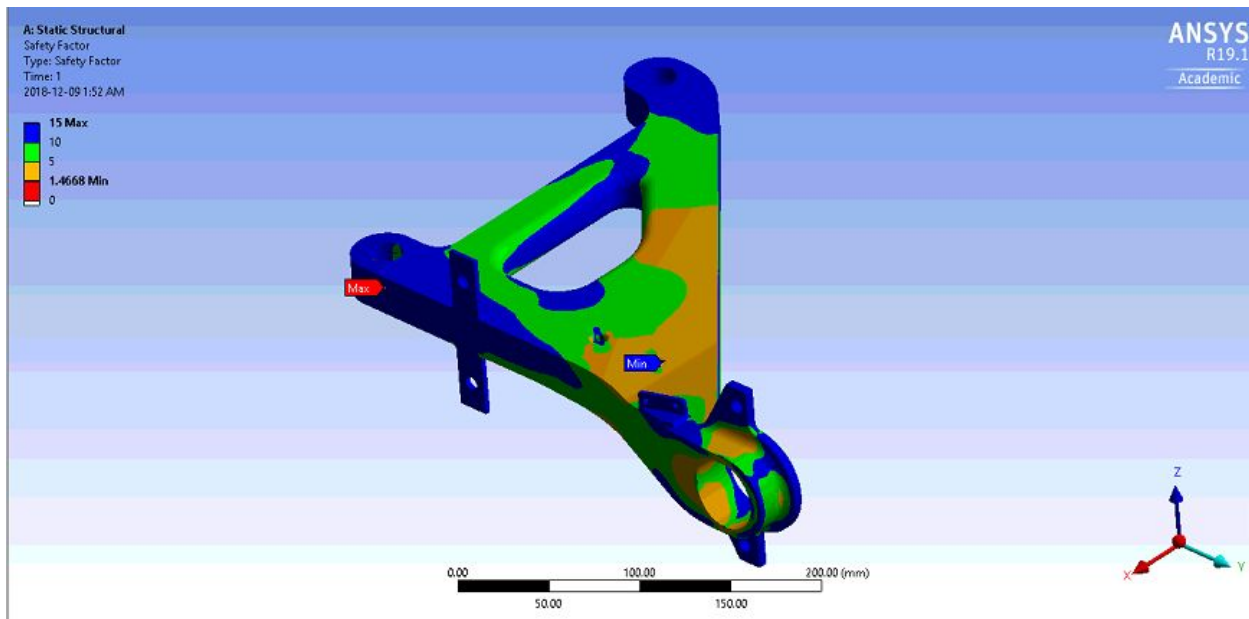
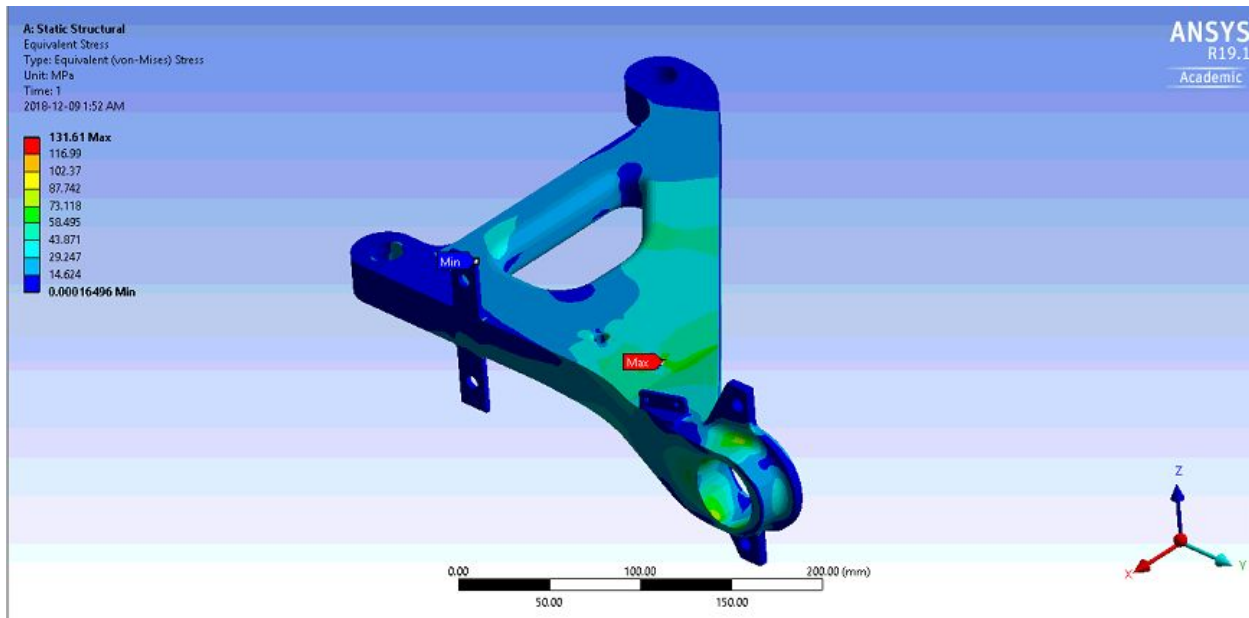
2,1,1





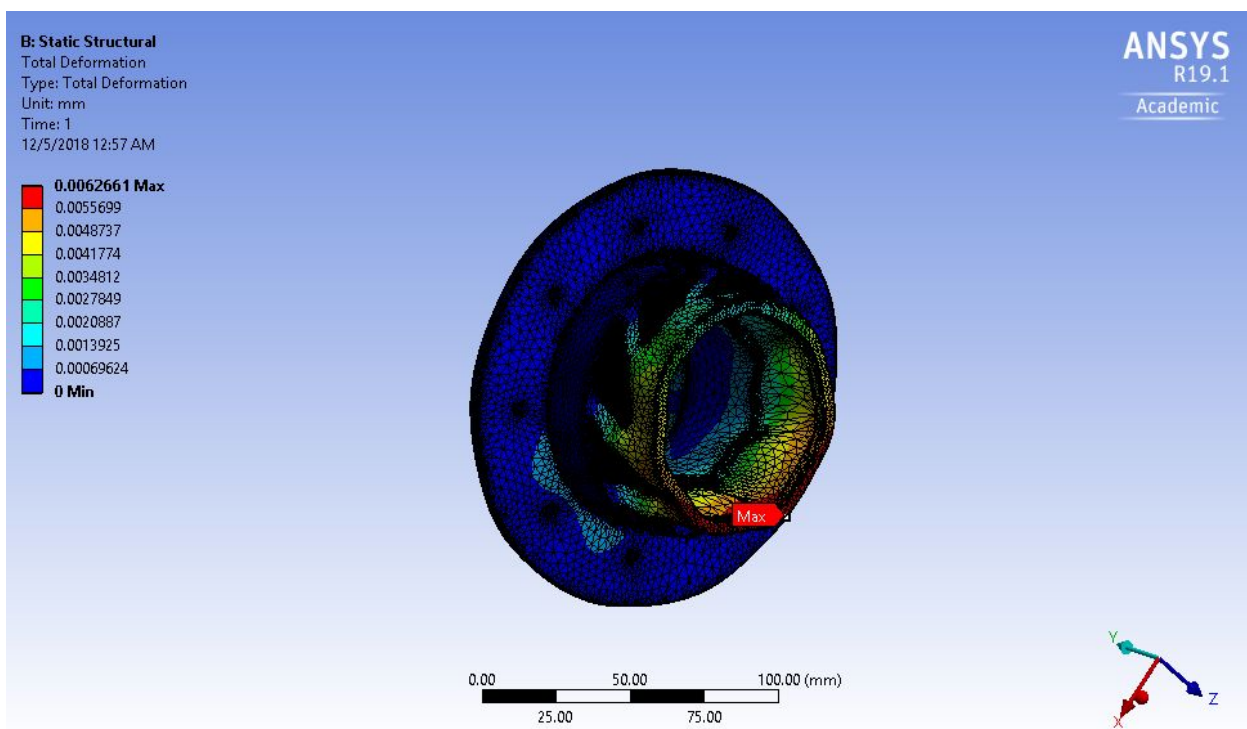
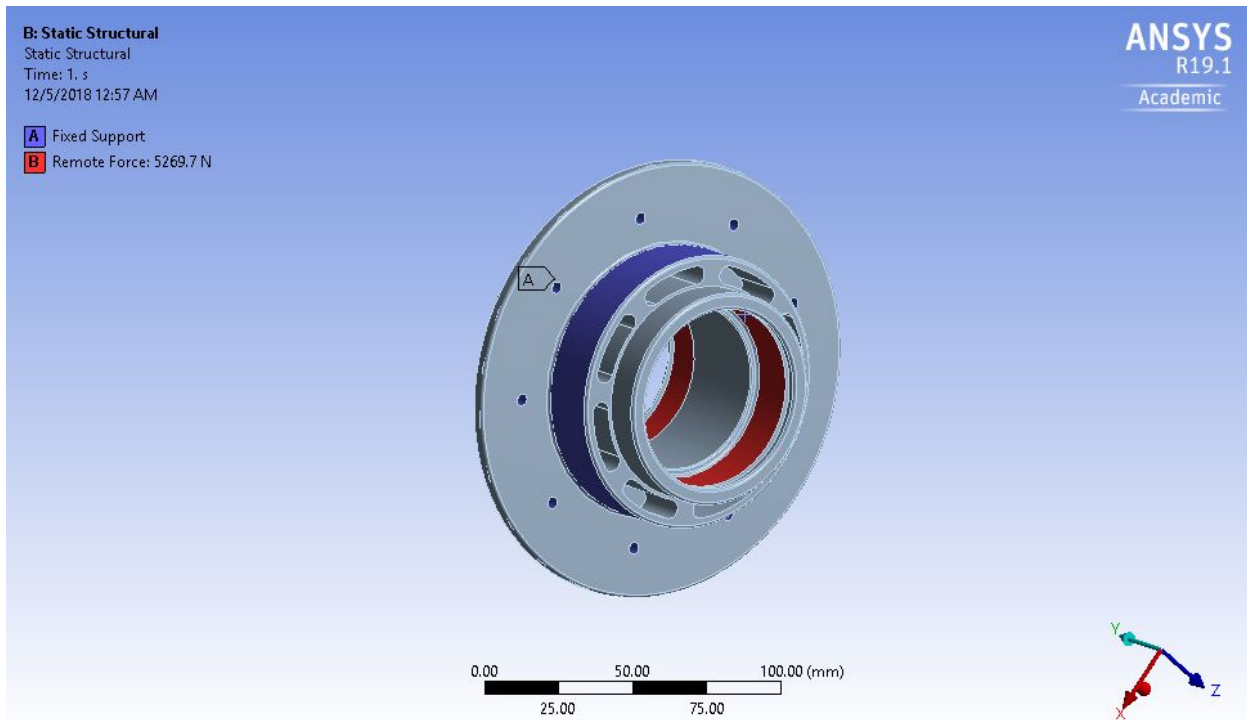
6,0,0

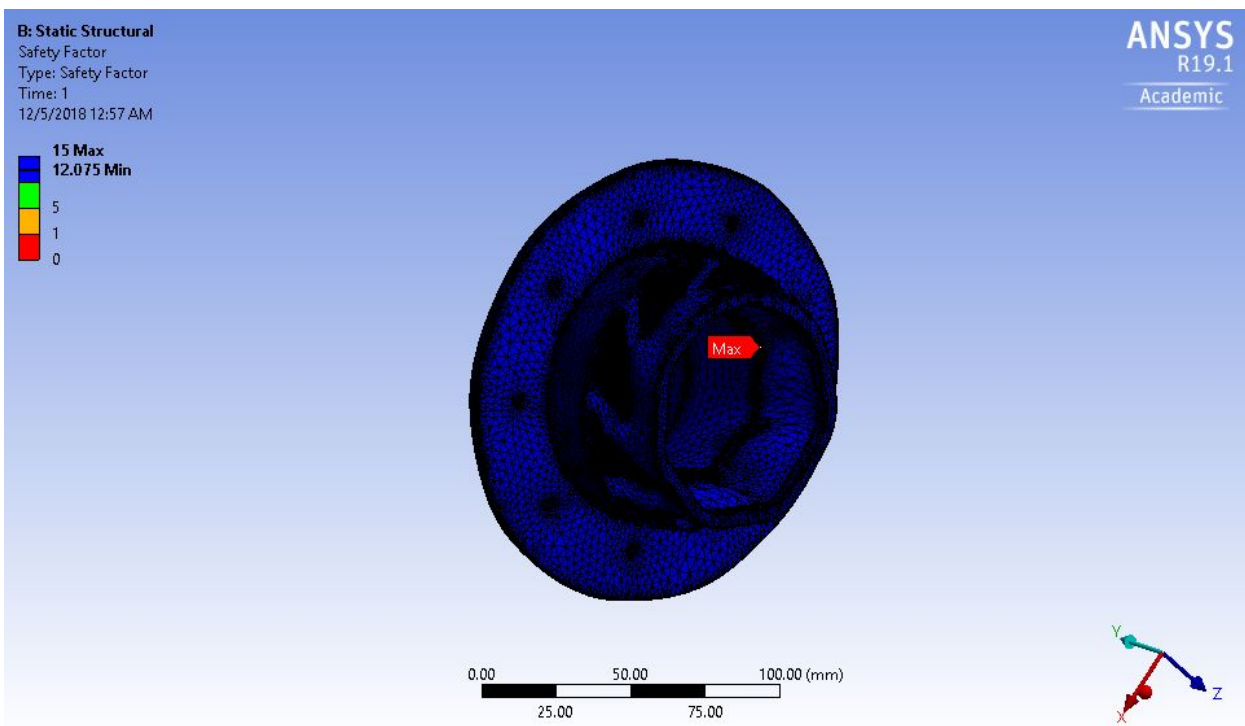
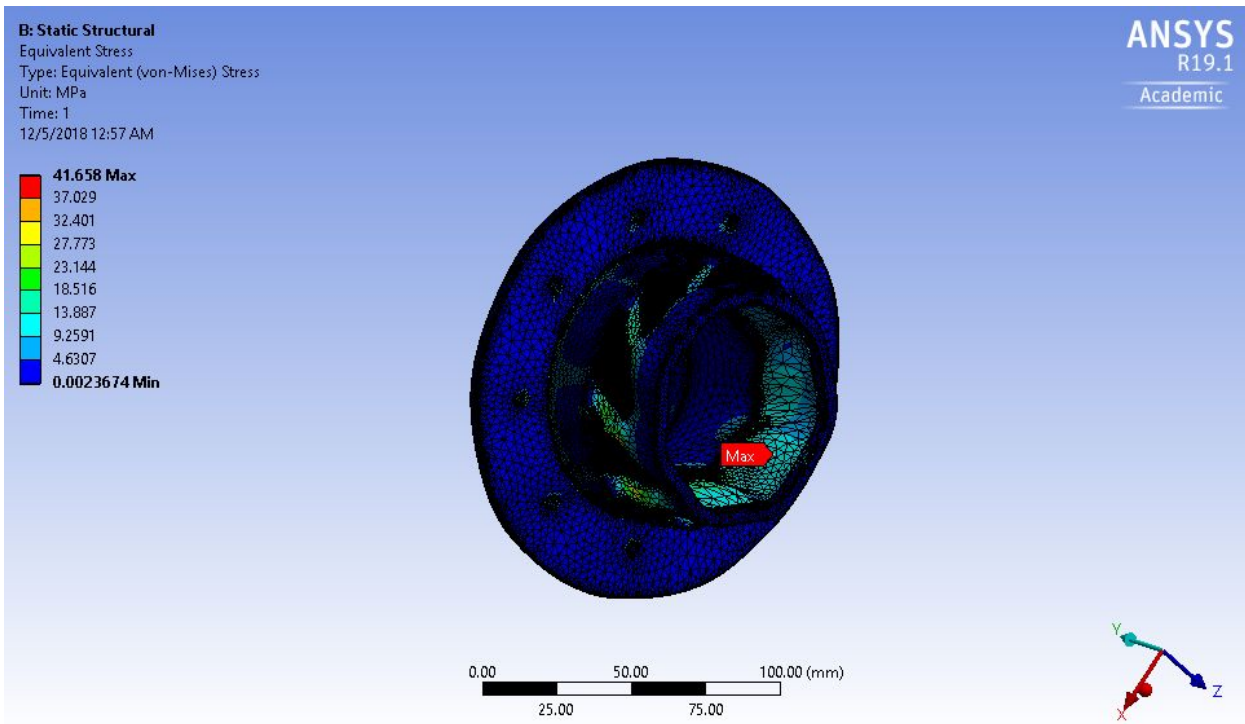




Appendix D: Hub Simulation Results

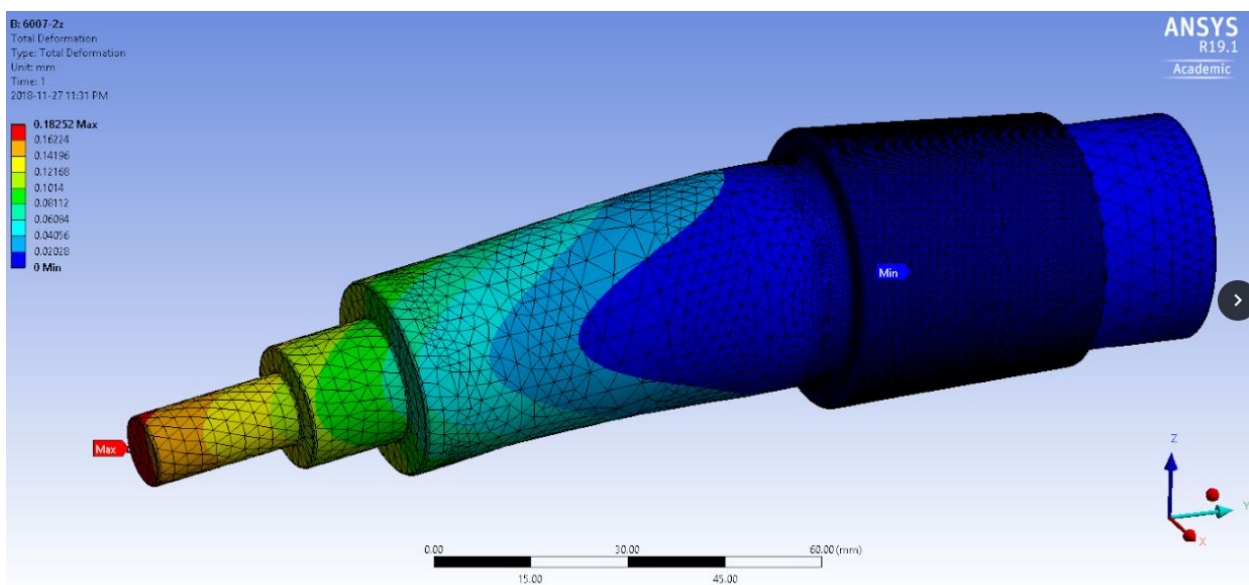
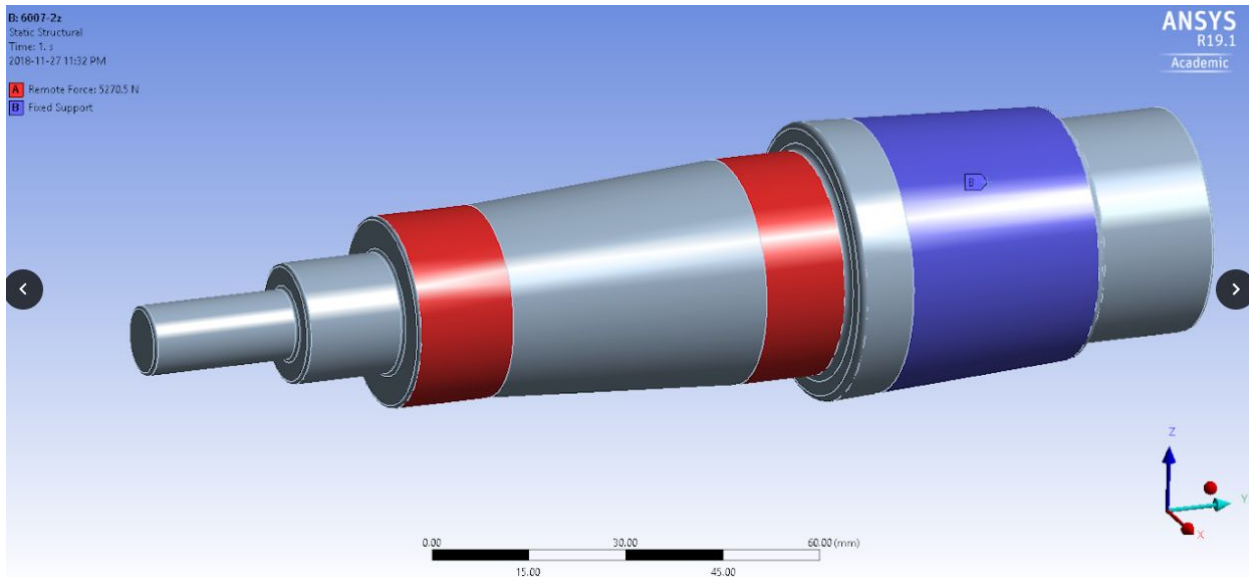
CASE 1: 2,1,-1

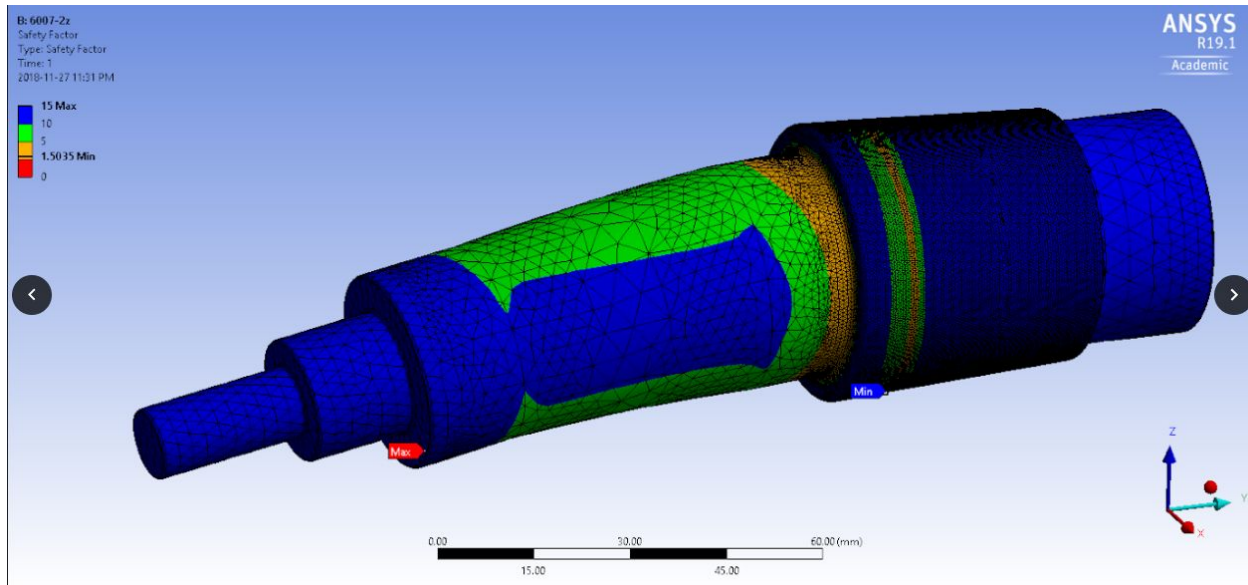
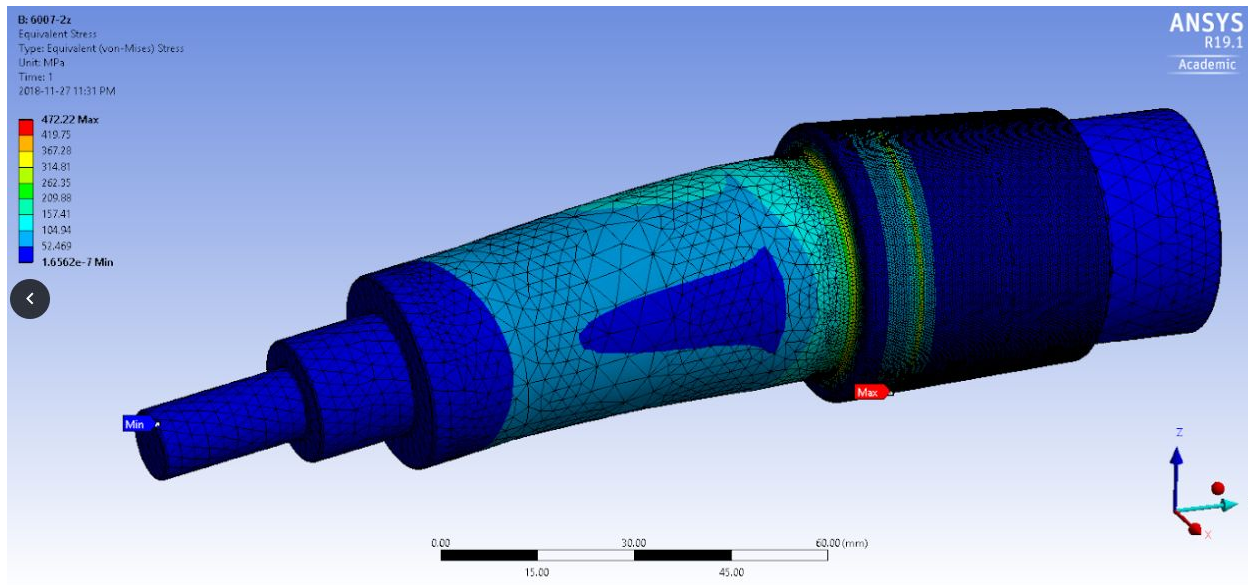




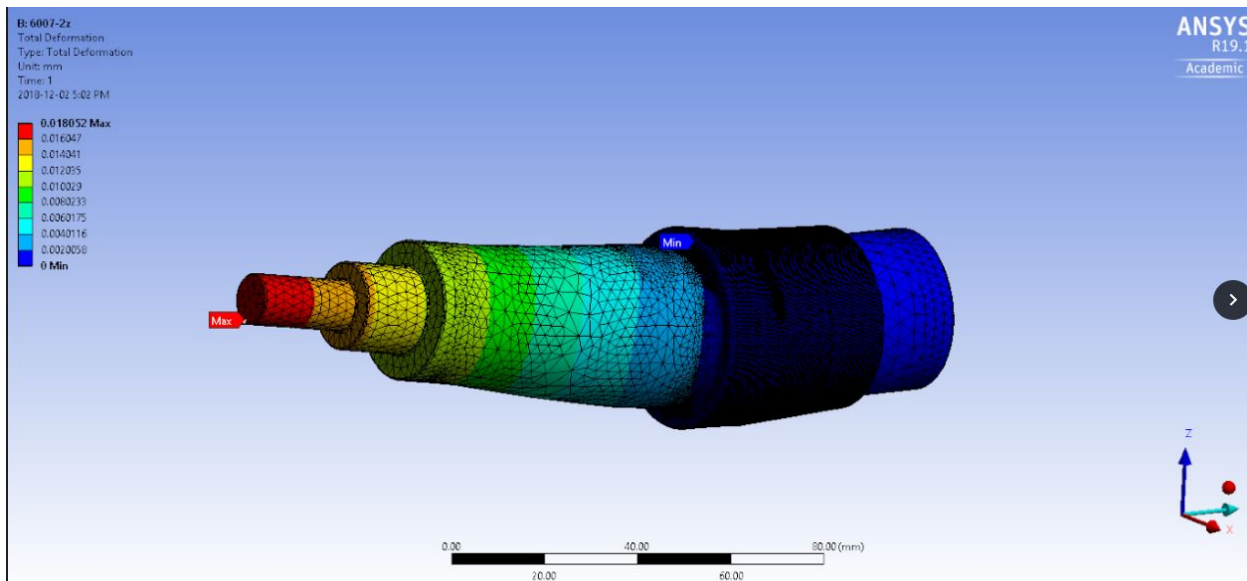
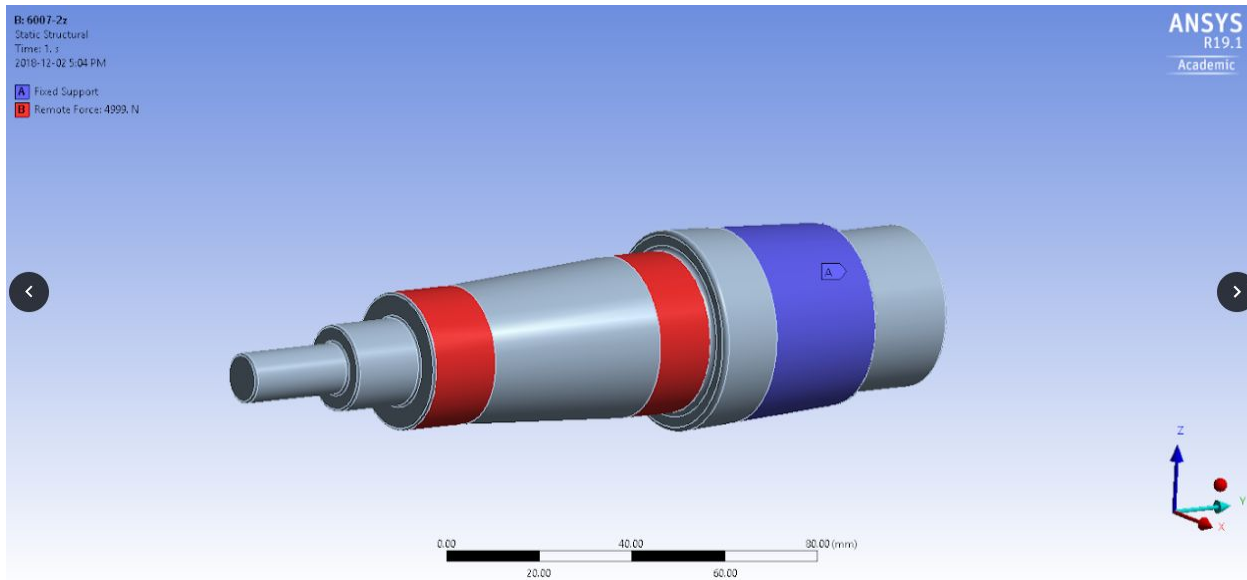
Appendix E: Axle Simulation Results

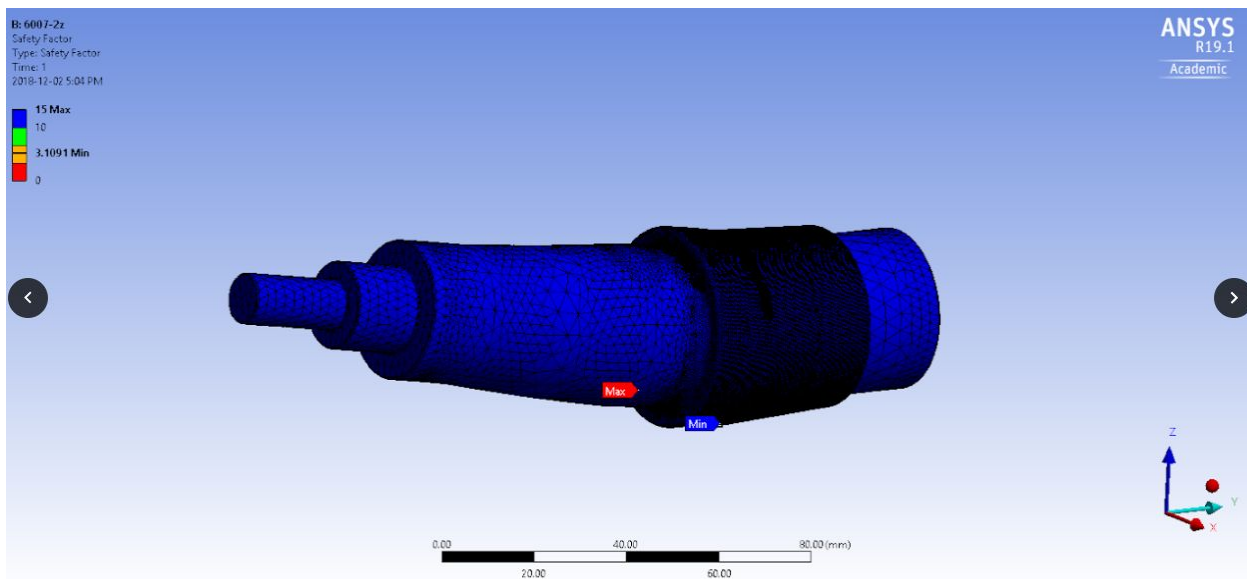
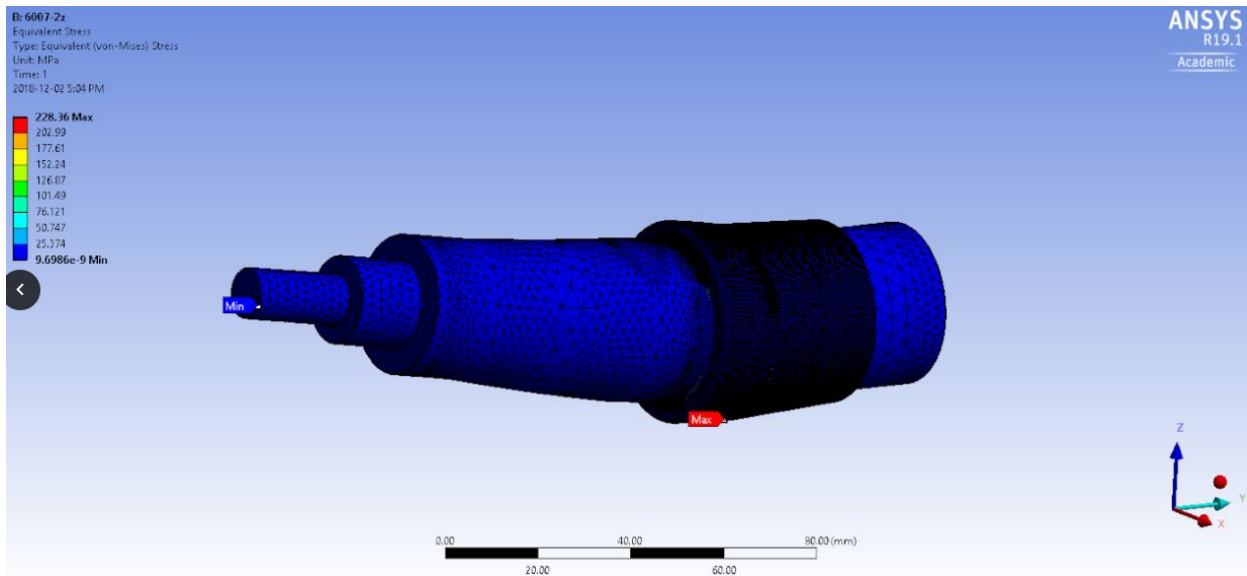
CASE 1: 2,1,-1





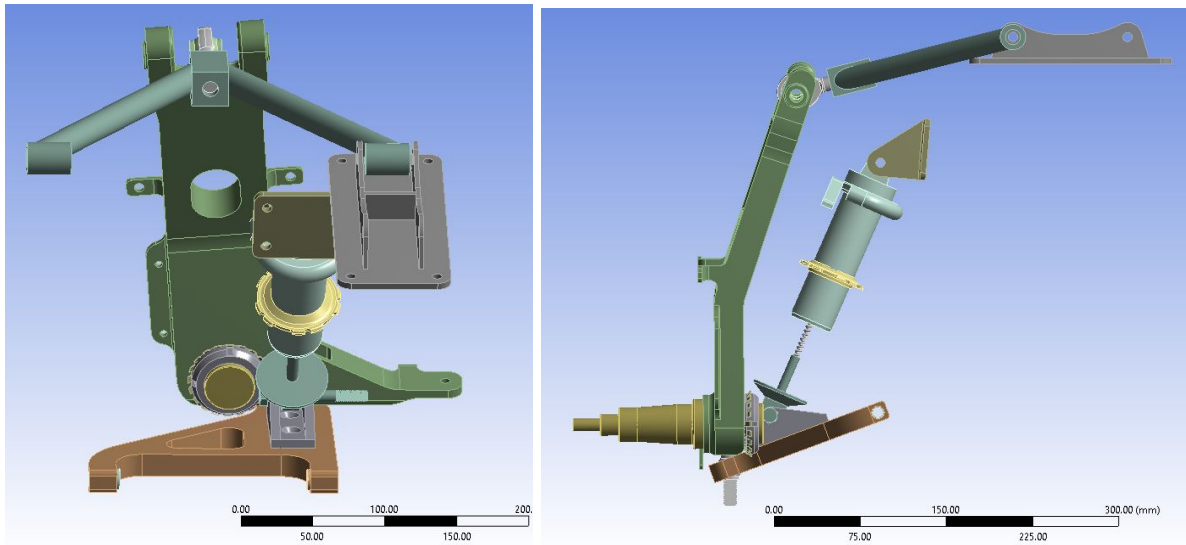
CASE 2: 6,0,0



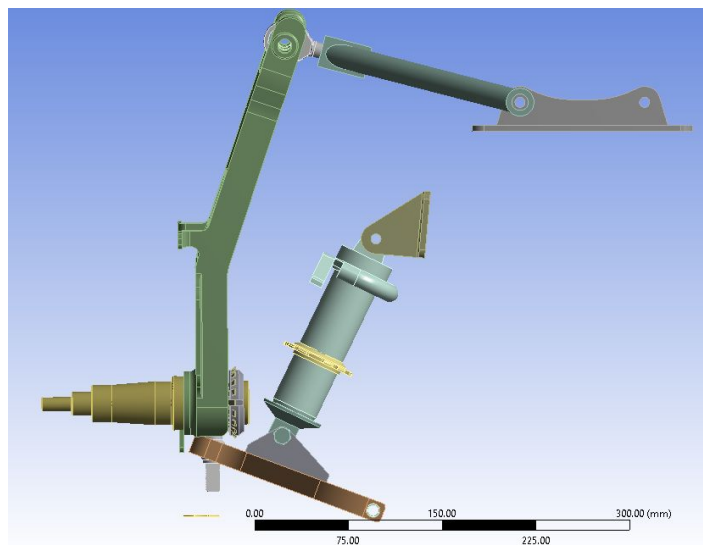


Appendix F: Front Suspension Rigid Dynamics

CASE 1: Bump/Droop

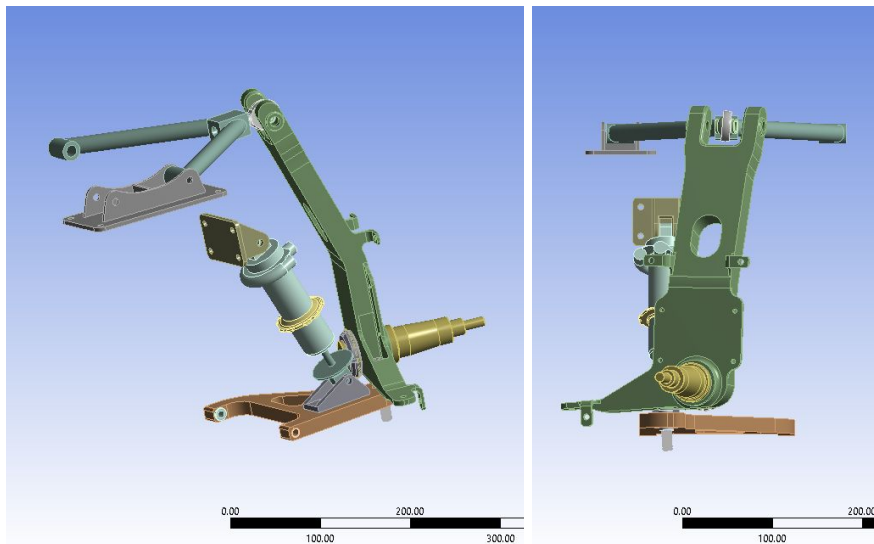


Full Droop

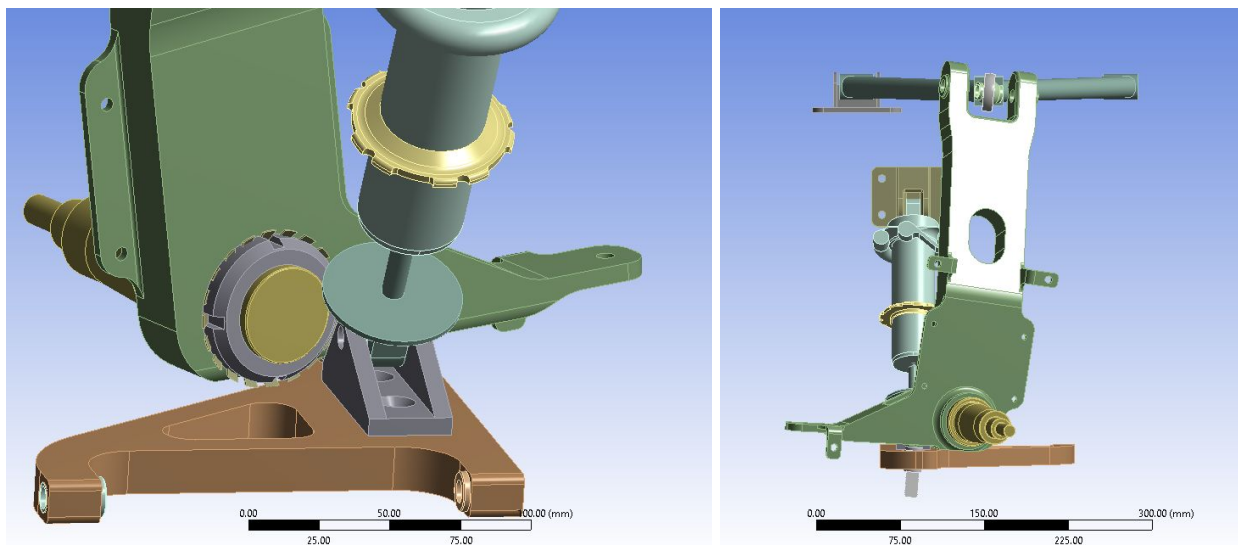


Full Bump

CASE 2: Steering

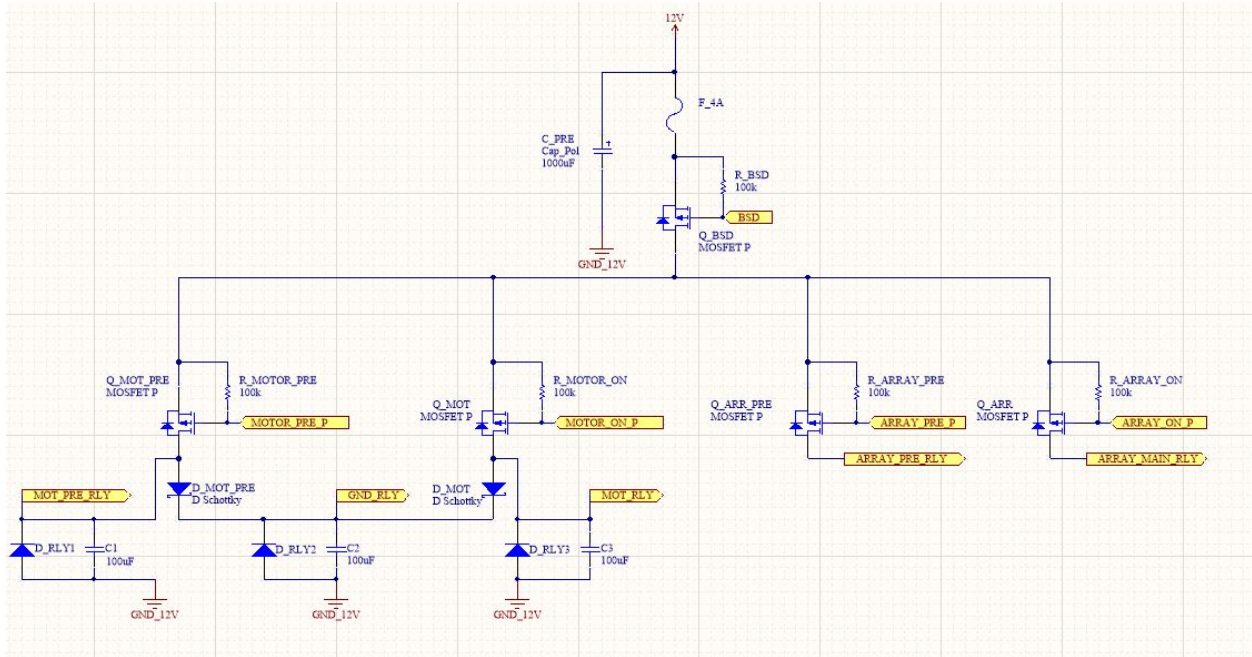


Full Left Steering



Full Right Steering

Appendix G: Polaris Relay Driving Circuit Schematic



Polaris Relay Driving Circuit Schematic. Note that the new system will drive half as many relays per circuit.

Appendix H: Samsung INR18650-35E Datasheet:

Spec. No.	INR18650-35E	Version No.	Ver. 1.1
-----------	--------------	-------------	----------



1. Scope

This product specification has been prepared to specify the rechargeable lithium-ion cell ('cell') to be supplied to the customer by Samsung SDI Co., Ltd.

2. Description and Model

- 2.1 Description Cell (lithium-ion rechargeable cell)
 2.2 Model INR18650-35E
 2.3 Site Manufactured in Korea

3. Nominal Specifications

Item	Specification
3.1 Standard discharge Capacity	Min 3,350mAh - Charge : 0.5C(1,700mA), 4.2V, 0.02C(68mA) cut-off @RT - Discharge : 0.2C(680mA), 2.65V cut-off @RT *1C=3,400mA
3.2 Charging Voltage	4.2V
3.3 Nominal Voltage	3.60V
3.4 Charging Method	CC-CV (constant voltage with limited current)
3.5 Charging Current	Standard charge: 1,700mA For cycle life : 1,020mA
3.6 Charging Time	Standard charge: 4hours
3.7 Max. Charge Current	2,000mA (not for cycle life)
3.8 Max. Discharge Current	8,000mA (for continuous discharge) 13,000mA (not for continuous discharge)
3.9 Discharge Cut-off Voltage	2.65V
3.10 Cell Weight	50 g max
3.11 Cell Dimension	Height : Max. 65.25 mm Diameter: Max. Φ 18.55 mm
3.12 Operating Temperature (Cell Surface Temperature)	Charge : 0 to 45°C Discharge : -10 to 60°C
3.13 Storage Temperature	1 year : -20~25°C (1*) 3 months : -20~45°C (1*) 1 month : -20~60°C (1*)

Note (1): If the cell is kept as ex-factory status (30% of charge),

The capacity recovery rate is more than 80%.

Spec. No.	INR18650-35E	Version No.	Ver. 1.1
-----------	--------------	-------------	----------

4. Outline Dimensions

See the Fig. 1

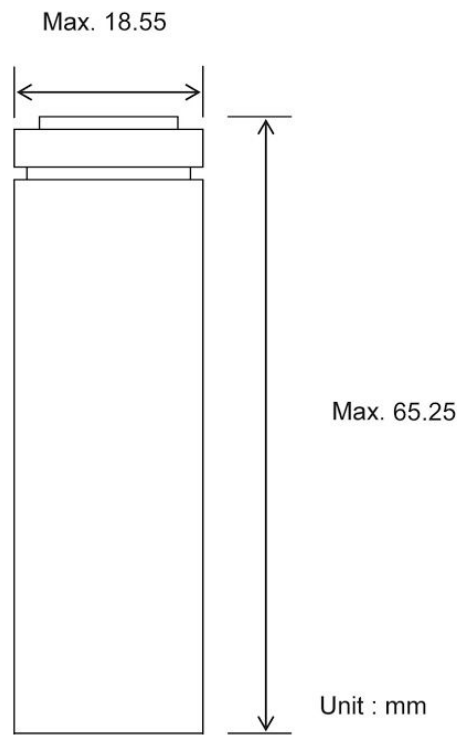


Fig. 1 Outline Dimensions of INR18650-35E